CEBAF PR 92-003

FAST SCINTILLATORS FOR HIGH RADIATION LEVELS

Stan Majewski and Carl Zorn
Continuous Electron Beam Accelerator Facility
12,000 Jefferson Avenue
Newport News, Virginia, U.S.A. 23606

Contribution to Instrumentation in High Energy Physics, edited by Fabio Sauli, and to be published by World Scientific Publishing Co. Pte. Ltd. in 1992.

CONTINUOUS ELECTRON BEAM ACCELERATOR FACILITY

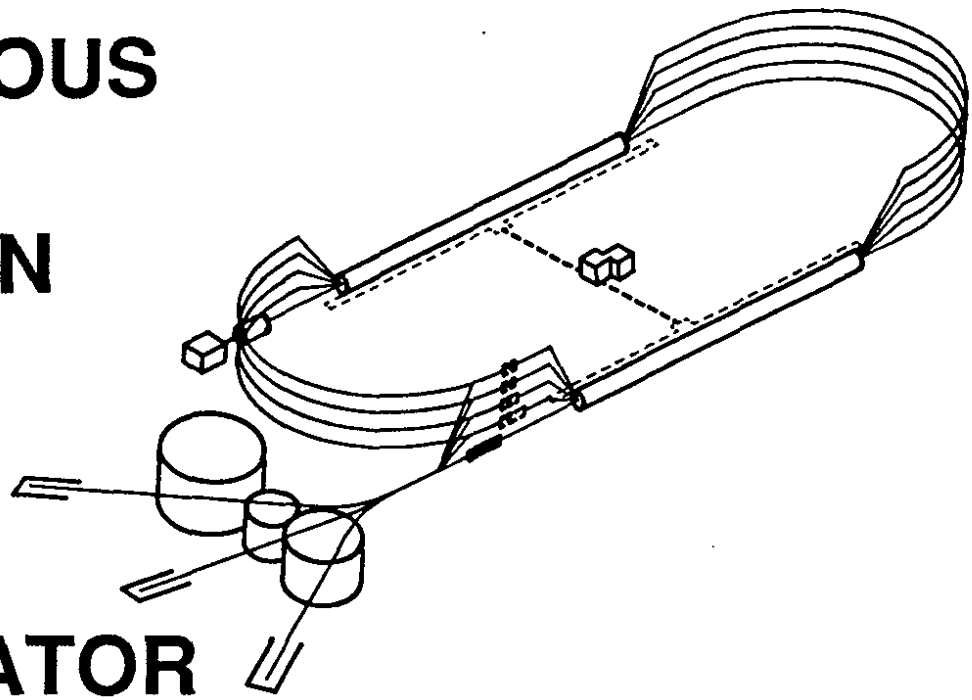

SURA *Southeastern Universities Research Association*

CEBAF
The Continuous Electron Beam Accelerator Facility

Newport News, Virginia

Copies available from:

Library
CEBAF
12000 Jefferson Avenue
Newport News
Virginia 23606

The Southeastern Universities Research Association (SURA) operates the Continuous Electron Beam Accelerator Facility for the United States Department of Energy under contract DE-AC05-84ER40150.

FAST SCINTILLATORS FOR HIGH RADIATION LEVELS

Stan Majewski and Carl Zorn
CEBAF, Physics Division
12,000 Jefferson Avenue
Newport News, Virginia, U.S.A. 23606
Email: MAJEWSKI and ZORN@CEBAF

Part I
Crystal Scintillators

Stan Majewski

Part II
Plastic and Liquid Organic Scintillators

Carl Zorn

ABSTRACT

The development of new high luminosity hadron colliders (SSC and LHC) has posed a number of new challenges to traditional detector technologies. In addition to the expected problems of cost, project management, fast timing, energy resolution, occupancy levels, etc., some detectors (particularly calorimeters) face new problems due to the unusually high radiation levels expected in the forward regions of the beam-beam intersections. Although not alone in this category, scintillators face this last problem as probably the determining factor for their use in the high radiation areas, especially in the calorimetric detectors.

This article is a review of ongoing developmental work to make scintillators a viable and important element of the next generation of high energy physics detector systems. Although the key problem is that of radiation tolerance, attention has to be paid to such questions as fast timing capability, energy resolution, light output, and photodetector spectral sensitivity and quantum efficiency in order to produce a realistic solution.

It is the intent of the authors to show that although the final solutions may not exist at present, the achievements of the past few years show that the solution is probably realizable with proper effort and attention within the time scale envisioned for the construction of the new colliders.

Contribution to Instrumentation in High Energy Physics, edited by Fabio Sauli, and to be published by World Scientific Publishing Co. Pte. Ltd. in 1992.

FAST SCINTILLATORS FOR HIGH RADIATION LEVELS

Part I

Crystal Scintillators

Part I: Crystal Scintillators

I.1. Introduction

With the increasing energies and interaction rates of the upgraded detectors either planned or under construction for the presently operational accelerators, and the detectors intended for experiments at the future machines such as SSC, LHC, UNK, K-factories and RHIC (in p-p experiments), there is an ever increasing demand for fast and radiation hard dense scintillators or Cherenkov radiators for high resolution electromagnetic calorimeters. The expected interaction rate will be around 10^8/sec at the SSC and up to 2.5 x 10^9/sec at the high luminosity version of the LHC. The differences in calculated radiation dose rates of two orders of magnitude exist between RHIC and SSC, with LHC at the top of the list [1, 2]. But even in the RHIC case, even if a small fraction of the beam is accidentally dumped or scattered into a detector, the damage can be serious. Figure I.1.1 shows the comparison of the calculated fluxes of secondary particles and integrated radiation doses per year for the SSC ($L = 1 \times 10^{33}$ cm^{-2}s^{-1}) and the high luminosity version of the LHC ($L = 4 \times 10^{34}$ cm^{-2}s^{-1}) [3]. The intensity scale factor between these two machines is 27 [1].

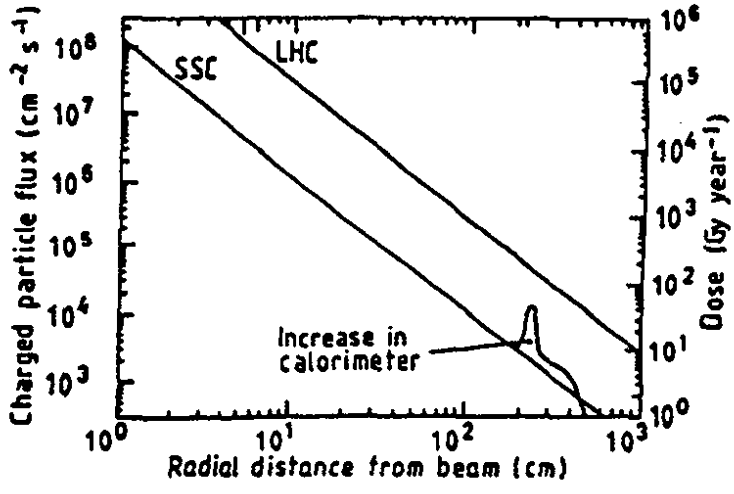

Figure I.1.1: The expected charged particle flux as a function of the radial distance from the interaction point for the SSC and the LHC with the corresponding integrated radiation doses/year due to ionization energy deposit [3]. The energy deposit will locally increase in calorimeters due to the showering process.

Heavy scintillating materials make possible the construction of hermetic detectors without local defects. The main advantage of fully active crystal scintillator electromagnetic calorimeters is their excellent energy resolution, making them the best tools for electron and gamma detection. This was found to be necessary for efficient electron identification at the SSC [4]. The most stringent limit on resolution is set by the requirement to study the 2g decay mode of a light Higgs [5]. In several recent review articles [3, 6, 7, 8] the analysis of possible solutions was performed. First, it was concluded that no candidates for high resolution calorimetry were available presently for the most forward regions due to

radiation damage and insufficient time resolution. The only possible solution to this problem (i.e. placing detectors far away from the interaction region in order to keep a safe radial distance), is impractical due to the sizes and costs involved. Therefore the main effort is focused on finding a solution for the central barrel calorimeter with short forward additions. Lorenz [3] has recently summarized the prospects and limitations for the use of electromagnetic crystal calorimeters in the SSC and LHC experiments. As expected, the result of the analysis was that such calorimeters can only be built in the central region and with a large radius of the central cavity to accomodate track density in space and time, and the total radiation load.

Under a critical review there seem to exist at present only a few proven and many potential candidates for crystal scintillator-based detectors for future high rate applications. Several short review papers discussing the new developments in solid scintillator research were recently published [9, 10, 11] and the reader is referred to these sources for more details than covered in this review. A systematic survey of fluorescence of over 400 inorganic compounds is in progress with a pulsed X-ray beam technique [12].

Table I lists the selected group of scintillating crystal materials. The included collection of data found during literature research in preparation for the present review is not complete, but it is meant to testify to the ongoing vigorous research on new potential candidates for fast, dense and radiation hard scintillators. In cases when discrepancies were encountered between different information sources, such as different values quoted for scintillation yield, emission wavelength, etc., the extreme limits and/or all the options are listed. It is interesting to note that the presently best known scintillation material, CsI(Tl) did not make the list because of its rather poor radiation resistance (but improving, see section I.5) and a long decay time. Even before the high rate high energy physics experiments were planned, in some nuclear physics applications the long luminescence of CsI(Tl) was seen as a major drawback, limiting its use to relatively low counting rate applications. For comparison, BGO, LXe, and scintillating glasses (see section I.7) are included in the table. BGO which is used on a large scale in the L3 detector at CERN, is only marginally acceptable due to its slow response and relatively poor radiation resistance (see section I.7).

Also many other listed crystals fulfill some but not all of the requirements for use at the high intensity SSC and LHC environments; requirements such as:

- fast speed and short decay constants (no tails)
- high light yield
- good energy resolution (yield+uniformity+stability)
- good radiation resistance (survival)
- short radiation length and Moliere radius (compactness)
- mechanical, chemical and thermal stability of operation.

The criteria for the selection of a crystal material include not only the obvious demands for high light output (> 500 photoelectrons/MeV) and short radiation length but also short pulse duration (decay time of under 10 ns) and radiation resistance (better than 1 Mrad and 10^{12} n/cm^2) to cope with instantaneous rates and integral radiation doses,

respectively. Many crystal scintillators have several scintillation components which are usually divided into "fast" and "slow" ones. The basic mode of operation is to use the fast component and to try to desensitize readout to the slow components. A classical example of this technique is barium fluoride, where much effort went into designing photocathodes insensitive to the slow (~600 ns) decay component (see section I.2). The effects of radiation damage in crystal and glass scintillators are primarily due to damage to transmission properties of materials, while damage to intrinsic scintillation yield has not been observed in some cases even up to the doses of 1 GRad (10 MGray).

To illustrate the serious problems encountered one might take a look at cerium. Cerium is an excellent rare-earth scintillator and can be incorporated into a wide range of matrices, but the speed of its emission is only marginally acceptable. The scintillation emission is due to the characteristic fast allowed 5d-4f dipole transition in Ce^{3+} in the region of 300 to 500 nm, depending on the host matrix. Only lattices in which Ce^{3+} ions fit and the formation of Ce^{4+} quenching centra is minimized are suitable for this class of scintillators [9]. Especially interesting are high density matrices. Examples of cerium scintillators are: cerium-doped gadolinium silicate (Gd_2SiO_5), yttrium aluminate ($YAlO_3$), rhenium aluminate ($ReAlO_3$), barium fluoride (BaF_2), and cerium fluoride (CeF_3).

It seems that at the time of writing this review there is one material which satisfies most of the above listed and discussed criteria: barium fluoride. Recently it was preselected as a possible solution for the GEM SSC detector. The planned detector will have a total of about 16,000 crystals. In section I.2 we will discuss properties and applications of this very important crystal scintillator. But even barium fluoride will not survive the radiation doses expected in the very forward regions of the SSC and LHC. A fast detector with liquid scintillator capillaries replacing scintillating fibers is a possible candidate for that region. Other possible candidates except BaF_2 are: CeF_3, cerium doped gadolinium orthosilicate (Gd_2SiO_5:Ce), pure CsI, and lead fluoride (PbF_2), a Cherenkov radiator material, listed in the order of their overall judged applicability.

Depending on the count rate and magnetic field expected in a particular region of a detector, different readout methods are applicable to crystal scintillators. In general, these can be silicon photodiodes, vacuum photodiodes, phototriodes and phototetrodes, and finally higher gain devices such as new type mesh photomultipliers to be used in magnetic fields and at high rates. It was shown, for instance, that the Hamamatsu photomultiplier type 2490 with 16 transmission dynode stages works even at a magnetic field of 1.5 Tesla, and at tilting angles up to 50° still can provide a gain of more than 10^3 [13]. New hybrid photomultipliers with a silicon PIN or APD active "amplifying" element are under development [14-18]. Efforts are also under way to minimize the effect of Cherenkov light produced in the photomultiplier as a result of the passage of particles through the PMT window by working on a special design of a thin glass photocathode support [19]. An example of a large readout system is the CLEO CsI(Tl) electromagnetic calorimeter where crystals are read by silicon photodiodes. This system is too slow for most of the future applications (shaping time of several microseconds), but new versions are being prepared with pure CsI in mind and shaping time in the range of 100 ns (see section I.5).

Table I
List of candidates for fast and radiation hard crystal scintillators

MATERIAL	DECAY Fast Comp. (ns)	FAST EMISSION @ λ (nm)	FAST LIGHT YIELD (BIALKALI PM) %, NaI(Tl) = 100 *(pe/MeV)* (phot./MeV)#	RADIATION LIMIT (Rad)	DECAY Slow Comp (ns).	DENSITY (g/cm^3)	RAD. LENGTH (cm)	MOLIERE RADIUS	NUCL. INT. LEN. (cm)	dE/dX (MeV /cm)	HYGRO-SCOPIC (?)	REFR. INDEX @Peak	ΔL/ΔT @20 C (%/C)
BGO	no fast co.	480	12-13, (8200)	10*7?	300, 60	7.13	1.11	2.2-2.7	22-23	9.2	No	2.19	-1.55
LXe	3, 25	170	(4-7 x10*4)	high	45	3.06	2.77	5.6-5.7	55	3.89	N/A	1.5@ 170nm	
BaF2	< 0.9	195, 220	3-5,*(130-400)* (1800-2500)	>10*7	~600 (see text)	4.88-4.89	2.06	3.39-4.4	29.4-29.9	6.5	Slightly	1.56*	-2.4(slow) -0.6(fast)
CeF3	3-5, 20-30	300-310, 340,375	3-6,*(160)* (4000)	>10*6	*No slow component*	6.16	1.65-1.7	2.63	26.2		Slightly	1.68	+0.08
CeF3:Ca	30	340		>3 x 10*6		6.1	1.				Slighly (?)		
CsI (pure)	~ 10,36	305-320	4-6, *(125-400)* (16800)	>10*4	1000	4.51-4.53	1.86	3.5-3.8	36.4	5.6	Slightly	1.81*	~-1.5
GSO:Ce	30-60	435-450	20	>10*8	600	6.71	1.39	2.42			No	1.9	
CsF	2.8-4.4	(265-335), 390	5-7, (2500)	below 1000	*No slow component*	4.64	2.0				VERY	1.48	
Scint Glass	50-90	430	*(3)*, (100) SCG1-C	10*5		3.36-3.49 SCG1-C	4.12-4.35 SCG1-C	3.9 HED-1	44-45		No	1.60 SCG1-C	
PbF2	Cherenkov radiator	Cherenkov ≥300	*(1.3-1.8)*	>10*4	Cherenkov *No slow c.*	7.77	0.93	2.22-2.24 (1.8)^			No	1.82	
KMgF3	1.5	140-190	(800-3500)			3.16	7.72			5.2			
KLuF4	1.3-1.5	165-200	(170-400)			4.8	2.0						
LaF3:Nd	6.3	173, 216, 245	~5 (200)			5.94					No	1.70 @200nm	
LaF3:Ce (10 mol%)	3, 27 (86%)	290,305, (350)	(880-2200)		185 (4%)	>5.9						1.70	
LiYF4:Nd (0.9 mol%)	40	184, 230, 260	(~200@184nm)										
YAlO3:Ce	17-35	350-390	30-40, (17000-19700)	10*8	246 (2%?)	5.35-5.55	2.63	2.82			No	1.94	
ThF4	≤25	315,330, 450		high?		6.32	1.18	2.71					
BaYb2F8	Cherenkov radiator	Cherenkov (>310 nm)		~10*7	Cherenkov *No slow c.*	6.99	1.3	2.4					

* for fast component

photons emitted/MeV @20°C, unless otherwis specified.

^ apparent Moliere radius in PbF_2 due to insensitivity to slow electrons (see text).

Table I - cont.
List of candidates for fast and radiation hard crystal scintillators

MATERIAL	DECAY Fast Comp. (ns)	FAST EMISSION @ λ (nm)	FAST LIGHT YIELD (BIALKALI PM) %, NaI(Tl) = 100 *(pe/MeV)* (phot./MeV)	RADIATION LIMIT (Rad)	DECAY Slow Comp (ns).	DENSITY (g/cm^3)	RAD. LENGTH (cm)	MOLIERE RADIUS	NUCL. INT. LEN. (cm)	dE/dX (MeV /cm)	HYGRO-SCOPIC (?)	REFR. INDEX @Peak	ΔL/ΔT @20 C (%/C)
LiYbF4	≤25	400-500	(~BaF2)	high?		6.09	1.56	2.70					
BaLiF3	<1 (UV), <25 (vis.)	228,252, 435-440	(~BaF2 in UV)			5.24	2.13	3.13					
LiBaF3	1.9	203,234	~3,(900 - ~BaF2)			4.9	2.3						
KYF4:Rb	1.9	140-190	(~BaF2)			3.6							
K2YF5			(~BaF2@ 80°K)			~2							
RbF	1.3	203, 234, *380*	(→~BaF2)		*No slow component*	3.6					yes		
CsCl	.88	240, 270	(900-~BaF2 @ 80°K)		>500 @390nm	4.0					no		
CsBr	0.07 (!)	250	(20)		>500 @390 nm	4.4					no		
CsBr	1.34±0.05 @80°K	250	(~BaF2@ 80°K)			4.4					no		
RbCaF3	~1		(~BaF2)			2.83							
KCaCl3	~1@ 80°K		(~BaF2@ 80°K)										
KCaF3	<2	140-190	(~BaF2)			3.0							
CsCaCl3	<1	250, 305	(est. 5000)			2.9							
CsSrCl3	~1		(~BaF2)										
LSO:Ce	~40	420	75			7.4	1.14						
CdI2	3	540	10	~10*7		5.67	1.5	3					
Y3Al5O12: Ce (0.4 mol%)	65	550	(14000)			4.56	3.5	3.2					
BaCl2	1.2, 3.5		(25000)		58, ~μs?	3.9							
CeCl3	4.4, 23		(28500)		70, ~μs?	3.9							
BaI2	6	190-340			2500 @450nm	5.15					no, but air unstable		

A special class of crystal scintillator detectors are active preshower detectors. The crystal converter such as BaF_2 can be read out for instance by a multistep chamber photodetector with a solid CsI or CsI/TMAE photocathode (see subsection I.2.2). Good shower position resolution may give the measurement of the photon angles necessary to guarantee good Higgs mass resolution.

We will procede now with the detailed reviews of the five selected crystal materials: barium fluoride, cerium fluoride, cerium doped gadolinium orthosilicate, pure cesium iodide, and lead fluoride (Cherenkov radiator). This will be followed by a brief discussion of some other materials, such as CsF, $LaF_3:Nd^{3+}$, $KMgF_3$, BGO, and other.

I.2. Barium Fluoride (BaF_2)

At present two fluoride crystals are considered as the main potential candidates for a fast and radiation hard electromagnetic calorimeter: barium fluoride (BaF_2) for SSC and cerium fluoride (CeF_3) for LHC. Generally fluoride crystals have high chemical stability and compact crystal lattice and are good candidates for the formation of compact and radiation hard scintillating crystals.

I.2.1. Properties of Barium Fluoride

Barium fluoride seems to be at this moment (end of '91) "the material of choice", considering speed of operation and radiation resistance. Much experience in producing good quality crystals was gained in the past due to the construction of three large-size crystal systems for nuclear physics applications [20-22]. Recently barium fluoride was selected as one of the leading options for the SSC - GEM electromagnetic calorimeter [23-25].

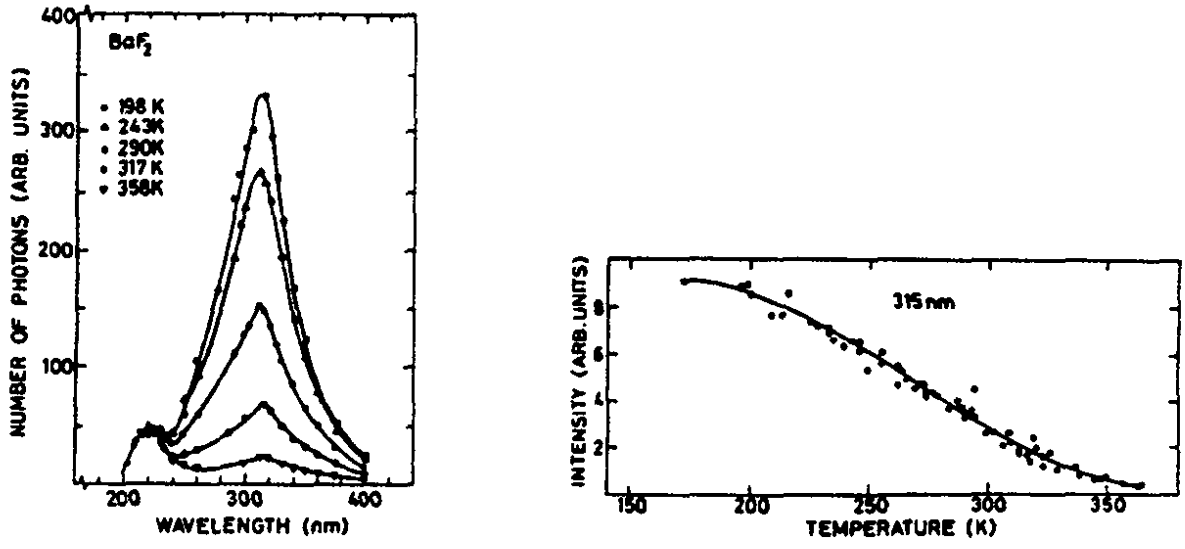

Figure I.2.1: Scintillation emission spectra of BaF_2 at different temperatures, measured under 35 keV X-ray irradiation (left), and scintillation intensity of the 315 nm emission peak as a function of temperature (right)[26].

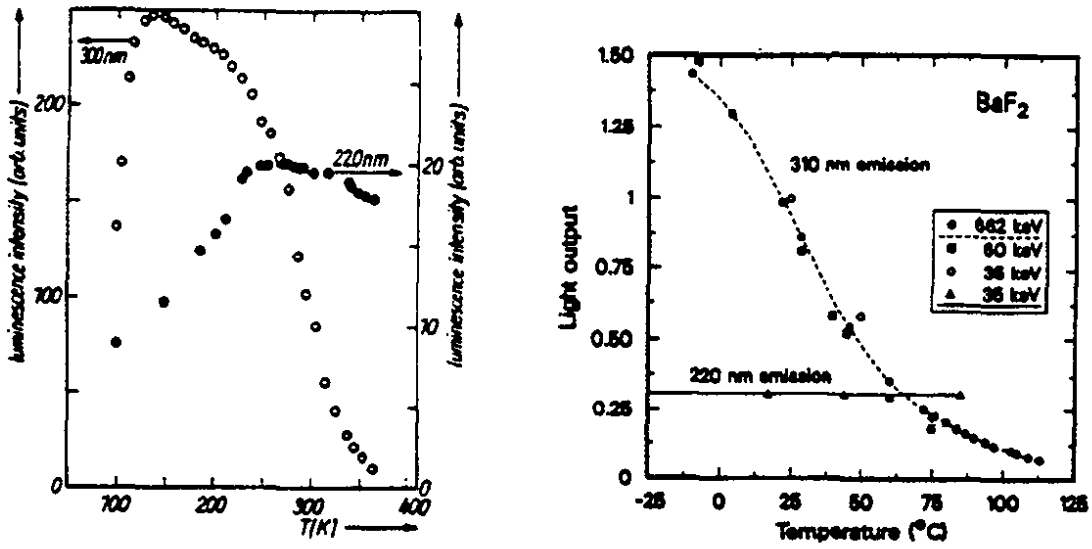

Figure I.2.2: Temperature dependence of the fast and slow emissions of barium fluoride [28] (left) and [30] (right).

Its fast subnanosecond decay component makes barium fluoride operable at high rates, and it was shown to be one of the most radiation hard scintillators, despite the fact that the effects of radiation damage on the performance of long modules were still not evaluated to satisfaction. Another big advantage of barium fluoride is that the intensity of the fast component is independent of temperature, while the intensity of the slow component decreases with increasing temperature [26-30] as shown in figures I.2.1 and I.2.2. This property of BaF_2 was actually exploited in order to yield a better gamma-ray energy resolution by cooling a BaF_2 crystal to 243 °K [31].

For applications in the precision crystal calorimetry, however, barium fluoride has at least two drawbacks: (1) a rather long radiation length and large Moliere radius, and (2) a small ratio of hadronic absorption length to radiation length making e/hadron separation difficult. Other disadvantages of BaF_2 include its mechanical fragility (it cleaves easily), and difficulty in detecting the short UV light component. It is also rather expensive. This is further compounded by a slight hygroscopic nature of BaF_2 which was found to affect the light yield [32-34]. After repolishing, the crystals regain their transmission and light yield. Taking all this into consideration, a vigorous research was initiated, especially in Europe, to identify a possible replacement for BaF_2, such as CeF_3 or other new materials [8]. But as of today, barium fluoride is a unique high density (4.88 g/cm^3) scintillator with subnanosecond timing properties (110-160 ps FWHM) [35-39] with three emission spectra with peaks at 195 and 220 (fast component) and 310 nm (slow component) [28, 40, 41]. The fast components have fast decay time constants measured to be 0.6-0.79 ns [35] and 0.85-0.88ns [40-43] (figure I.2.3) and the slow component was measured in the range of 100-1000 ns.

The fast emission in BaF_2 was explained to be due to a so-called "radiative core-valence transition" or "cross-over transition" following the direct electron-hole recombination [40, 43-46]. The same phenomenon also occurs in CsF. A different mechanism of self-trapped

hole centers was proposed for the slow component. Figure I.2.4 [11] shows a model used to describe fast scintillation components in barium fluoride. A core electron transition to the conduction band is immediately followed by an associated valence electron transition to the core hole.

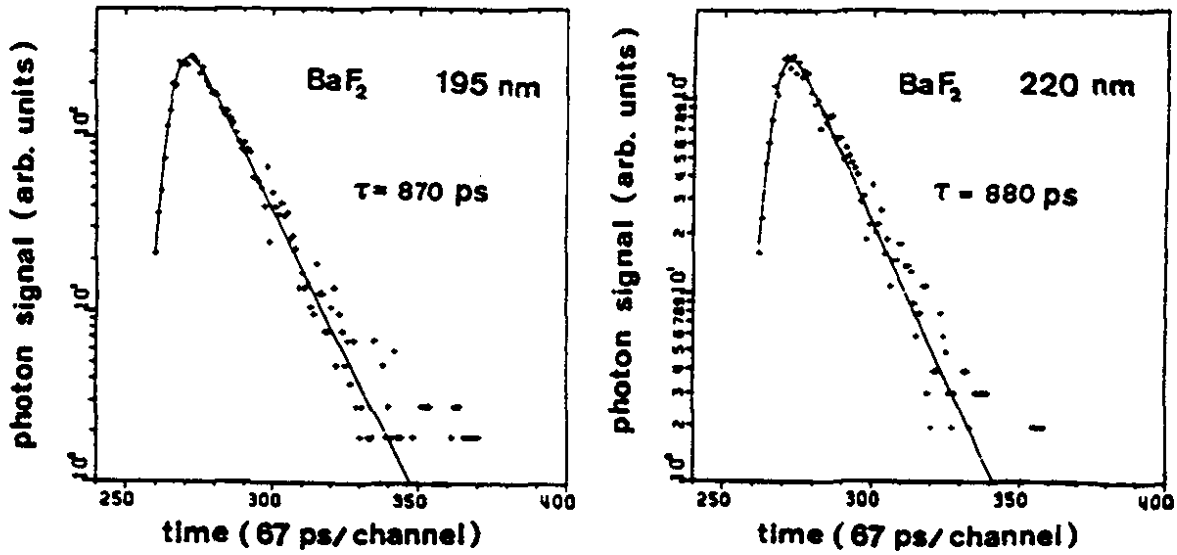

Figure I.2.3: Decay of the 195 nm and 220 nm scintillation light components of BaF_2 [41].

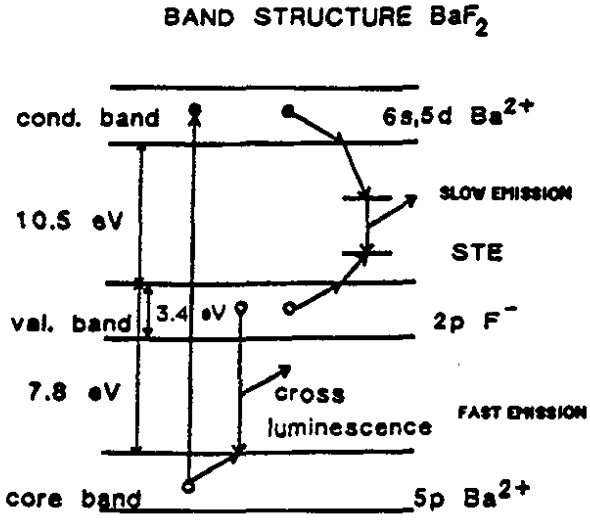

Figure I.2.4: The band structure of BaF_2 and the scintillation mechanisms [11].

Different values of slow decay constants were obtained in different studies. In the original paper describing the discovery of the fast component [35] two components with 430 ns and 620 ns decay times were found for excitation with ^{137}Cs gamma-rays. In a different study with electron excitation the 310 nm component was measured to have two lifetimes of 600 ns (main component) and 100 ns [40]. In yet another study two slow decay

components were identified with decay times of 730±60 ns (80%) and 240±30 ns (20%) [47]. The weighted average is 630 ns which is in good agreement with previous results. In a recent high statistics measurement two slow components of BaF_2 emission were identified with 340 ns and 920 ns decay constants [30] (figure I.2.5).

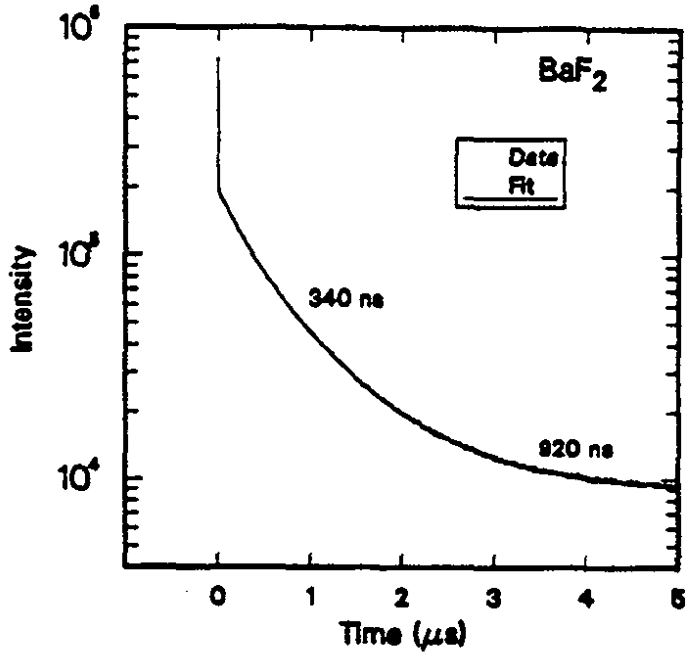

Figure I.2.5: Single-photon measurement of the scintillation decay of BaF_2 showing the fast and two slow components of 340 ns and 920 ns [30].

Table II lists intensities of the fast emission component and of the total light intensity obtained in different studies with bialkali PMTs, a solar-blind Cs-Te PMT and a TMAE gas photodetector. The measured photoelectron signal depends on many factors, such as the way crystal surface is treated, the wrapping material, the type of PMT photocathode, and how a crystal is coupled to a PMT. Also, the fast/slow photon ratio depends on particle type and is about 0.2-0.3 for gamma-rays and electrons. For alpha particle excitation the fast component is scarcely observed [40].

The importance of surface treatment, particularly polishing, on the amount of fast scintillation detected was reported in several studies [32, 33, 48, 55-57]. Other studies stressed the importance of reflector around crystals [33, 38, 56, 58, 59]. The best results were obtained with the teflon film. Teflon film, however, becomes semitransparent in contact with leaking coupling grease from the junction of the crystal and the PMT window. Silicon rubber gaskets were reportedly used to seal in the leakage [38]. Also, standard teflon is known to be radiation soft when irradiated in air, and further studies are needed to confirm its applicability to the high total dose environment. A new radiation-hard teflon wrapping made of interlocking meshes of silicone rubber and PTFE was proposed [25]. Also, optical coupling is sensitive to pressure [60]. Using TFE teflon UV reflector and a 50%/50% mixture of RTV and Viscasil silicon oil produced best results in a PET detector [61]. RTV

silicone rubber such as type KE103 was recently shown to be radiation resistant up to a dose of 10^7 Rad throughout the 200-600 nm transmission region and, therefore, can be used in gluing BaF_2 [62]. It was shown that the reflectivity of CaF_2 powder was not much inferior to that of a teflon tape in a canned BaF_2 crystal [56].

Table II
Photoelectron yield of BaF_2 for gamma-rays/electrons.

Fast (pe/MeV)	Total (pe/MeV)	Reference	Comments
385	1850	35	4 cm x 2.4 cm dia.
157	1370	48	1 cmx 1 cmx 4.5 cm
158	1124	49	2.5 cm x 2.5 cm dia.
145		50	6 mm x 22 mm dia.
403	2518	51	2 cm x 3 cm dia.
380	1430	52	0.5 cm x 4 cm dia.
445	2672	23	av. for 3 small cryst.
55-65♦	675-825♦	53	2 cm x 2 cm x 5 cm
80-200#	400-900#	33	2.5 cm x 2.5 cm dia.
60-80*	115-140*	23,33	2.5 cm x 2.5 cm dia.
50-60*		23	25 cm long crystals
19.2$		54	5 cm x 5 cm dia.
26.7$		53	2 cm x 2 cm x 5 cm

♦ Measured with no optical contact compound.
Measured with a Dow Corning 200 fluid and for different wrappings.
* Measured with a Hamamatsu R3197 Cs-Te solar-blind PMT and an air gap.
$ Measured with a TMAE gas photocathode

It was found that for a homogeneous response from long crystals, compensating surface treatment of the crystals might be required [63]. A combination of partial wrapping with teflon tape with an air gap coupling to a PMT with a Cs-Te solar-blind photocathode was found to secure uniform (within 1-2%) response of 25 cm long crystals tested for use in electromagnetic calorimeters [60, 64]. In the same study it was also shown that ray-tracing Monte Carlo simulations can well reproduce the observed behaviour. Uncorrected for pulse height variation, a time resolution of about 160 ps (rms) was obtained for minimum ionizing muons in the same study (energy deposit of about 20 MeV). However, it has to be demonstrated that the optical conditions will not change with time. Using simple aluminum wrapping a uniformity of ~2% was obtained in a 25 cm long crystal [23, 24] (figure I.2.6).

I.2.2. Photodetectors

Quartz window photomultipliers must be used to detect the fast component of BaF_2 light. One should comment that it is not only the quantum efficiency of the PMT used that is important, but also the collection efficiency of the fast photoelectrons originated from UV photons. Strong differences of up to a factor 3 were found in the collection efficiency of fast photoelectrons for two types of photomultipliers [36]. These effects are also well known in Cherenkov counters. A Monte Carlo study of the timing resolution of BaF_2 counters predicts that transit time spread of the photomultiplier plays a very important role,

especially for crystal lengths below 4 cm [65]. Also, care must be taken when coupling a crystal to a PMT by choosing an appropriate coupling grease transmitting well below 200 nm and the layer must be made as thin as possible in order to minimize absorption of the fast component [37, 52]. It was found that a 12.5 micron layer of a selected grease had good transmittance [29].

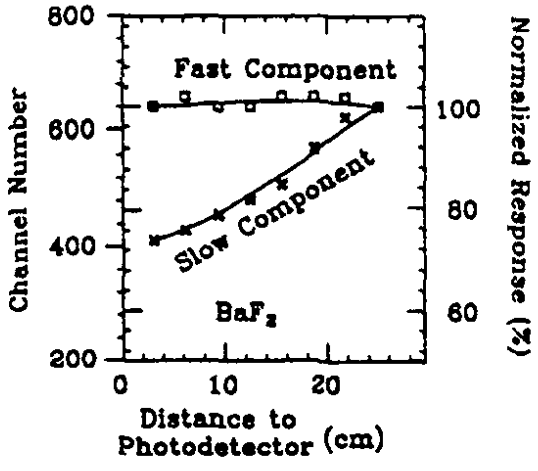

Figure I.2.6: The longitudinal light collection response of BaF_2 crystals measured with a collimated ^{137}Cs source for aluminum wrapping [23, 24].

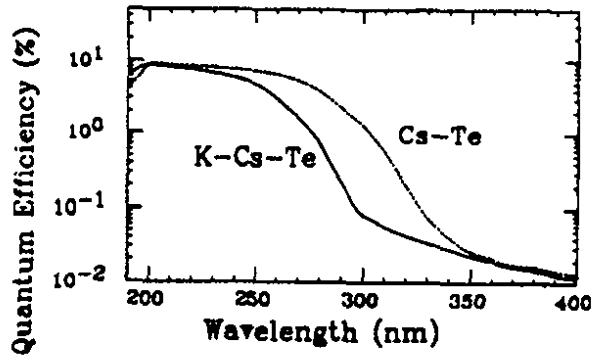

Figure I.2.7: Quantum efficiency of a new K-Cs-Te photocathode as compared to a Cs-Te photocathode [23, 24].

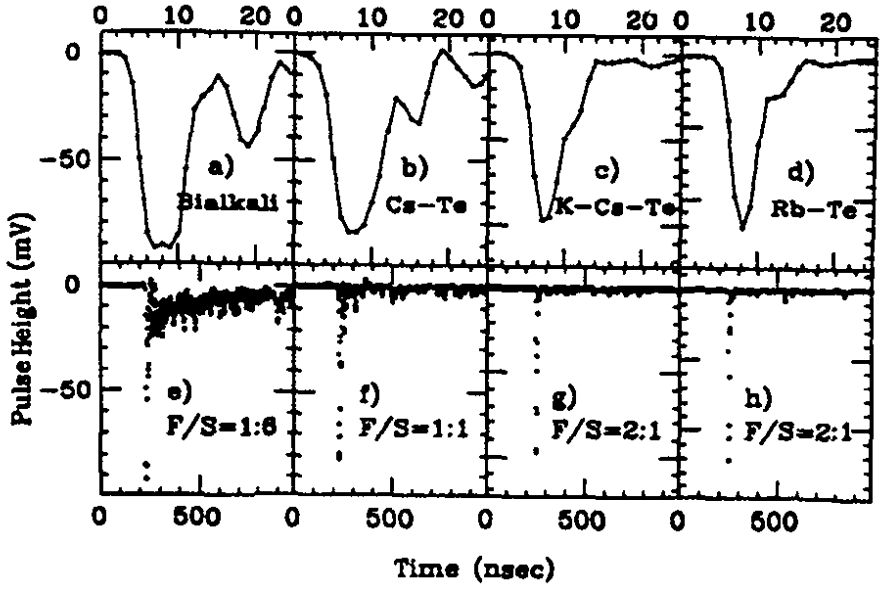

Figure I.2.8: Scintillation light pulses and ratios of fast to slow components from pure barium fluoride crystal observed using PMTs with bialkali, Cs-Te, K-Cs-Te and Rb-Te photocathodes [25].

It is an obvious idea to limit the response of a photomultiplier, or photodetector in general, to a fast component of barium fluoride light by a proper choice of a solar blind photocathode. Already in one of the first papers following the discovery of the fast

component in BaF_2 it was suggested to use photomultipliers with a Cs-Te photocathode[36]. Several types of solar blind photocathodes were tried, such as Cs-Te [29, 36], Rb-Te and K-Cs-Te, with the best result obtained for the latter photocathode [25, 33]. Figure I.2.7 shows quantum efficiency curves for Cs-Te and K-Cs-Te photocathodes. Examples of scintillation light pulses from barium fluoride crystals observed with four PMTs with different photocathodes are shown in figure I.2.8 [25]. The Cs-Te photocathode improves the fast/slow ratio by a factor of 6 (from a ratio of 1:6 to about 1:1), and a further improvement by a factor of 2 is obtained by using a K-Cs-Te or Rb-Te photocathode.

Another method is to couple barium fluoride to an ultraviolet sensitive gas chamber [66]. Figure I.2.9 shows an overlay of the fast BaF_2 emission spectrum with a quantum efficiency curve of tetrakis(dimethylamine)ethylene (TMAE) vapors [41, 53]. The average quantum efficiency of TMAE for the fast component was measured as 7.6 % ± 0.7% [53]. Many different small-size detectors were built with TMAE gas vapor used as a photocathode. However, characteristic to this solution is a lack of necessary operational stability of gas detectors additionally compounded by the severe ageing of TMAE. TMAE is unstable in air, corrosive and poisonous and therefore requires complicated purification and handling. Another solution for a gas photocathode is a more stable triethylamine (TEA), but its overlap with BaF_2 emission is poor. In recent studies [67] more stable photocathodes made of ethyl ferrocene and decamethylferrocene were shown to be matching well the fast component of BaF_2 scintillation light. However, the quantum efficiency of the produced photocathodes was too low for most applications (about 0.3%).

High quantum efficiency of 35% @190 nm was obtained for a CsI photocathode coupled to a gas chamber filled with methane [68]. The obtained detector is relatively efficient and fast. Potentially the most severe problem in these devices is the stability of the photocathode [69], especially under ion bombardment which gradually destroys it [70-72]. Also, ageing of the detector due to radiation induced chemical reactions can potentially seriously limit its application at high rates. To exploit the fast timing property of BaF_2, parallel-plate multistep structures are optimal. These however are unstable, prone to breakdown and to photon feedback at the photocathode [73].

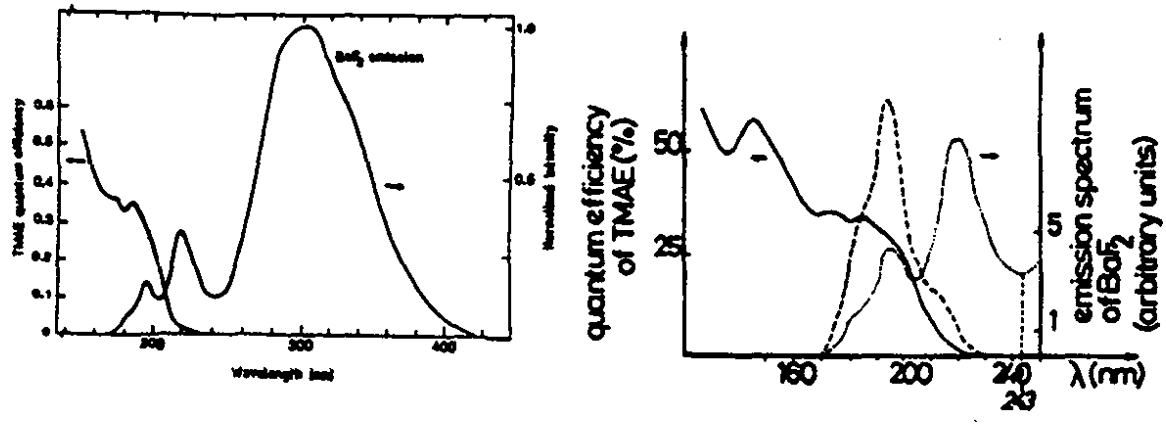

Figure I.2.9: Left: Emission of barium fluoride and quantum efficiency of TMAE vapors [41]. Right: Fast emission of barium fluoride (dotted line), overlayed with quantum efficiency of TMAE vapors (full line) and the product of the two (broken line) [53].

The best selective photocathode known at present is the reflective photocathode of CsI with adsorbed layer of TMAE [68, 75] (figure I.2.10). A comparison of the photoelectron yield for an infinite TMAE gas layer and a CsI-TMAE photocathode is also shown [74]. Again, a serious question is a stability and ageing of such a photocathode in actual experimental conditions, including effects of gas impurities and ion production [72, 75].

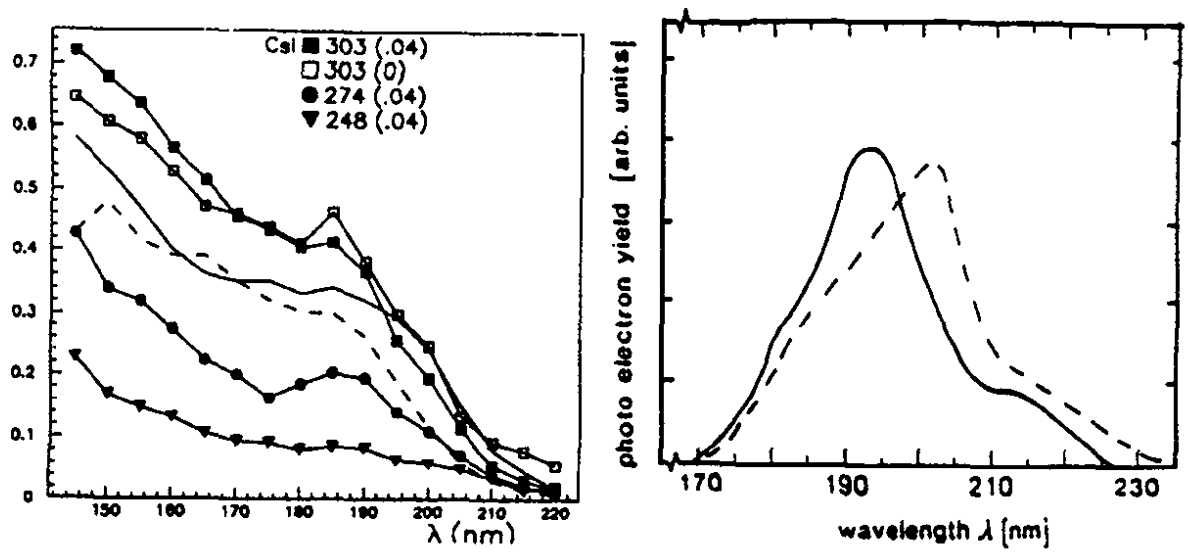

Figure I.2.10: Left: Quantum yield versus photon wavelength of the 500 nm thick CsI photocathode with solid, liquid, or adsorbed film layers of TMAE. For each curve the photocathode temperature is given in °K and TMAE partial pressure in Torr (in brackets); the solid line is for the TMAE gas, and the dashed line is for pure CsI [68]. Right: Comparison of the photoelectron yield for a TMAE gas photocathode (solid line, an infinite absorption thickness is assumed [41]) and for a surface CsI-TMAE photocathode (dashed line) [74].

A possible application for the gas-filled photodetectors in connection with barium fluoride is in the preshower counters where superior position resolution can be obtained [76]. Figure I.2.11 shows a design of the proposed preshower detector with a pad photocathode array coupled to a parallel plate avalanche chamber (PPAC) electron amplifier [76].

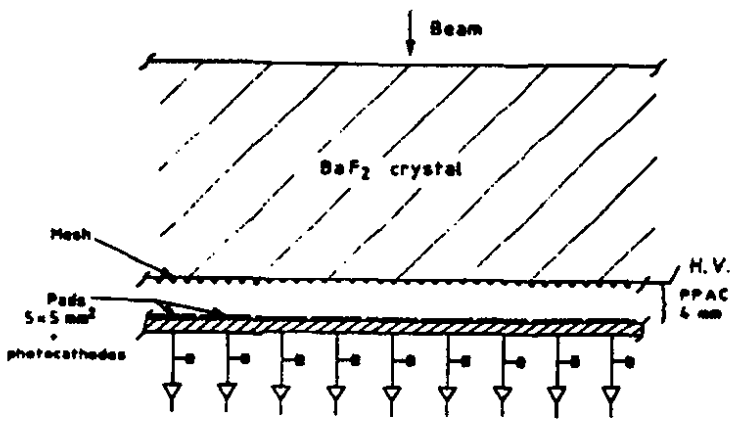

Figure I.2.11: Design of the BaF_2 preshower counter [76].

Several waveshifters, such as p-therphenyl (PT) and p-p' diphenylstilbene (DPS) were tried in an effort to avoid the necessity of using quartz window photomultipliers by converting BaF_2 light to a longer, typically blue, spectral region [77-79]. The time resolution was degraded by a factor of 2 [77, 78] associated with slowing down of the rise time caused by the radiative energy transfer from the BaF_2 to a waveshifter. Decay time constant of the fast component increased from 0.6 ns to 2.5 ns with p-terphenyl [78]. In one of the studies with a newly rediscovered waveshifter material DPS [80] an improvement in energy resolution was obtained as compared to direct light detection [79]. This was explained by the layer of shifter working as an additional diffuser of light.

The disadvantage of the waveshifting technique is that both fast and slow components are mixed together and no separation on the basis of their different emission spectra is possible. In one study [81] a prototype barium fluoride calorimeter was tested with silicon photodiode readout. Waveshifter plates were used to collect and guide BaF_2 light to the photodiodes. However, due to the spectral response of the waveshifter used (BBQ), both fast and slow components were converted and the time response was slow, characteristic of the slow component of BaF_2 emission. No efficient waveshifter selectively sensitive only to the fast component was developed until now. New UV-sensitive silicon photodiodes optimized at 220 nm (Q.E. >50%) enable direct readout of the fast component, they cannot however discriminate against the slow component. A solution to this problem might be to use narrow band interference filters with transmission peaking in the 190-210 nm region. Such a filter could be in principle incorporated in the photodiode entrance quartz window.

I.2.3. Doped Barium Fluoride

A disadvantage of barium fluoride is that the fast scintillation component is in the short UV region and expensive PMTs with quartz windows must be used. Also handling of crystals and selection of materials in optical contact with crystals is more delicate at these short wavelengths. It would be very advantageous if a shift to longer wavelengths were achieved without seriously compromising speed and radiation resistance of pure crystals. Doping of BaF_2 crystals was done not only to shift emission to longer wavelengths to enable the use of glass window photomultipliers, but also in order to suppress the slow emission component. In order to shift light emission to longer wavelengths, BaF_2 was doped with a few tenths of a mole% of Ce^{3+}, typically 0.2-0.5 mol%. Studies were performed in a wide range of concentrations from 0.002 mol% to 30 mol% [30, 82-87]. Doping leads to a change in both transmission properties and emission properties of the material (figure I.2.12 [86]). Slow and fast scintillation components of pure BaF_2 crystal disappear completely. New emissions due to 5d-4f transitions in Ce^{3+} ions appear above 300 nm. New time components are rather long and equal to 35 (97) ns and 210 (469) ns at 0.2 (0.5) mol% doping level. Figure I.2.13 shows the decay time spectrum of a 30 mm x 30 mm x 4.5 mm BaF_2 crystal doped with 0.5 mol% Ce^{3+} [86].

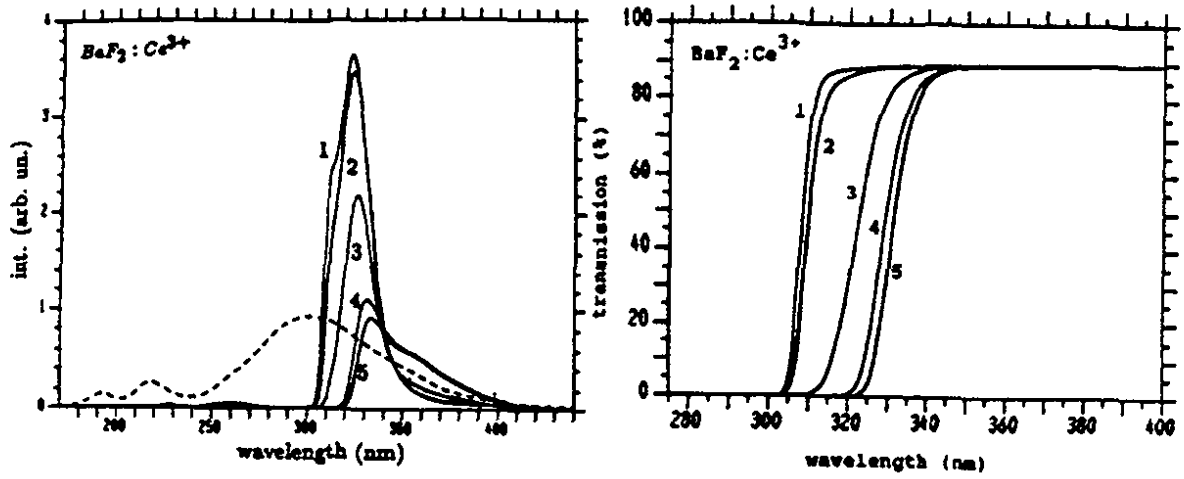

Figure I.2.12: X-ray induced emission spectra (left) and transmission curves of Ce doped 1" dia. x 1" BaF_2 crystals. Spectrum 1: 0.2 mol% Ce; 2: 0.3 mol%; 3: 0.5 mol%; 4: 0.8 mol%; 5: 1.0 mol% [86]. The dashed emission curve shows the emission spectrum of a pure BaF_2 1" dia. x 1" crystal.

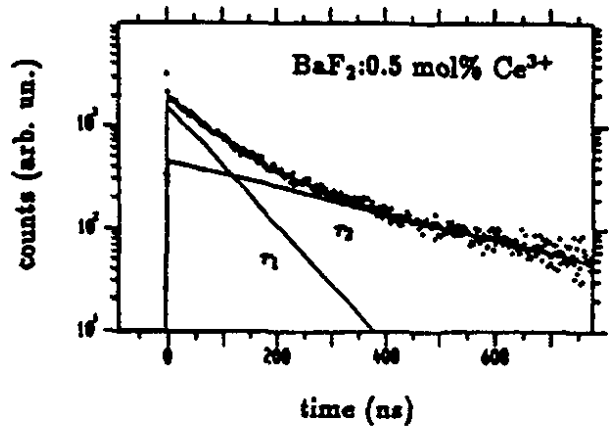

Figure I.2.13: Decay time spectrum of a BaF_2 crystal doped with 0.5 mol% cerium [86]. The decay time spectrum was fitted with two slow components: $\tau_1 = 75 \pm 4$ ns and $\tau_2 = 340 \pm 40$ ns.

The ratio of the relative intensities of the shorter to longer components is changing by almost a factor of 9 in the above range of doping levels, from 0.33 at 0.2 mol% to 2.8 at 1.0 mol%. This implies that even at 0.2 mol% the decay time is dominated by a decay component with a 210 ns decay constant. There is also a very slow emission with a decay time of about 0.2 ms. This component achieves maximum for Ce^{3+} concentrations of about 0.2 mol% and disappears for Ce^{3+} concentrations larger than 1 mol%. The photoelectron yields of doped crystals have values between those reported for BGO crystals and pure BaF_2 crystals and show a maximum for Ce^{3+} concentration near 0.2 mol% [87] (figure I.2.14).

Light intensity of cerium doped barium fluoride is a slowly changing function of temperature depending on doping level [87]. For a 4.4 mol% cerium concentration the intensity drops only by 50% between room temperature and 200 °C [30, 83].

Summarizing, cerium-doped BaF_2 is not a suitable material for very high intensity applications.

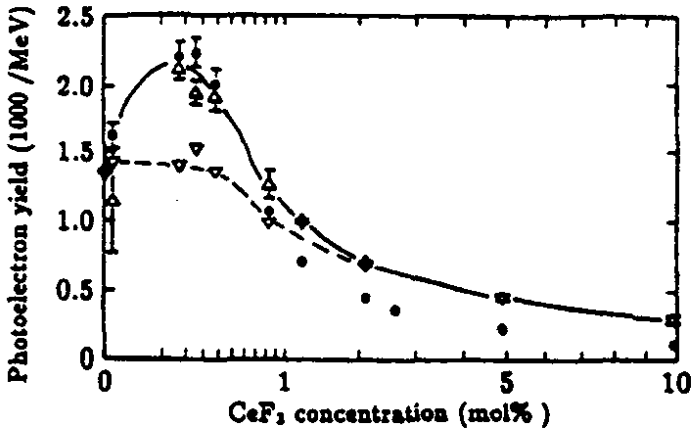

Figure I.2.14: Photoelectron yields/MeV of gamma energy and the relative X-ray induced light yield of pure and Ce^{3+} doped BaF_2 [87]. Δ: total photoelectron yield/MeV, ∇: photoelectron yield created within 4 μs after absorption of a gamma-ray, •: X-ray induced light yield, in arbitrary units. The concentration was plotted on a square root scale.

An interesting technique devised to suppress the slow component of barium fluoride is by doping it with lanthanum, La^{3+} [47, 84, 88, 89]. Figure I.2.15 shows changes to emission spectrum [88] and intensity of the fast and the slow components with increasing lanthanum concentration [89].

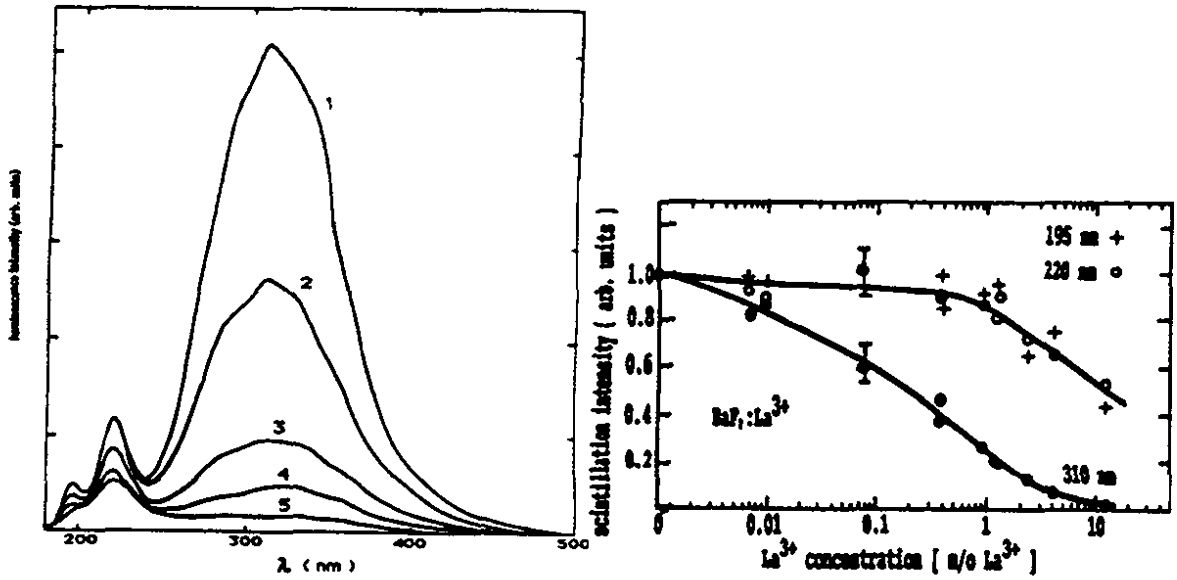

Figure I.2.15: Left: X-ray excited luminescence spectra at room temperature of La-doped BaF_2 [88]. Curve 1: pure BaF_2, curve 2: 0.9 mol% La^{3+}, curve 3: 2.37 mol%, curve 4: 4.2 mol%, curve 5: 13.3 mol% La^{3+}. Right: intensity of the fast and slow scintillation components of La-doped BaF_2 excited with X-rays as a function of the La^{3+} concentration, normalized at zero concentration [89].

The effect of La doping on the fast scintillation components is much smaller than that on the slow component. A suppression factor of 6 was obtained for the slow component by doping BaF_2 crystal with 1% lanthanum, accompanied by only a 10% reduction in the fast component intensity [89]. The average decay time of the slow component decreases with increasing La^{3+} concentration (figure I.2.16). As an example, the decay time spectrum of a crystal doped with 2.37 mol% La^{3+} is shown [88]. The suppression effect was attributed to the presence of interstitial F ions causing quenching of the slow luminescence by dissociation of self-trapped excitons. The inclusion of an additional quenching mechanism is consistent with the observed weaker temperature dependence for the lanthanum-doped samples [84]. This implies that heating is less effective in suppressing the slow component in the doped material.The radiation hardness of the small lanthanum-doped BaF_2 samples was found not to be affected significantly up to at least 1MRad [84].

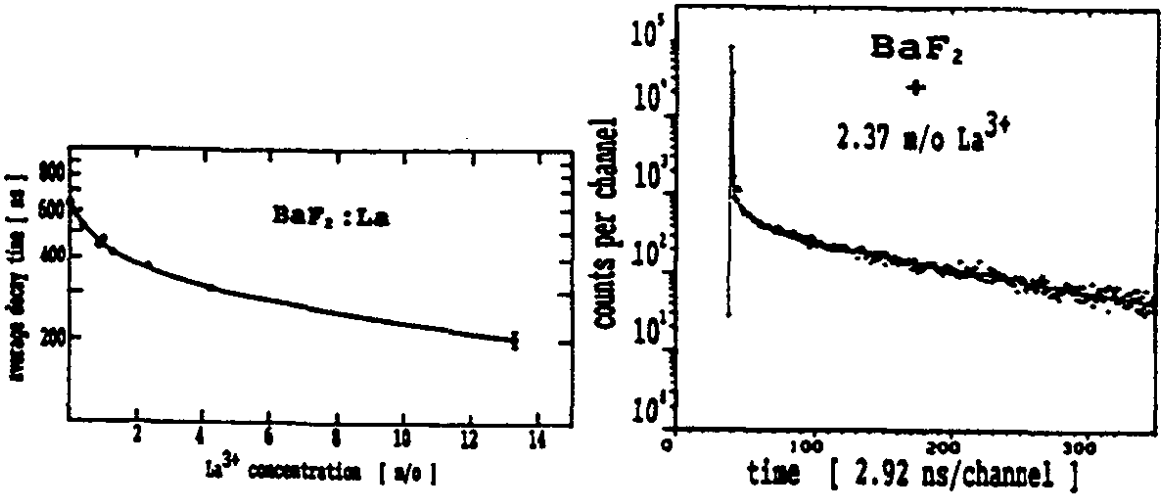

Figure I.2.16: Left: average decay time of the slow component of BaF_2:$La3^+$ as a function of the $La3^+$ concentration [89]. Right: decay time spectrum for the luminescence of BaF_2 doped with 2.37 mol% $La3^+$ [88].

However, this method is only partially succesful, and studies to find an appropriate dopant to obtain more significant improvement in the fast/slow ratio were proposed [90]. Doping with trace amounts of transition or post-transition metal ions was proposed.

The suppression of the slow component might be achieved by a combination of doping with lanthanum and the use of a solar blind photocathode. A combination of Cs-Te photocathode and La-doping was shown to decrease the ratio fast/slow to 5:1 [33]. Figure I.2.17 shows emission spectra of pure and lanthanum-doped BaF_2 and quantum efficiencies of a regular bialkali and a Cs-Te photocathodes.

Attempts to exploit the fast barium fluoride component went beyond using pure or doped crystals. A PMMA plastic scintillator doped with barium fluoride powder (70-86% by weight) was developed and its properties studied [91-94]. Its operation is based again on the principle of waveshifting of the barium fluoride emission by dopants/dyes, but this time dissolved in the mixture of barium fluoride and plastic. The emission spectrum is

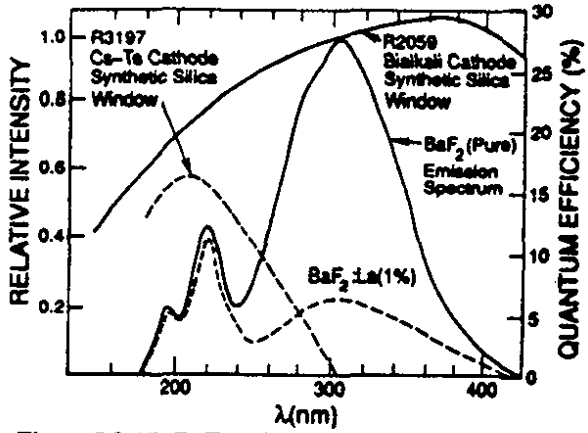

Figure I.2.17: BaF_2 scintillation spectra and PMT quantum efficiencies [33].

conveniently peaked at 410 nm, however the decay constant is a mixture of the fast and slow BaF_2 components which cannot be separated anymore on the basis of their different emission wavelengths after conversion.The new material has been shown to have a capability of particle identification based on pulse shape discrimination (fast component vs. total, see also subsection 1.2.5).
Neutron elastic scattering on hydrogen contained in the plastic was exploited as an additional mechanism for neutron detection [93, 94]. An excellent pulse shape discrimination between neutrons and gamma-rays has been obtained. The disadvantages, however, include high sensitivity to gamma-rays and poor energy resolution.

1.2.4. Radiation Resistance

The first general comment that can be made regarding the radiation resistance of barium fluoride and of many other scintillators is that the intrinsic scintillation process (light yield) does not appear to be affected even after subjection to multi-megarad radiation doses. This conclusion has been reached on the basis of experimental results. The main difference between scintillators is at the level of damage to transmission, due to the formation of color centers, as well as surface damage.

It was already known for some time that UV windows made of BaF_2 were extremely radiation hard when irradiated with 1-2 MeV electrons [95]. Subsequent studies performed with good quality (high purity) small samples [24, 33, 50, 55, 76, 96-98] have confirmed that BaF_2 is one of the most radiation resistant solid scintillator materials. No change in scintillation yield was seen in a small crystal irradiated to a dose of 13 MRad with 800 GeV/c protons [50]. Figure I.2.18 shows examples of the two apparently highest radiation doses delivered to BaF_2 samples. A 5 cm sample irradiated to 170 Mrads has shown a 50% loss in transmission due to acquired blue discoloration [76]. No effect on scintillation was observed at a lower dose of 50 Mrad.

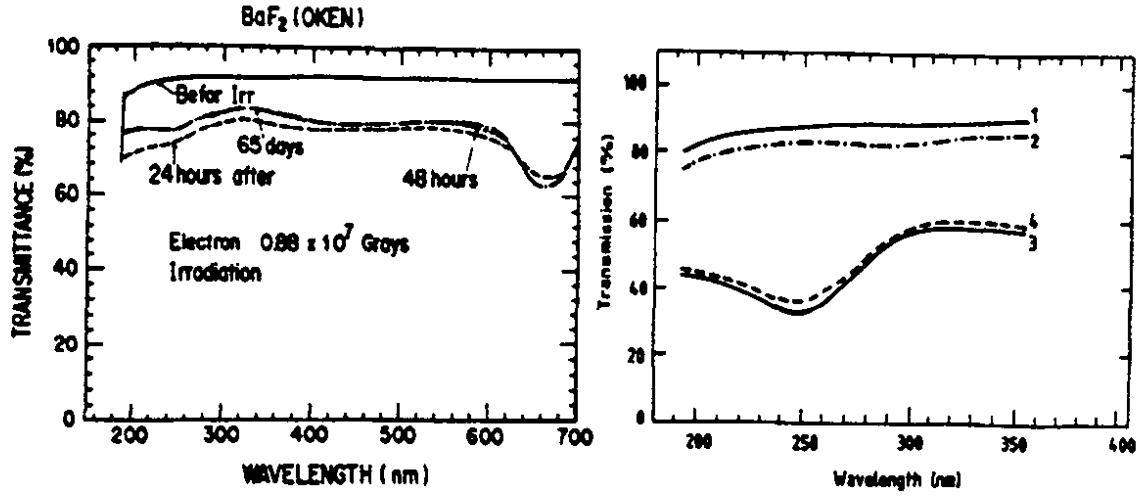

Figure I.2.18 Transmission of two crystals before and after irradiations and during recovery. A 1 mm thick sample at the left [96] was irradiated to 88 Mrad with 2 MeV electrons. A transmission of a 5 cm sample at right [76]: before irradiation: 1; after 50 Mrad: 2; after 170 Mrad: 3; after three weeks recovery: 4.

On the other hand, not surprisingly, the crystals of a lesser quality were observed to be much more susceptible to radiation damage [24, 33, 34, 96, 99, 100]. The common underlying source of post-irradiation effects might be the presence of impurities or defects inside the crystal. It was suggested that radiation damage in BaF_2 is not caused by intrinsic color centers in the bulk material, but rather by externally introduced impurities [24, 34]. The observed saturation of radiation damage in the case of gamma-rays and neutrons supports this suggestion [101], but is not the only possible explanation. Figure I.2.19 [57] shows almost no change in transmission up to a gamma dose of 10^4 Rad, and a saturation in radiation-induced absorption at a dose of 10^6 Rad. Small BaF_2 samples were irradiated up to a dose of ~620 MRad, and no change of the intensity in the fast component was detected. The samples were irradiated in sealed glass containers to avoid the effects of moisture. A very efficient and almost complete recovery of both transmission and scintillation output was stimulated by exposure to UV light from a mercury lamp. This result indicates that no permanent damage was produced in these crystals by irradiation. After a dose of 50 MRad the absorption length is still relatively long (~25 cm).

Defects and observed increased damage in the surface region due to surface treatment and/or water/oxygen absorption are also being investigated as possible contributing factors. The key issue is if large size crystals with low enough levels of impurities can be produced. Research both on chemical and other methods of material impurity analysis is currently underway, as well as investigations of the possible mechanisms responsible for color center formation [25, 33, 101]. For example, the absorption dip around 285 nm in transmittance of some 25 cm long crystals is attributed to cesium contamination. Another impurity identified to cause color center formation in BaF_2 is lead, manifesting itself in an

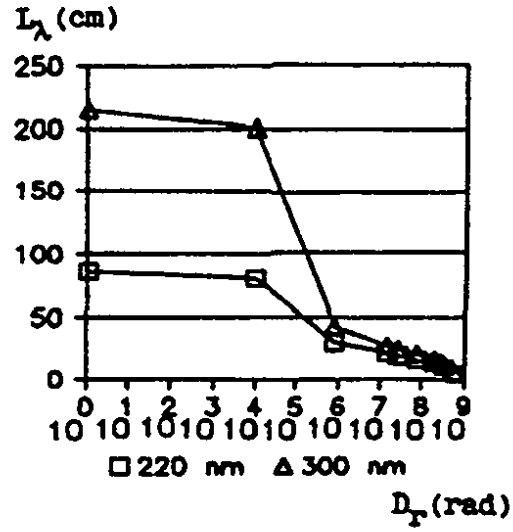

Figure I.2.19: The dependence of the attenuation length on the ^{60}Co gamma dose in the irradiated 3 x 3 x 1.5 cm^3 BaF_2 samples [57].

absorption band at 205 nm and an extra emission band at 257 nm [7, 63, 89, 96, 102]. It is assumed that harmful impurities will be identified and removed from the raw material. Lead contamination, however, sometimes originates from the fact that lead fluoride is added during the crystal growth process to avoid the incorporation of oxygen and OH^- ions in the fluoride lattice [63]. The presence of oxygen and OH^- was shown to have a very serious effect on the light transmission in barium fluoride. A replacement for the lead fluoride additive was found recently [101].

Even in "pure" crystals, however, color centers are produced due to the formation of so-called F-centers and M-centers on negative-ion vacancies [103]. Absorption bands at 611 nm and 720 nm obtained in that study in gamma-irradiated samples were linked to F-centers and M-centers, respectively. Partial thermal bleaching of color centers at temperatures of up to 220 °C was observed.

Almost complete recovery in transmission was observed after gamma and electron doses of 50-100 MRad [76, 97]. Substantial and quick, though not complete, recovery of transmission and scintillation light yield of the thin BaF_2 samples irradiated to 11 MRad with ^{60}Co gamma-rays was obtained by sunlight exposure [98]. This indicates that at least some part of damage is annealable with UV-light. Saturation of light yield and transmittance damage after doses of 1MRad (10^4 Grey) was also observed in that study. Damaged transmission after subjection to gamma-ray doses of up to 20 MRad and neutron fluences of up to 10^{14} n/cm^2 was found to recover fully after the irradiated crystals were annealed for 3 hours at a temperature of 500 °C, and after the outer surface was subsequently repolished to remove a layer oxidated in the annealing process (figure I.2.20) [24]. This observation agrees with a proposed explanation that the stable impurities in the crystal itself are responsible for the color center formation. Some natural recovery was also seen at room temperature, but it was very slow. It is important to mention here that according to a new study [57] the annealing of BaF_2 crystals with moisture surface layer at temperatures above 350 °C results in the irreversible pyrohydrolysis process. The formed

chemical groups OH^- and O_2^- produce wide absorption bands and substantially reduce the transmission of crystals. Strong absorption in the 190-250 nm region was induced in samples deliberately produced with a high oxygen content [104]. This is believed to be caused by O_2^- ions or ion pairs. Under irradiation the dissolved oxygen atoms or molecules will be transformed into oxygen ions, thus producing the absorption in the 190-250 nm region. The moisture from air leads to the appearance of a several micron thick surface layer. This is the reason why the transmittance of crystals kept in air deteriorates with time. Removal of moisture may be achieved by annealing @ ~300°C.

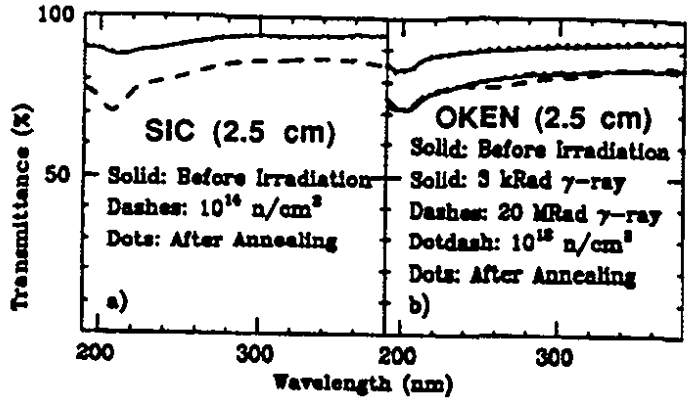

Figure I.2.20: Transmittances before and after irradiation showing recovery from neutron damage (a) and a typical saturation effect and recovery in the case of gamma damage (b) [24].

It should be commented here, that the detected light output changes that cannot be explained by simple internal transmission losses do not necessarily mean that there is a decrease in the intrinsic scintillation yield. Changes in surface reflectivity, amplification of absorption losses due to multiple photon reflections in the crystal and, finally, absorption at the exit surface can contribute to the net effect of decrease in the light output. Determination of the possible impact of these phenomena is presently being studied through simulation programs [34, 101]. The above interpretation claiming that there is no damage to intrinsic scintillation yield is supported by the results of measurements of induced scintillation emissions in two 1" diameter x 1" long samples during irradiation. No change of emission intensity was observed up to 10^6 Rad [34]. This confirms the result of the original measurement showing no damage to scintillation yield at a charged particle dose of 1.3 x 10^7 Rad [50] and the new results reported [57].

In recent high dose-rate (3.4-3.8 x 10^4 Rad/hr) gamma irradiation tests of 1 inch diameter and 1 inch long samples to about 5 Mrad, a strong post-irradiation afterglow phosphorescence was observed [34]. The emission, however, peaked at around 330 nm, well above the region where the solar blind photocathodes such as Cs-Te are sensitive. Also, the intensity of induced phosphorescence died away quickly with three time decay components in the range of 2-220 s. The longest component was of highest intensity. Some crystals showed signs of phosphorescence months after irradiation, proving that much longer phosphorescence components were also present. Exposure to roomlight or sunlight, or an increase in the crystal's temperature accelerates the deexcitation by

increasing (activating) the intensity of its emission. A two days long exposure to sunlight completely eliminated phosphorescence emissions. It seems that in the real experimental conditions of considerably lower dose-rates the phosphorescence effect will not be expected to cause problems.

The phosphorescence showed signs of saturation at the same dose of 10^4 Rads for which saturation in transmission and light output was observed. A large, up to 30-40%, decrease in light output was seen in some samples at this dose. (A similar 30% light output change vs. 10-15% transmission change was measured [98], but saturation was obtained at a much higher total dose of 10^6 Rad.) This suggests that there is a link between the three observed radiation induced effects.

Recently the GEM SSC collaboration performed first radiation resistance studies with several 25 cm long crystals of different origins [34, 101, 104]. Large changes of a factor of 2-4 in transmission accompanied by a very substantial loss in light output were exhibited in the tested crystals already after a low gamma radiation dose of 10^4 Rad. A very different pattern of absorption bands was observed in each sample, convincingly illustrating the effect of different production "histories". Contamination with oxygen or OH^- ions during crystal growth, traces of rare earth and cerium impurities, or defects related to residual stress in the crystal were suggested in different studies as possible sources of observed radiation effects [34]. Transmission spectra measured on small samples cut from a 30 cm long crystal irradiated to 1.6 MRad have shown that the amount of damage increased from the bottom end, grown first, to the top end, grown last [104]. The crystal was grown by the Bridgman-Stockbarger method, and the top part of the ingot was found to have a higher percentage of impurities due to zone refining (which happens in this growth technique). An improvement should therefore be possible through the selection of a higher purity raw material and through a reworking of the growth technique. A more systematic study of the effects of particular impurities on radiation resistance as well as a full analysis of the irradiated samples for impurities and defects is needed before conclusions as to the practical applicability of long BaF_2 crystals in high dose environments can be reached.

1.2.5. Applications in Nuclear Physics

There are several applications of BaF_2 in nuclear physics. The compound is suitable for fast coincidence measurements, such as those of the many particles, neutrons and gammas produced from interactions on nuclei [105]. Barium fluoride can be used to identify energetic heavy and light ions, since its time response shows strong correlation of slow and fast integrated pulse components with the particle type [22, 40, 58, 77, 99, 106-108]. Good separation based on the ratio of the fast component to the total light yield and good energy resolution were obtained among the particle species. Figure I.2.21 shows a scatter plot of the fast component vs. the total light output for photons and charged particles, as well as a corresponding projection of the particle separation components in the TAPS detector [22].

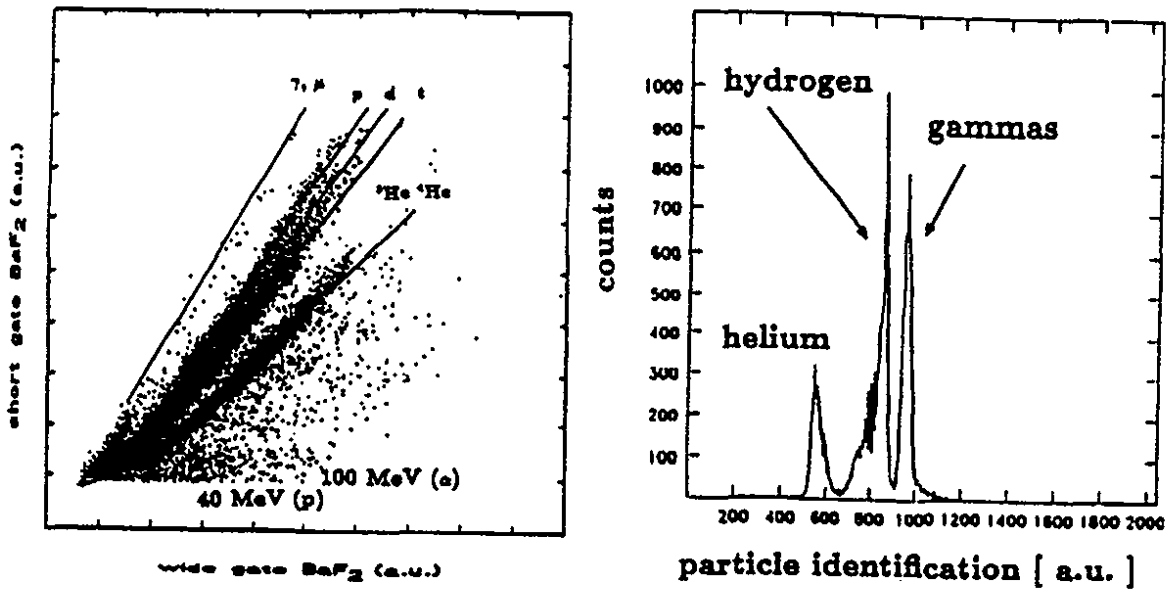

Figure I.2.21: Scatter plot of the fast scintillation component vs. the total light output (left). Projection of the separated particle lines after linearization (right) [22].

Time and energy response of BaF_2 to intermediate energy ions have been studied. Timing properties as good as for plastic scintillators were obtained [109]. The response to neutrons below 22 MeV was measured and a conclusion was reached that partial discrimination between neutrons and gammas was not possible in the energy range studied, but that it might be possible at higher neutron energies [110]. It was also concluded that BaF_2 scintillators of a relatively large size are a favorable alternative to BGO for the detection of high-energy gamma-rays [111]. The superior timing properties of BaF_2 scintillators were found to be particularly suitable for in-beam gamma-ray spectroscopy [112]. Combined time-of-flight measurement and pulse shape analysis enabled separation of hard gamma photons with energies up to 130 MeV from charged particles and neutrons [106]. At these high photon energies detection and summing of the shower leakage in a ring of six hexagonal neighbouring modules significantly improved the energy resolution as compared to the resolution of a single module for photons of up to 50 MeV [113]. Good agreements with Monte-Carlo simulations of gamma response were obtained [106, 113, 114]. The response function of a BaF_2 detector for electrons of energies 50-150 MeV was found to be in excellent agreement with computer simulations [115].

Three large size detectors have been built with BaF_2 crystals: the Strasbourg crystal castle [20], the Karlsruhe 4π detector [21] and the TAPS Darmstadt detector [22, 116]. The Strasbourg detector was the first large volume BaF_2 detector built with 74 hexagonal crystals arranged in several plane structures meant to achieve a high efficiency of gamma-ray detection. The Karlsruhe 4π detector, consisting of 42 hexagonal 15 cm long crystals, was found to have a nearly 100% efficiency for gamma-rays of up to 10 MeV. It was built for precise measurements of neutron capture cross sections in the neutron energy range of 3 to 200 keV. The overall achieved time resolution was 500 ps and the peak efficiency was

90% at 1 MeV. Time and energy resolutions superior to BGO were obtained. In these large crystals the energy self-calibration was provided by the alpha-lines from radium impurities in the crystal.

The TAPS (Two/Three Arm Photon Spectrometer), a system consisting of 384 hexagonal, 59 mm flat-to-flat size, 25 cm long crystals arranged in the form of 6 arrays of 64 crystals each, has been designed to detect high energy photons and neutral mesons such as π^0 and η in relativistic heavy ion collisions or in the experiments at the tagged photon facility. An excellent time resolution of 110 ps FWHM of the BaF_2 module in the test with 43.5 MeV electrons was obtained. By adding total energies (fast and slow components) deposited in the six neighbouring detectors to the response of the central crystal, the energy resolution has improved from 20.2% to 12.9% FWHM at this electron energy. The same procedure applied to 186 MeV tagged photons lead to a drastic improvement of the energy resolution from 16% FWHM down to 7% FWHM [22]. Already in the preliminary studies it was confirmed that other advantages of the TAPS detector include excellent response to charged particles, high quality of photon/particle discrimination by pulse shape technique (up to the highest tested energies of about 400 MeV; see figure I.2.21), and high efficiency in detecting neutrons. Other operational BaF_2 detectors are the ~28 cm diameter inner BaF_2 ball of the NORDBALL detector [117] consisting of 60 concentric BaF_2 elements and used in nuclear structure studies, and the HECTOR detector at the Niels Bohr Institute consisting of several large 14.5 cm x 17.5 cm BaF_2 crystals used to detect gamma-rays of up to 100 MeV [118].

1.2.6. Possible Future Applications in High Energy Physics

The most important project to include BaF_2 scintillators is the proposed BaF_2 electromagnetic calorimeter for the SSC GEM detector [23-25]. About 16,000 50 cm long crystals in a central barrel detector and two endcaps obtained by glueing pairs of 25 cm long crystals would have to be produced. The calorimeter has following design features: radiation resistance up to at least 10 MRad (10^5 Grey), energy resolution of $2\%/\sqrt{E} \oplus 0.5\%$, π/e suppression ratio of 10^{-4}, and a fast shaped bipolar signal output with a residual tail of less than 10^{-4} after 35 ns. To achieve this set of parameters a serious R&D effort is underway. Some important factors influencing this development include the need for an adequate production technology that would permit the growth of large, good quality crystals with low levels of impurities (to secure necessary optical quality and radiation resistance, as was discussed in subsection 1.2.4.), as well as the optimization of the readout of the fast component.

An important issue in large detectors is the implementation of a practical method of maintaining the calibration of the whole crystal matrix to secure a good energy resolution of the detector. A precise novel calibration technique with a pulsed photon source based on a radio-frequency quadrupole proton accelerator was proposed in the case of the planned BaF_2 detector by the SSC GEM collaboration [119]. With a proper normalization an absolute (relative) calibration precision of 0.7% (0.4%) is expected.

Another issue related to the use of this superfast material is the need for adequately fast electronics which would be able to exploit its speed of operation [24, 25]. An improvement of the parameters of a constant fraction or leading edge timing discriminator with fast GaAs

comparators was demonstrated [120]. The main advantage of these new circuits is a substantially reduced walk of ±20 psec for a dynamic range of 100:1.

1.2.7. Other Applications

The potential of BaF_2 for positron emission tomography (PET) was acknowledged immediately after the discovery of its fast component [36, 37, 48, 121, 122], and BaF_2 tomographs were built [61, 123-126] since they could provide time-of-flight (TOF) information in addition to projection measurements. This lead to an improved signal-to-noise ratio. A special version of a PET camera based on a BaF_2 scintillator coupled to a low-pressure MWPC filled with TMAE gas photocathode was developed [47, 53, 127-133]. The capabilities of this detector include over 40% quantum efficiency of detection of annihilation gammas for a 50 mm thick BaF_2 crystal, 5.6 mm FWHM spatial resolution, and a 2.4 ns time resolution [127]. A version of this detector to operate at atmospheric pressure and with a CsI photocathode is under development [134]. BaF_2 was also recently considered for well logging applications, but it was found that the intensity of its fast component is too weak [30, 135].

I.3. Cerium Fluoride

Cerium Fluoride (CeF_3) with its two originally reported [136, 137] fast scintillation components of 2-5 nsec (310 nm) and 30 nsec (340 nm) (figure I.3.1), no slow component, and light output equal to one-half of that from pure CsI (and 4-5% of that of NaI(Tl)) is intensively studied for LHC [6-8]. Besides the applications in high energy and nuclear physics, CeF_3 is also proposed for positron emission tomography.

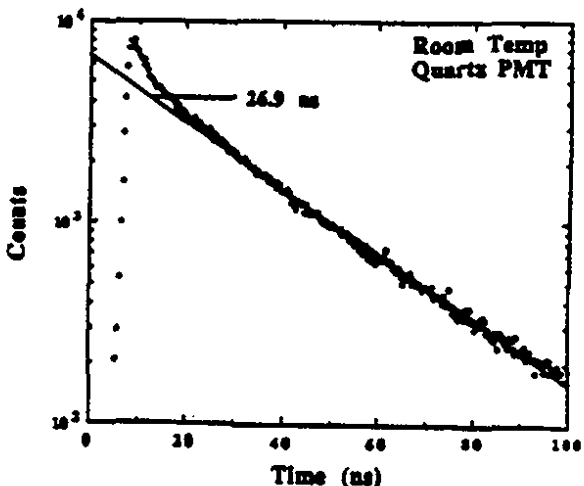

Figure I.3.1: Scintillation decay curve with a quartz PMT at room temperature of CeF_3. Scintillation was excited with gamma-rays from ^{22}Na [137].

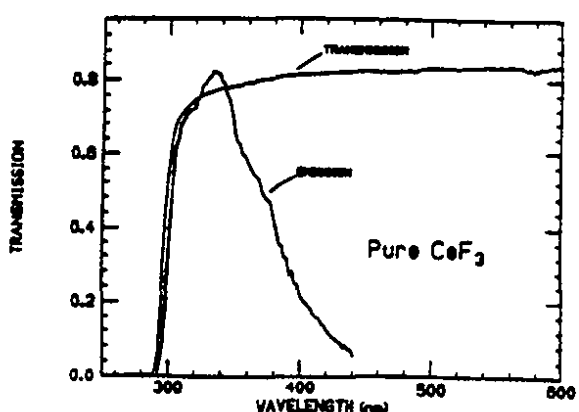

Figure I.3.2: Emission spectrum and transmission as a function of wavelength at room temperature Emission excited with 254 nm UV light [137]

CeF_3 is 25% more dense (6.16 g/cm^3) than BaF_2 with the advantage of about 20% shorter radiation length (1.68 cm) and about 25% smaller Moliere radius (2.63 cm). Also its

emission is more conveniently placed at a longer wavelength that the fast component of BaF_2.

Like in many other cases, the positions of the fluorescence bands obtained in different studies [8, 136-143] vary due to the differences in the quality of samples (such as levels of impurities) to the methods of excitation of emission used in a particular study and also due to the differences in the thicknesses of samples. Since the transmission is lower at a shorter wavelength (figure I.3.2 [137]), the excitation light and the emission spectra are more suppressed at shorter wavelengths in thicker samples than in thinner ones. In one study two luminescence bands one at 290 and one at 390 nm were seen [140]. The 290 nm emission had a shorter attenuation length. Fast luminescence of the 290 nm band was explained as corresponding to the radiative transition 5d-4f in Ce^{3+}. It can be excited with UV light centered at about 270 nm [8]. It is expected that luminescence of the same type should also occur in $CeCl_3$, $CeBr_3$ and CeI_3.

The lifetime for the 290 nm band was found to be 4±1 ns [140], in agreement with the earlier observations [136, 137]. In a different study [141] no fast component was detected. Three emission components were seen at 284, 300 and 360 nm in powder samples excited with 22.7 keV pulsed X-rays [142]. The 284 and 300 nm components (which were absorbed significantly in the tested crystal sample) were found to decay with a 9.5 ns decay constant. The 340 nm component had a decay time of 27 ns. In a recent paper [143] three components were detected with 2.1ns, 17.3 ns and 32.6 ns decay constants. The first ultra fast component was explained in that study by a rapid non-radiative quenching of the Ce emission. According to the authors the elimination of this quenching, if possible, should improve CeF_3 light output by a factor of 2. Additionally, reduction of self-absorption and decrease in decay time to 20 ns at room temperature is expected by elimination of secondary luminescence centers competing with unperturbed Ce emission. To achieve these goals further improvement in technology is needed.

CeF_3 has the advantage of its light yield being stable and temperature independent (figures I.3.3 and I.3.4 [137]). No temperature dependence was observed in the region of 77-300 °K [140]. A very different temperature dependence of decay times and emission spectra was obtained in another study [143]. The emission was shifted to a longer wavelength at low temperatures in that experiment, while in the original study [137] the intensity of the short wavelength band associated with the ultra fast component increased for lower temperatures (figure I.3.3). In the former case it was speculated that the differences were due to the respective qualities (types and levels of impurities) of the samples used in these two studies. Figure I.3.5 [143] shows emission spectra measured at room temperature for the three different decay components identified in that experiment.

Cerium fluoride samples doped with rare earth dopants (deodymium, erbium and praseodymium) have shown a substantial loss in light output. A faster light component with a several ns decay constant has appeared in samples doped with Er and Dy [141].

Radiation induced absorption at a 1-2% level was observed in a 2 mm thick sample after ^{60}Co gamma doses of 10 kRad [136]. In a recent radiation damage test of a 7 mm thick CeF_3 crystal carried out with ^{60}Co gamma-rays [144] no sizable degradation of the transmission spectrum has been observed up to the dose of 10^6 Rad (figure I.3.6). There

was no significant effect of irradiation on the emission characteristics even after a dose of 10^8 Rads.

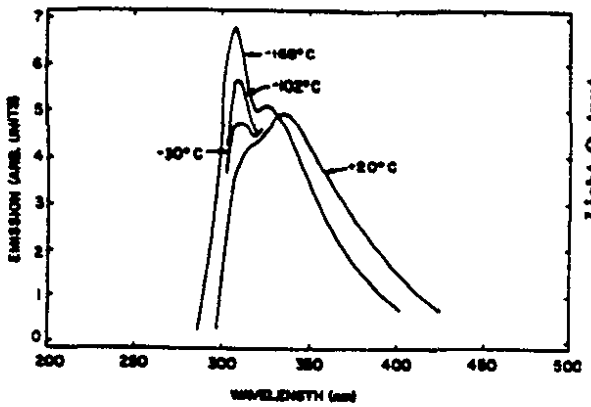

Figure I.3.3: Emission spectra of CeF_3 excited with 511 keV photons from a ^{22}Na source at different temperatures [137].

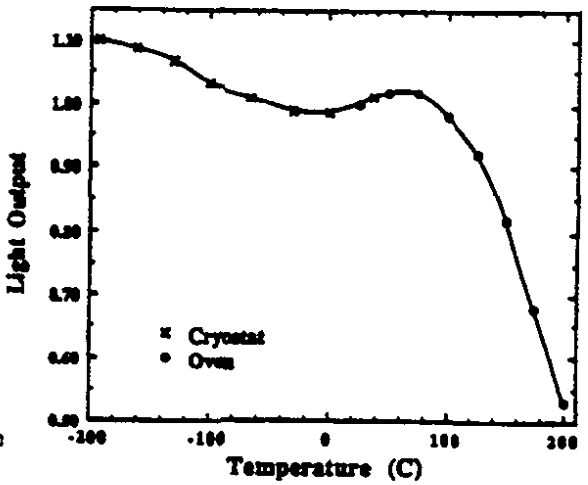

Figure I.3.4: Light output of CeF_3 as a function of temperature [137].

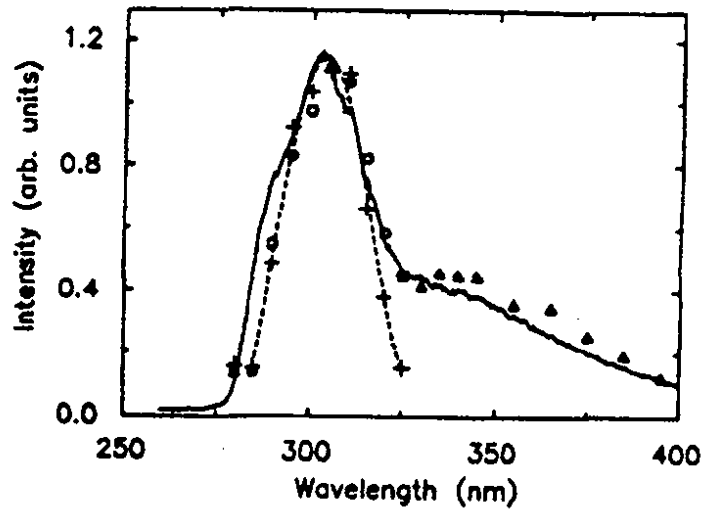

Figure I.3.5: Emission spectra of CeF_3 excited with 270 nm UV laser pulses (solid line) and under Ru/Rh beta/gamma source excitation for the three identified decay components (+: 2.1 ns, o: 17.3 ns, and Δ: 32.6 ns). Broken line is a polynomial fit to the 2.1 ns component [143].

The radiation damaged transmission recovered with an exponential time constant of about 40 days. No effects of accelerated recovery due to exposure to sunlight were observed. These results place CeF_3 just next to BaF_2 in radiation resistance. Preliminary irradiation of a 8 cm long crystal to 100 KRad showed positional variation of color center formation due to changing gradient of impurity concentration in the melt [8]. In some parts of the crystal the damage was very severe, but at one end the damage level was acceptable. Characterisation

of color centers is in progress and improvements are expected soon. Gamma-ray irradiations of small 7 mm thick crystal samples of pure CeF_3 and CeF_3:Ca with doses of up to 10^8 Rad have shown that the doped crystals have less transmission damage than pure samples [146].

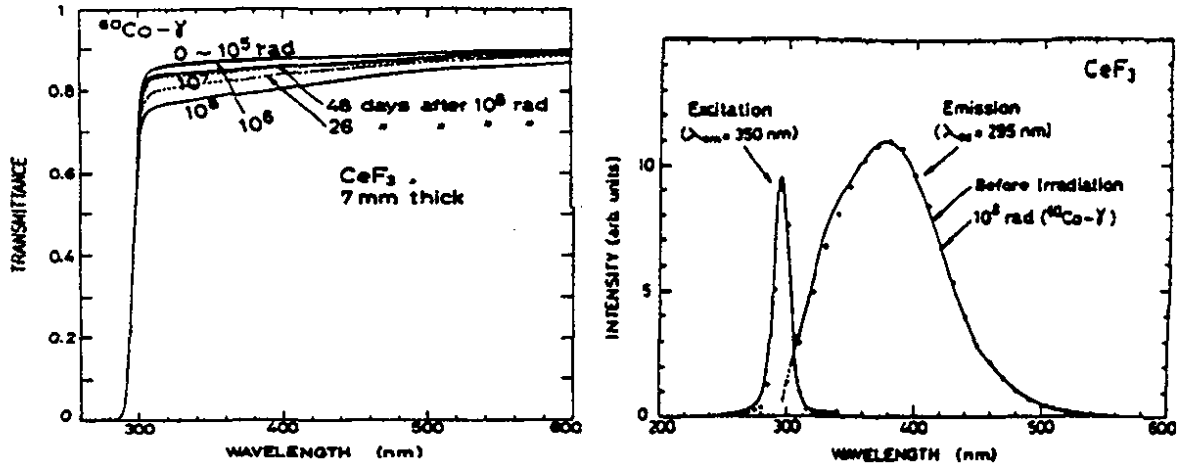

Figure I.3.6: Transmission (left) and emission (right) of CeF_3 before (solid lines) and after (dotted transmission curves and solid emission points) ^{60}Co irradiation to the indicated gamma doses [144, 145] (in Rad).

As a final comment one might say that the decay time constant of cerium emission of 20-35 ns is almost too long for the SSC or LHC applications. An ADC gate about 100-200 ns wide must be used to integrate the signal [144]. This situation is actually more difficult than in the case of barium fluoride, where the difference of nearly three orders of magnitude in the decay constant as well as a distinct difference in emission wavelength makes a selective detection of its ultra fast component practically possible.

I.4. Cerium doped gadolinium orthosilicate

Gadolinium orthosilicate activated with Ce^{3+}, Gd_2SiO_5:Ce or GSO(Ce), is a fast, dense (6.7 g/cm^3) and efficient scintillator with high light yield equal to 20% of NaI(Tl), and therefore higher than BGO. Its emission excited with 661 keV gamma-rays and UV light is centered at 440 nm and is shown in figure I.4.1 [147]. GSO(Ce) is an attractive candidate for calorimetry [145, 148-150]. It is considered for possible applications at future supercolliders [8].

GSO(Ce) scintillator was first reported in 1983 [152]. GSO(Ce) was employed in PET systems already for several years, but until recently was not available in crystal sizes sufficiently large for applications in high energy physics experiments. It has an extremely high thermal neutron absorption cross section due to Gd, implying that it should be a sensitive detector of thermal neutrons. Unfortunately this could also mean that GSO(Ce) may be too sensitive to neutron fields in accelerators whenever a substantial amount of

neutron thermalizing hydrogen-rich material is present. Its applicability as a gamma-ray detector for nuclear well logging applications was evaluated and found promising [153].

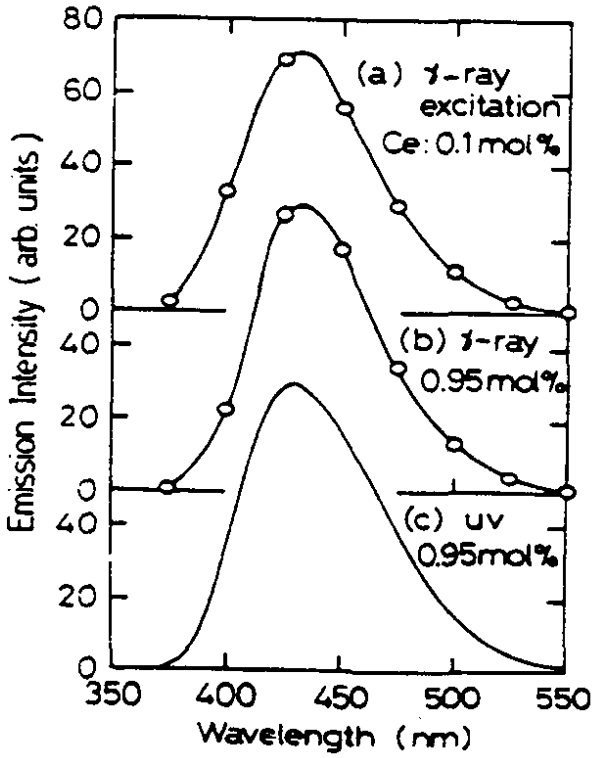

Figure I.4.1: Emission spectra of GSO(Ce) with a Ce concentration of 0.1 mol% (a) and 0.95 mol% (b) when excited with 662 keV gamma-rays @ 295 °K, and with 0.95 mol% when excited by UV photons (c) [147].

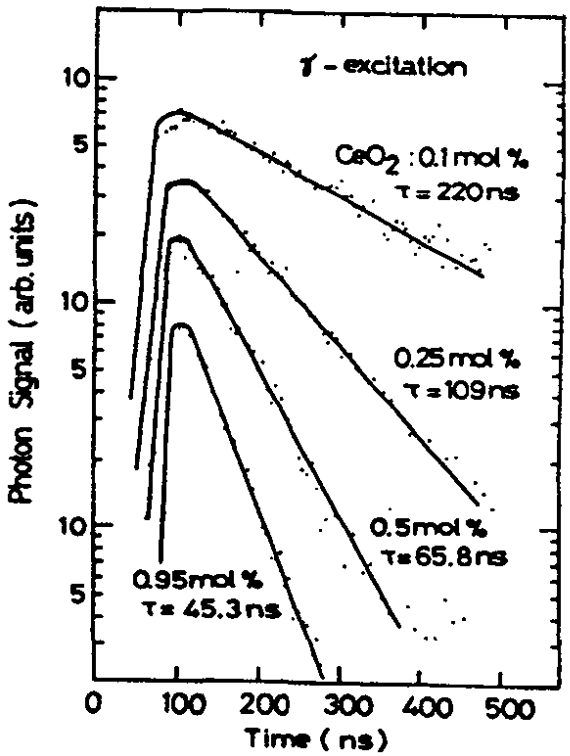

Figure I.4.2: Decay curves for GSO(Ce) with various Ce concentrations excited by ^{137}Cs gamma-rays [151].

Fast rise times of 3 ns and fast decay constants down to 30-60 ns were observed [151] (figure I.4.2), depending on the Ce concentration and temperature, together with slow decay times up to 2 μs [147, 153]. Figure I.4.3 shows scintillation decay of a 2 cm x 2 cm x 2 cm GSO crystal doped with 0.5 mol% cerium [153, 154]. A fit was made to the experimental spectrum with the sum of two exponential terms with decay constants (and fractions of total scintillation light) of 57 ns (85-90%) and 600 ns (10-15%). The time constants of both decay components are strongly dependent on the concentration of the cerium dopant (Table III). The light output is greatest for the 0.5 mol% doping level and decreases for both higher and lower concentrations [151]. About 10-15% of the total scintillation output is contained in the slow component. Due to the slow component, ADC integration gates with widths of up to 500 ns had to be used to collect light.

It is interesting to note that with 5 mol% of cerium activator, the slow component's decay time decreases to 70 ns. Both light output and decay times decrease monotonically with increasing temperature (figure I.4.5) [153]. Over the temperature range of 20-170 °C the light loss is comparable to the loss for NaI(Tl) and is equal to about 40% @ 150 °C. The

experimental results of the decay time measurements are well explained by the recombination luminescence following recombination between Ce^{2+} (formed by thermal electron capture on Ce^{3+}) and self-trapped holes (i.e. V_k-centers) produced by ionizing particles [147]. The fast rise of about 3 ns corresponds to the lifetime of Ce^{3+}.

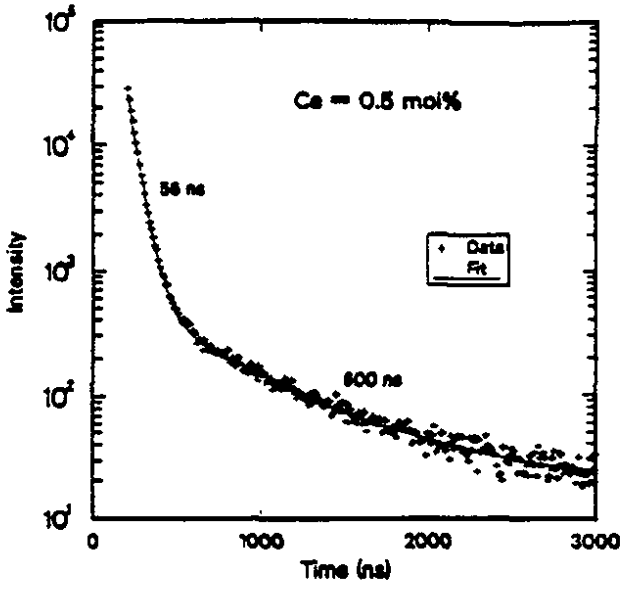

Figure I.4.3: Scintillation decay of a GSO crystal doped with 0.5 mol% cerium [153].

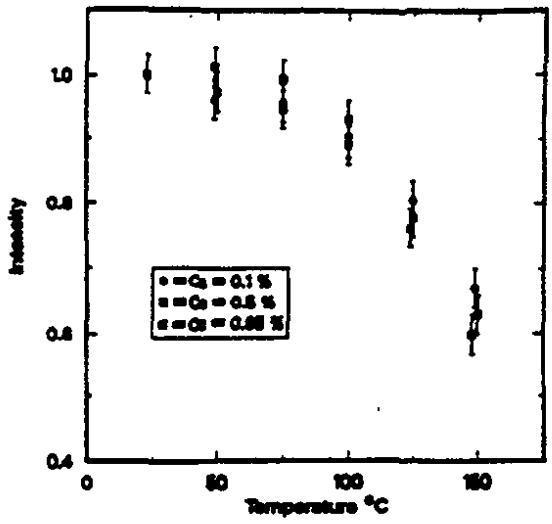

Figure I.4.4: The light output of GSO crystals doped with 0.1, 0.5, and 0.95 mol% cerium as a function of temperature [153].

Table III
GSO decay constants vs. cerium concentration.

Ce conc. (mol%)	Primary decay (ns)	Secondary decay (ns)
0.1	190	1200
0.5	56	600
0.95	40	418
1.5	32	307
2.0	27	215
5.0	19	70

In a recent radiation damage test with ^{60}Co gamma-rays [150] of several small GSO(Ce) samples doped with 0.5%, 1.5%, 2% and 2.5% cerium, the crystals showed an excellent radiation resistance comparable to or even better than BaF_2. No sizable degradation in transmission and scintillation was detected up to 10^8-10^9 Rad in all the crystals tested. In figure I.4.6 transmission and emission spectra for GSO samples doped with 0.5 mol% before and after irradiation are shown [150]. Only a small change in the excitation and emission was measured. Recovery of radiation damage was also observed.

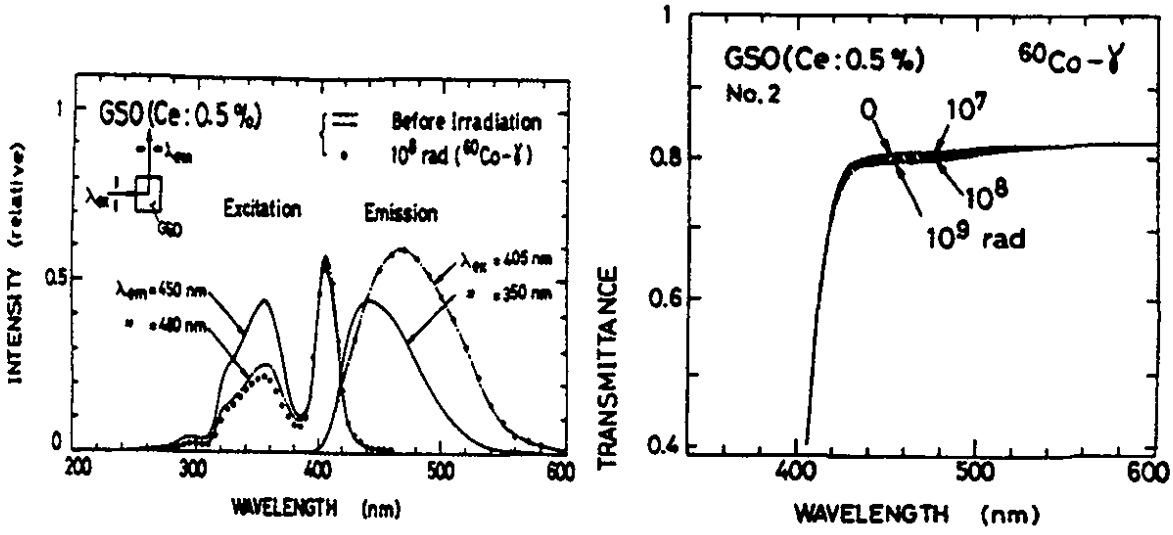

Figure I.4.6: Excitation-emission and transmission spectra of GSO(Ce) samples doped with 0.5 mol% of Ce measured before and after ^{60}Co gamma irradiations to 10^8-10^9 Rad. Transmission measured across a 1 cm thickness [150].

Disadvantages of GSO are (1) its high melting point (1900 °C) and (2) the high segregation factor of cerium in this matrix resulting in a low pulling rate of 1-2 mm/hour [8].

In many cerium-doped crystal scintillators there are means to alter the matrix with Li or Ni resulting in a reduction of scintillation lifetime. But, quite possibly, this might have an adverse impact on radiation resistance of the new material.

I.5. Pure CsI

I.5.1. Properties

Pure CsI, whose emission was already observed in the 1960s, re-emerged recently as an attractive candidate with superior mechanical properties to those of BaF_2 and easier to detect scintillation light in the longer wavelength region [155]. It has a dominant emission band occuring between 305-320 nm [156] (figure I.5.1) of scintillation light with fast 10, 23 and 36 ns decay constants originally reported [155].

CsI is only slightly hygroscopic, with a surface weakly sensitive to exposure to humidity. It is however highly shock resistant, thermally stable, and easy to process. CsI is not susceptible to cleavage or cracking under mechanical or thermal stress. In the more recent studies two components of about 6-7 ns and 29-30 ns [157], and 2.1 ns (35%) and 21.7 ns (65%) according to a different study [158], were identified. A slower 1 μs component associated with lattice defects and centered at 450 nm was also seen [158] (figure I.5.2). The fast/total ratio depends on the purity of material and the highest attainable value is about 0.8 [157]. In a new study [159] decay time measurements were made on pure CsI scintillators prepared by different methods. The main conclusion of that study was that the presence or absence of the slow component was strongly correlated with the production

method via different purity of samples (figure I.5.2). The differences in measured decay times in various studies may be understood in this way.

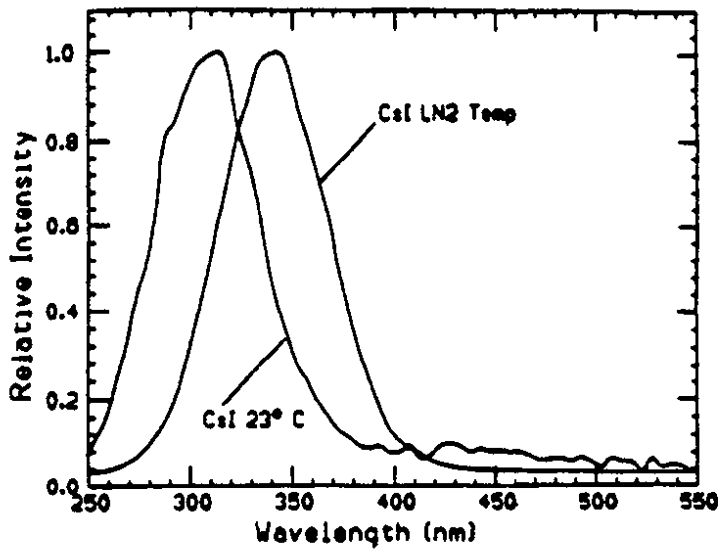

Figure I.5.1: Emission spectrum of undoped CsI at 23 °C and at liquid nitrogen temperatures [157].

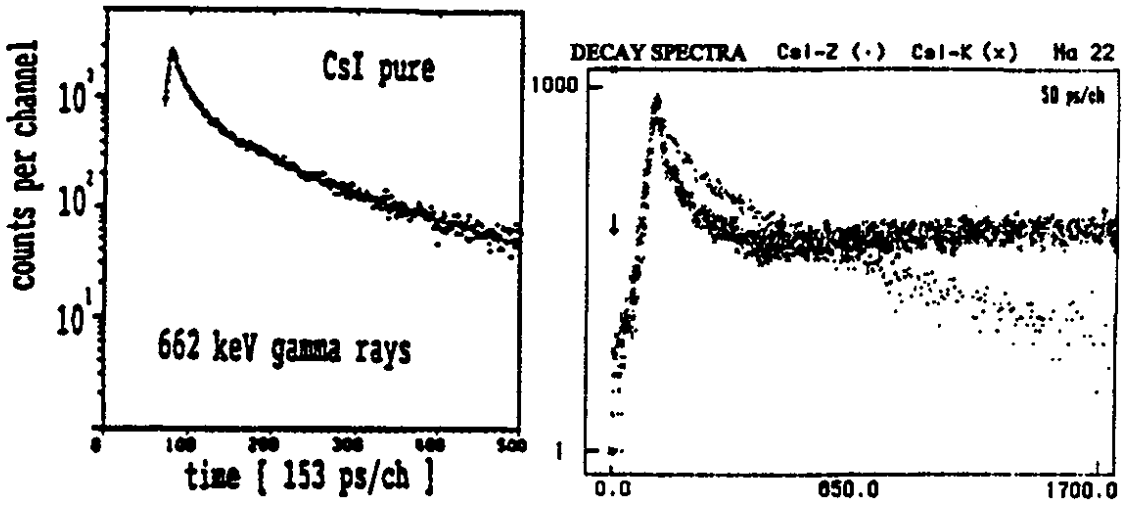

Figure I.5.2: Left: decay spectrum of undoped CsI excited with gamma-rays [158]; Right: Decay time spectra for Na^{22} excitation of two different CsI samples produced by the zone melting technique (Z) and by the Kyropoulos method (K) [159].

The best results were obtained for crystals prepared by the cold press technique where practically no slow component was present. Also, a zone melting technique gave good results. In the same study a fast (about 1 ns) component of nearly the same fractional intensity of nearly 25% for gammas (electrons) as reported previously [158] has been confirmed. It was reported that 70-80% of the total light output is in the fast component within a 100 ns gate to ADC. Thus the slow component in CsI is considerably less intense

than the fast one, and will cause less pileup at high rates. The scintillation mechanism of the fast band at 315 nm is explained in terms of the radiative decay of self-trapped excitons [158, 160]. The slow 450 nm component is attributed to the presence of vacancies and other defects [158, 160]. Chemically pure crystals with as little defects as possible are therefore required. The intensity of the slow component, the shape of the emission spectrum and transmission properties were shown to be at least partly related to the level of impurities, such as Tl, in the crystal [156].

A potentially serious drawback of pure CsI is the steep dependence of its light yield on temperature, requiring precise temperature monitoring in large detector systems (figure I.5.3) [157]. Decay constants of the fast (7 ns and 29 ns) components of CsI scintillation light increase with decreasing temperature. At -190 °C they are 180 ns and 320 ns, respectively. This is accompanied by an increase in the total light output by a factor of 6. Also, a shift in emission spectrum to longer wavelength occurs at lower temperatures [157, 162]. Figure I.5.1 shows a shift in the peak emission from 310 nm at room temperature to 340 nm at liquid nitrogen temperature [157].

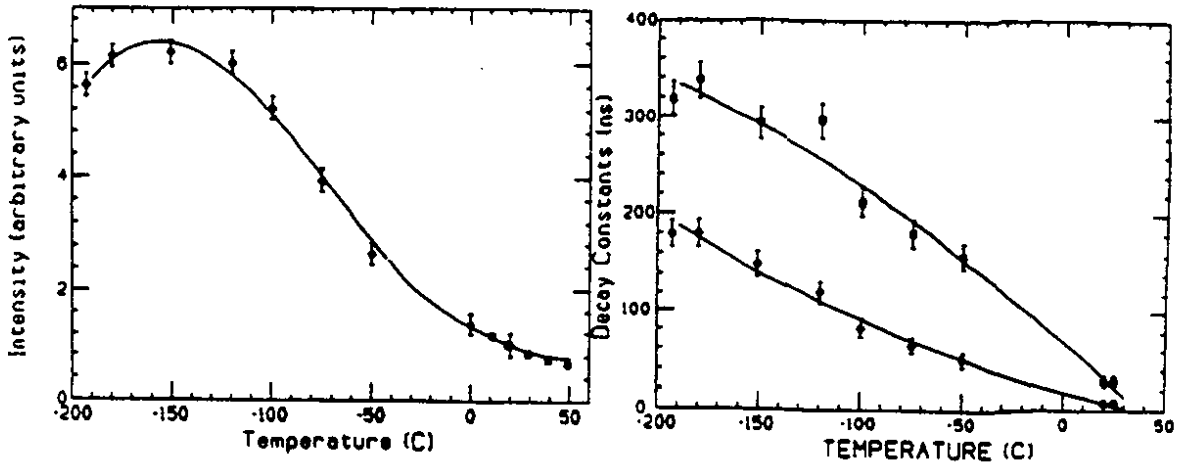

Figure I.5.3: Variation in the light intensity of the fast light output (left) and in the decay constants (right) of the two fast components in undoped CsI as a function of temperature [157].

CsI can be grown like CsI(Tl) into very large ingots. Large detectors such as the 7800 crystals CLEO II [163, 164] and Crystal Barrel were built with CsI(Tl). A high-resolution, large-acceptance spectrometer for neutral mesons was constructed at LAMPF with two pure CsI calorimeters, each made with 60 large 4" x 4" x 13.5" long crystals [165]. The same developed techniques can be used to produce pure CsI. New improved purification and production processes developed for CsI(Tl) resulting in considerably better uniformity of scintillation efficiency [166] help with pure CsI production. Large 30 cm long good quality crystals became recently available [167, 168]. Fast light yield of 250-300 pe's per MeV was measured in these crystals with a 100 ns effective ADC gate (figure I.5.4). Total light output was measured with a 1 μs gate.

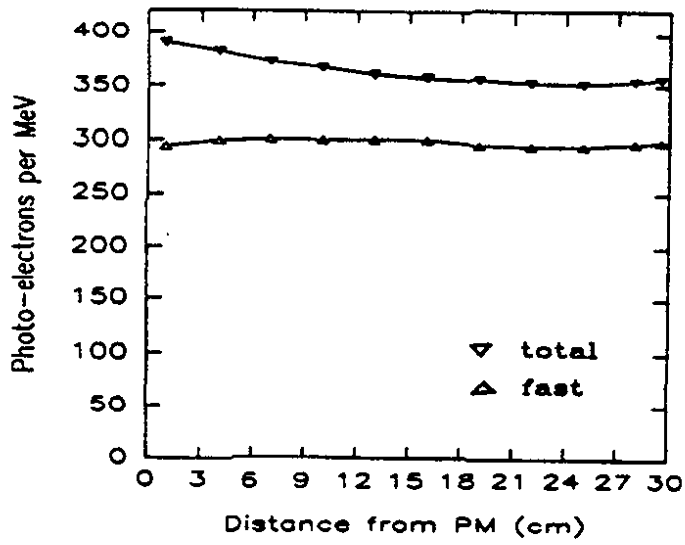

Figure I.5.4: Fast and total light output versus distance for a 3.5 cm x 3.5 cm x 30 cm crystal sample measured with a quartz window photomultiplier [168].

By using optical filters, waveshifters or selective photocathodes to suppress the slow component (as in the case of BaF_2) it is possible to improve the speed of operation of this scintillator. An improvement was seen in the fast to total ratio in poor quality samples when using a broad band filter centered around 320 nm [157]. Plastic waveshifters used in the same study also allowed the possibility of employing regular window PMT's instead of quartz window PMT's necessary to detect directly the fast CsI component. Also, large crystal arrays can be read with a limited number of photomultipliers. In a preliminary study with a piece of Bicron 408 scintillator used as a waveshifter, the number of photoelectrons obtained per MeV of deposited energy was ~25% of the number detected directly with a quartz window PMT [157]. The result of a beam test with 3 GeV electrons indicated that at least at higher energies it was possible to obtain a resolution comparable to the direct readout. The authors pointed out the interesting possibility of reading out many crystals with a single wavelength shifter bar and with a PMT on each end. The waveshifter is primarily excited by the fast component and any slow emission coming at longer wavelength should be suppressed, since the PMT does not view any direct light emanating from the crystal. Since there was very little difference in the percentage of the fast component in the total light signal with the waveshifter as opposed to the direct readout, the conclusion was reached that part of the slow emission in CsI occurs also at a shorter wavelength, in the region close to the fast component. In a special embodiment of the waveshifter idea, scintillating fibers may be used to transport the shifted light over long distances [157].

I.5.2. Radiation Resistance of CsI

The first studies indicated that CsI is susceptible to radiation damage at rather low doses [169]. Doses of only 100 Rad were found to decrease substantially the transparency of crystals resulting in a serious decrease in detected light. New results obtained by Woody et

al. [157, 167], however, show that it can be made radiation resistant to at least a fraction of a megarad of a ^{60}Co gamma dose. Figure I.5.5 shows the radiation induced absorption during irradiation and recovery for one of the best among the tested samples. The samples were irradiated at a dose rate of 3.4 x 10^4 Rad/hr in a dry nitrogen atmosphere to prevent any surface deterioration due to moisture during the exposure.

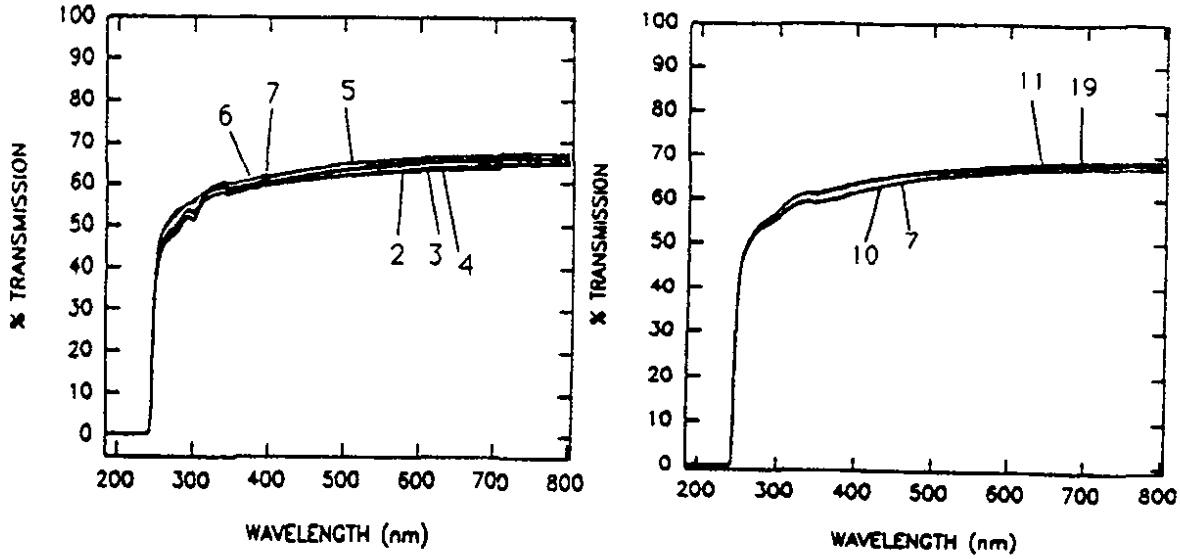

Figure I.5.5: Transmission vs. wavelength for the undoped Quartz & Silice 1" dia. x 1" long CsI sample: (2) 10^3 Rad, (3) 10^4 Rad, (4) 6 x 10^4 Rad, (5) 2.6 x 10^5 Rad, (6) 9.0 x 10^5, (7) 4.2 x 10^6 Rad, (8) 7 hours after 4.2 x 10^6, (10) after 54 hours, (11) after 20 days, (19) after 26 days plus 63.5 minute exposure to UV light [167].

Decrease in the light output of the same Quartz & Silice 1" dia. and 1" long sample with a gamma dose is shown in figure I.5.6. A ~35% loss of light output is seen. This loss exceeds what would be expected from loss in transmission only (which is very small in this sample; see figure I.5.5). Other 1" dia. x 1" long tested samples have shown worse performances, and large sample to sample variations in transmission and light output damage were measured.

Scintillation emission spectra measured during gamma irradiation have shown some increase in the spectral region of the slow component, while little change occured in the region of the fast emission (figure I.5.7). Within experimental errors the intensity of the fast component did not change up to the highest doses used. Hence, the observed changes in light output cannot be accounted for by the combined measured effect of the losses in transmission and in light yield. One of the investigated possibilities is the potential role played by radiation effects near or at the surface, which could change light collection efficiency. A slow recovery with time was seen in all irradiated samples. Exposure to UV light from a mercury lamp did not induce acceleration of recovery. All five samples of a 2.54 cm diameter and 2.54 cm long used in the study have shown a prominent absorption band at 800 nm and several bands in the 250-500 nm region. No recovery was observed in the latter region for this sample, while a substantial recovery was shown for the 800 nm

band. Also, no recovery under UV exposure was detected. Large sample to sample variation in relative intensity of induced absorption bands and recovery behaviour was observed, indicating the role of different amounts of impurities.

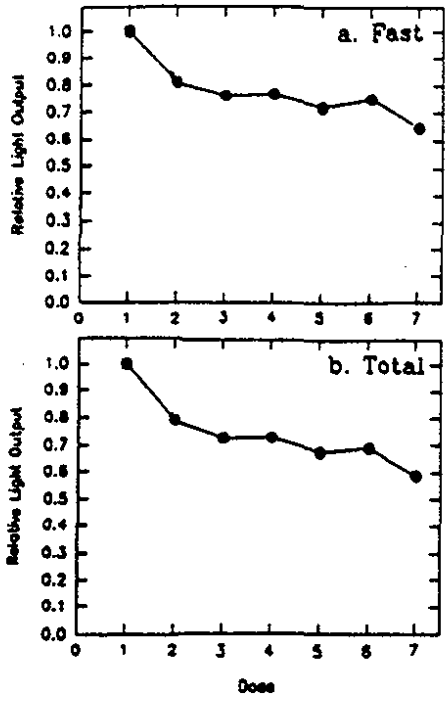

Figure I.5.6: Relative light output for the same Quartz & Silice sample as in figure I.5.5 as a function of dose for the fast and slow scintillation components: (1) before irradiation, (2) 10^3 Rad, (3) 10^4 Rad, (4) 6×10^4 Rad, (5) 2.6×10^5 Rad, (6) 9.0×10^5, (7) 4.2×10^6 Rad (adapted from Woody et al. [167]).

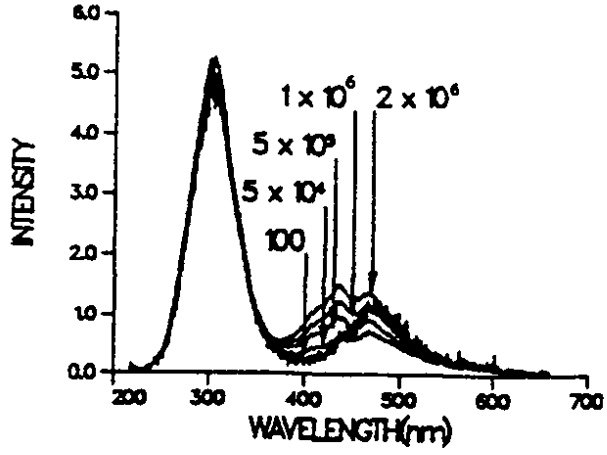

Figure I.5.7: Scintillation emission spectrum of undoped CsI measured during irradiation for various doses, as indicated. The curves are not corrected for the spectral response of the spectrophotometer and do not give the exact shape of the spectrum [167].

A change in light output varied from 10 to 40, considerably more than would be expected from the decrease in transmission. This implies that there is an additional loss due to a reduction in the scintillation yield in the crystal. Further studies are necessary to solve this problem. It would be particularly interesting to correlate any observed radiation damage with impurity concentration as indicated by the light output and fast/total ratio.

Tests with long samples have begun. A 3.5cm x 3.5cm x 30 cm long sample was recently irradiated in a dry nitrogen atmosphere [167]. There was a substantial change in the apparent absorption at doses greater than 10 kRad (100 Grey) with some indication that there was a position dependence of the light output, possibly due to different concentrations of impurities. Much improvement in quality control is needed before the same radiation resistance seen in the best small samples, such as the Quartz & Silice sample (figures I.5.5 and I.5.6), will be attained in long samples.

A phosphorescence emission was observed in the CsI crystals immediately after irradiation [167]. Several decay constants in the range of many seconds were identified, and some residual emission was detected in samples even several days later.
Another study of radioluminescence and radiation damage in single crystals and in polycrystal CsI thin infrared windows was performed with 100 kRad 14 ms wide reactor pulses with 5 kRad neutron and 95 kRad gamma components [170]. After radiation doses of more than 2 MRad the radioluminescent intensity in the visible range decreased to about 60-70% of the pre-irradiation value and then recovered completely after bakeout at 150 °C. Apparently the quenching centers that were at the origin of the decrease of the emission have been annealed. Heat treatment of one non-irradiated pure CsI crystal at a higher temperature of 550 °C led to cloudy appearance, lowered intensity of the fast component, and longer wavelength emission bands extending from 350 nm to 550 nm [156].

Interestingly, new samples of CsI doped with thallium were also found to be radiation hard [167, 171]. This indicates that impurities in the meltstock rather than thallium were then responsible for the observed radiation damage of CsI(Tl), already with doses of under a kilorad [169, 172-174]. Actually, thallium is expected to "protect" material against radiation damage by "scavenging free carriers before they can find a more damaging site" [175]. Impurities such as Rb, K, Na and Ba were found in a sample damaged by a ^{60}Co gamma dose of less than a 1 kRad, in contrast to other 1 cm^3 samples which have displayed good radiation resistance up to the doses of over 50 kRad [171]. An interesting effect was observed when comparing radiation resistance of two samples cut from the same boule. The sample cut from the first grown part of the ingot (bottom) was much more radiation hard than the sample from the top, pointing to the accumulation of impurities in the top part of the ingot grown by the vertical Bridgeman method. A chemical analysis has confirmed a higher concentration of impurities (Fe, Rb and Ba) in the top sample. No difference in radiation resistance was obtained by varying Tl content from 0.01% to 0.6%, proving that impurities and not thallium are responsible for radiation damage in CsI(Tl) crystals.

In a study of undoped (pure) CsI crystals a correlation was shown to exist between the light yield in the fast component and the vertical position in the ingot (grown by the Stockbarger process) from which the sample was taken [176]. A continuous decrease of the fast component and increase in the concentration of impurities with height were found.

One can point out to a similar experience with different samples of BaF_2 where contradictory radiation damage results were encountered until the role of relevant impurities and defects became more clear (the studies are continuing) and production of crystals of improved quality was made possible. This problem is presently further compounded by the fact that radiation damage tests are often done with small, better-than-average quality samples, and the predictions to the large actual-size samples are risky, and usually lead to an underestimation of the expected damage.

In general one would expect pure CsI crystals to be radiation hard. If proven, CsI would be a natural candidate for a B-Factory electromagnetic calorimeter [177]. Also, being faster than the thallium doped CsI(Tl), it should be a better solution than the latter choice proposed for a tau-charm factory electromagnetic calorimeter [178]. It was also selected as an

option for a calorimeter detector at RHIC [179, 180]. Another considered option in that case is PbF_2.

I.5.3. CsI-CsBr mixtures

In an attempt to increase light output of pure CsI (0.05-0.08 of NaI(Tl)) mixed crystals of CsI-CsBr were developed. The light output was increased to 0.18 of that of NaI(Tl) [181]. Three fast components of 11, 23 and 36 nsec were measured. Crystal emission was found to be in the region of 280-340 nm. In the preliminary tests, good quality middle-sized CsI-CsBr samples had no detectable slow component [182]. On the other hand problems were detected with light attenuation length and mechanical properties of the crystals. In a another recent study [183], an extra slow (decay time 8-10 μs) scintillation component centered at 450 nm was detected. In addition, an absorption band centered at 300 nm appeared and the intensity of the fast component decreased due to a quenching process. The conclusion of that study was that in spite of the fact that Br-doped CsI emited more light, there seemed to be no advantage in using this material since the extra components are very slow [9].

I.6. Lead Fluoride

The non-scintillating Cherenkov material lead fluoride (PbF_2), which was first studied for applications in calorimetry already in the late 60's [184] was rediscovered by Anderson in 1989 [185]. Lead fluoride does not scintillate because its Pb^{2+} ion luminescence is quenched at room temperature [186]. Several new experiment proposals (for example for RHIC [179]) consider the use of the PbF_2 electromagnetic calorimeter. PbF_2 has a high density of 7.77 g/cm^3, a radiation length of 0.93 cm and a Moliere radius of 2.22 cm. It was noted [187] that for a PbF_2 Cherenkov radiator the "apparent" Moliere radius is about 20% smaller (1.8 cm) than the physical shower radius. This occurs since the electrons in the outer regions of the shower are slow and produce almost no contribution to the Cherenkov light. These properties enable the building of a calorimeter even more compact than BGO. Lead fluoride is transparent down to about 265 nm, much better than lead glass (see figure I.6.1), has a high refractive index of 1.86, and a low critical energy of about 9 eV. As a result of this a signal of 1300 pe's per GeV was measured [188] which was higher than for standard lead glass materials. An even higher number (1800 pe's/GeV) was recently reported in a TRIUMF test [189].

Lead fluoride is also the fastest of the available radiation resistant materials. It only produces instant Cherenkov light. A signal from a 14 X_0 long and 4.3 cm flat-to-flat hexagonal cross section crystal has a 3 ns rise time and a fall time of 11 ns. PbF_2 is stable in air and is unaffected by moisture. It has a low melting point of 822 °C and the material in its raw form is abundant [188].

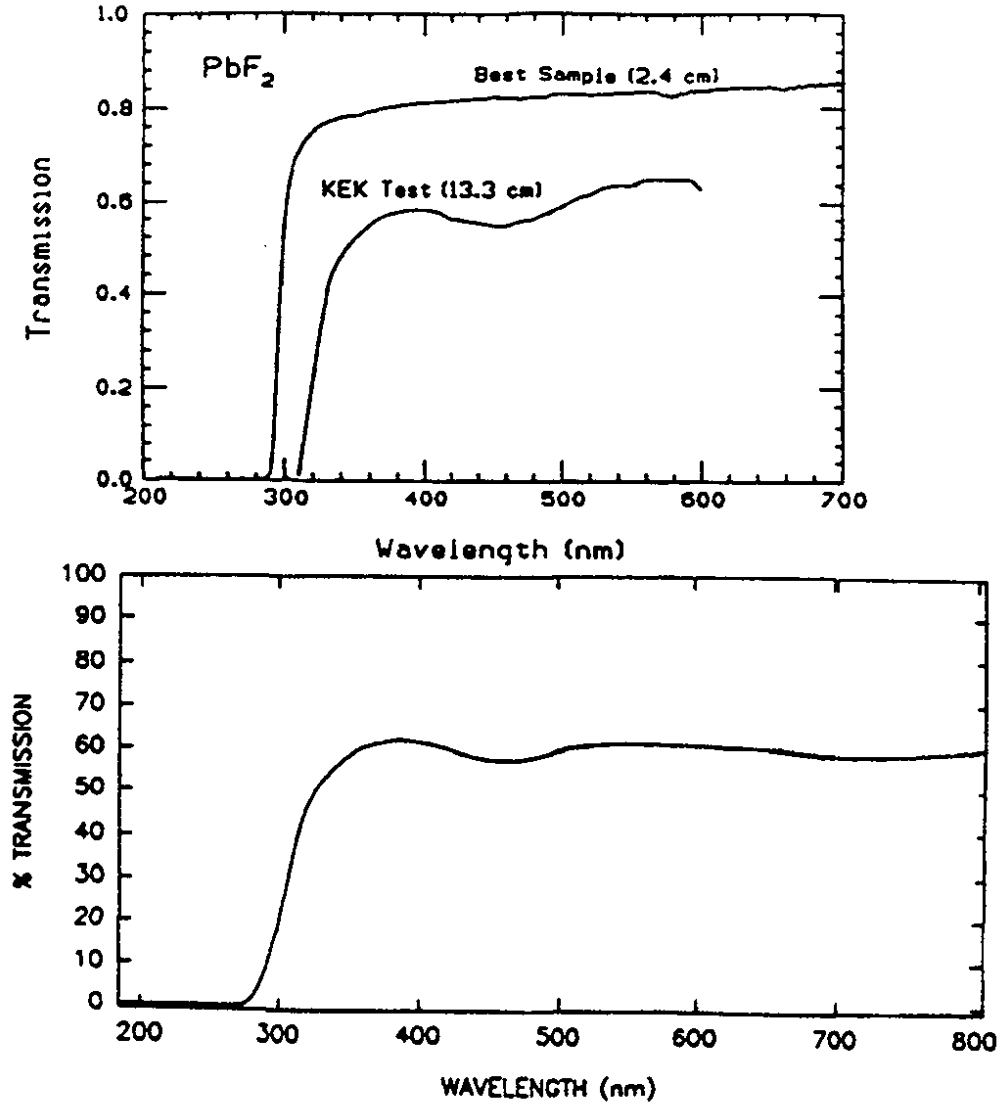

Figure I.6.1: Transmission as a function of wavelength of a small good quality sample and a 13.3 cm long KEK crystal (upper spectra, adapted from ref. [188]), and of the new 17.5 cm sample tested [190] (lower spectrum). The curves shown have not been corrected for the ~17% loss due to reflections from the two end surfaces.

Doped with some fast scintillators such as TbF_3, the ratio of the Cherenkov to the scintillation signal can be used to correct the visible hadron energy on an event by event basis [187]. There are plans to dope this crystal with other cations and to produce more complex structures such as $CsPbF_3$ and $Pb_2(Zn,Th)F_6$, which could be expected to show some scintillation [8]. Breaking the local symmetry (believed to be the reason for the luminescence to be hidden) of the Pb^{2+} ion in the fluoride lattice is expected to produce a scintillating material [8]. Other heavy crystals such as CdF_2 ($\rho = 6.33$ g/cm^3), $BaYb_2F_8$ ($\rho = 6.99$ g/cm^3) and YbF_3 ($\rho = 8.17$ g/cm^3) are studied as scintillator hosts [8, 146]. It was

shown that $BaYb_2F_8$ is radiation hard to 10^7 Rads and is suitable for the Cherenkov radiator [146].

The first measurements have shown that PbF_2 is substantially more radiation resistant than lead glass. On the other hand it turned out to be much more susceptible to radiation than the fast crystal scintillators such as BaF_2, CsI or CeF_3. Figure I.6.2 [188] shows the transmission of 1 cm cube good quality PbF_2 samples before and after irradiations with the reactor neutrons and gamma-rays. It was discovered that exposure to UV light (365 nm) led to the complete recovery from damage of a sample irradiated to 4 x 10^5 Rad.

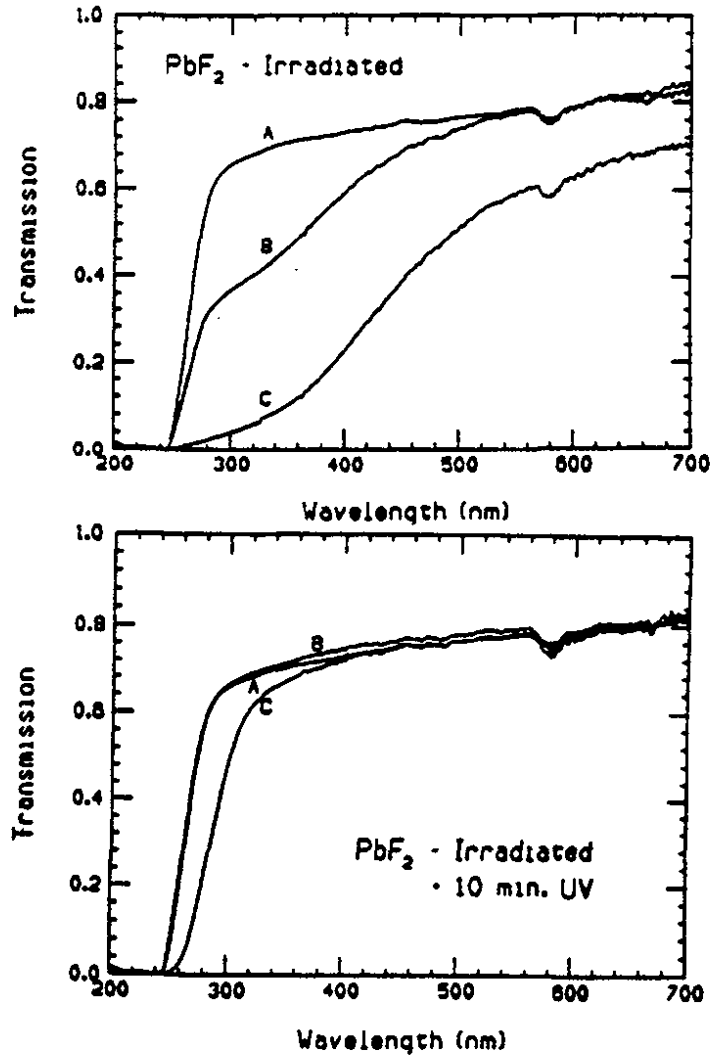

Figure I.6.2: Transmission as a function of wavelength for several PbF_2 samples before and after irradiation (upper figure) and after a 10 min UV exposure (lower figure): (A) before irradiation, (B) after $3x10^5$ Rad of neutrons and $1x10^5$ Rad of gamma-rays, and (C) after $3x10^6$ Rad of a neutron dose and $1x10^6$ Rad of a gamma dose [188]. The absorption feature at 580 nm is the measurement artifact.

Some residual permanent damage at the shortest wavelength remained in the sample irradiated to 4 x 10^6 Rad. In another measurement it was reported that a rather poor quality 1 cm thick sample, made from 98% purity raw material, showed effects of radiation damage after a ^{60}Co gamma dose of 10^4 Rad [145]. The research on this question continues. In figure I.6.3 the result of an irradiation test to 1.4 MRad with one of the new crystals of improved quality is shown [190]. The radiation resistance has significantly improved as compared to older samples. Except for the study of impurities responsible for the damage, it would be interesting to find an additive that would make PbF_2 more radiation-hard, much like different oxide dopants were found to supress the production of color centers in lead glass [191, 192]. It was suggested that in order to improve radiation properties of PbF_2, some metal fluorides of Li, Na, K, etc. may be used as additives [146].

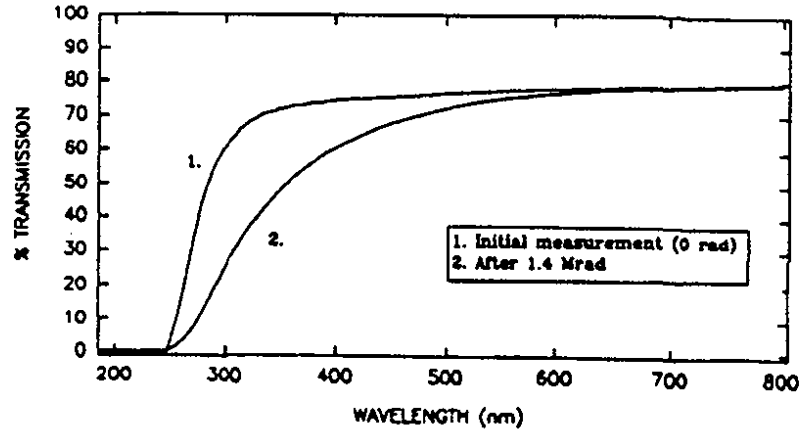

Figure I.6.3: Transmission spectra before and after a 1.4 MRad gamma irradiation of a 1" dia. x 1" long PbF_2 sample [190].

The first batch of 20 radiation length long PbF_2 crystals were recently produced and are undergoing tests [190] but the feasibility of production of large quantities of good quality crystals has yet to be demonstrated.

I.7. Brief discussion of some other materials

The search for new scintillating materials accelerates [9-12, 186, 193]. Blasse [186] has critically reviewed some of the efforts. For example, he has pointed out that lead carbonate ($PbCO_3$) and many other studied heavy lead-based materials, such as PbF_2, $PbCl_2$, $PbBr_2$ and $PbWO_4$ were found to have their luminescence quenched at room temperature, and therefore were not good candidates for scintillators. According to Blasse new and potentially interesting scintillating materials include $ZnGa_2O_4$, and several bismuth, gadolinium, barium and lead compounds. The main conclusion of his report is that the present level of understanding of the properties of luminescent materials can be used in order to search for new scintillators in a much more efficient way. At the present time there exists no fundamental approach in the search for new scintillating materials which would

take into account the achievements of today's luminescence science [90]. In his paper [90], after formulating five basic requirements defining good scintillator material, Lempicki proposed a class of excitation experiments intended to shed light on the basic mechanisms of scintillation in order to select material candidates.

In recent reviews [6, 8, 9, 11, 194] three groups of potentially promising fast scintillating crystals were listed: binary mixtures of cross-luminescence exhibiting fast scintillators such as CsCl, CsBr, CsF, RbCl, RbF and KF; binary compounds with rare earths such as $LaF_3(Nd^{3+})$, $YF_3(Pr^{3+})$; and three component heavier materials such as $KMgF_3$, $KCaF_3$, $KLuF_4$, BaY_2F_8, $LiYF_4$, $ErYF_4$, $TmYF_4$, and $HoYF_4$, where adding a third heavier component has no effect on optical properties. Luminescence components of CsF, CsCl, CsBr and RbF have been studied [43]. Except for CsBr, which was found to have very low light output at room temperature (but at the same time is the fastest known scintillator with a decay time of 0.07 ns), all other tested scintillators were comparable in light yield to pure CsI. KF, $KMgF_3$ and $KCaF_3$ have fast luminescence components in the VUV/UV region of 140-200 nm and therefore can be detected with the photocathodes developed for BaF_2 [195]. Luminescence of $KMgF_3$ and several other ionic crystals such as KYF_4:Rb, K_2YF_5, and $KLuF_4$ was also recently reviewed [10, 11]. Fast UV emission with a decay constant of about 1.5 ns and more intense than in BaF_2 was obtained for the first two crystals. This fast scintillation is of the same radiative core valence transition (cross-over transition) type as in BaF_2. The problem with most of the crystals studied up to now is that they are not high density scintillators, and only $BaLiF_3$ is a fast (< 1 ns) and slightly heavier (5.2 g/cm^3) crystal than BaF_2. $LiBaF_3$ (or $BaLiF_3$), has a UV photon yield @230-250 nm comparable with that of BaF_2, while it only has a fast (< 1 ns) component [46, 196]. Its density is 4.9 (5.2, resp.) g/cm^3, and its radiation length is 2.3 cm. $LiBaF_3$ can be coupled to a UV sensitive gaseous photodetector with a TMAE vapor or CsI solid photocathode. The presence of lithium in this crystal may be interesting from the point of view of neutron detection. Tested samples in one of the studies [196] contaminated with Pb showed a strong absorption band in the region of 185-205 nm. A strong $BaLiF_3$ emission centered @435-440 nm was reported [8]. There are plans to increase its density by preparing a solution with up to 20% of $PbLiF_3$ [8].
Also, several other materials related to BaF_2 (such as $BaCl_2$, $BaBr_2$, and BaI_2) are being investigated. BaI_2, for instance, has a fast component of 6 ns at 190-340 nm [43] and $BaCl_2$ has a dominating fast component of 1.2 ns [12] (see below).

The family of heavy tetrafluorides (Zn, Zr, Hf, Th) F_4 is also under investigation [8]. An interesting case is that of $LiYbF_4$. The tested samples of this fast and dense (6.09 g/cm^3) crystal demonstrated an actual increase in transmission after a gamma dose of 100 KRad [8]. A newly studied CdI_2 heavy (5.67 g/cm^3) scintillator has a fast 3 ns emission centered at 540 nm and a light yield approximately 10 times that of the fast 3 ns component of CeF_3 [146].

Another recently discovered cerium-doped scintillator is lutetium oxyorthosilicate ($Lu_{2(1-x)}$ $Ce_{2x}(SiO_4)O$ or LSO) [198]. It is a bright (scintillation intensity equal to 75% of that of NaI(Tl)) and dense (7.4 g/cm^3) scintillator with a fast (~40 ns) decay constant. Its peak emission is conveniently located at 420 nm and its radiation length is 1.14 cm.

A heavy material tested for a Cherenkov radiator is $BaYb_2F_8$. It has a density of 6.99 g/cm^3, and was shown to have good radiation resistance up to 10^7 Rad [146]. $BaYb_2F_8$ and other heavy crystals such as CdF_2 (6.33 g/cm^3) and YbF_3 (8.17 g/cm^3) are studied as possible scintillator hosts [8].

Lead carbonate ($PbCO_3$), a heavy (6.6 g/cm^3) scintillator was recently studied [207]. Its scintillation light output is temperature dependent and has many decay components from 3.9 ns up to 1.4 μs at room temperature. Following the rediscovery of lead carbonate, a report appeared on a naturally occuring lead sulfate ($PbSO_4$) in the form of anglesite [199]. In a new study of lead sulfate samples it was measured that its emission, peaking at 335 nm, has two fast decay components of about 1.8 ns (5%), 19 ns (36%) but also long components with decay times of 95 ns (36%) and 425 ns (23%) [200]. The slow component is the dominant one (about 60% of the total light output). Lead sulfate has a density of 6.4 g/cm^3, and is not affected by air or moisture. It is, however, difficult to grow because it decomposes when heated. As a result of this good quality synthetic crystals are still not available at this time.

Yet another interesting development is the study of a new crystal scintillator with an unusually long wavelength of emission. CdS has an intense red emission between 600 and 800 nm [197]. In a preliminary study about 10^4 photoelectrons per MeV were detected when the scintillator was coupled to a silicon photodiode [197]. The material is hard and non-hygroscopic and has a density of 4.8 g/cm^3. It could be expected to be radiation hard due to a long wavelength emission bypassing the usual absorption region caused by color centers. However, a serious disadvantage of this scintillator is its extremely long decay time (amounting to about 4 μs).

$YAlO_3$

A promising new material is cerium doped yttrium aluminate ($YAlO_3$(Ce) or YAP(Ce)) [8, 146, 201, 202]. It has a high relative light yield of about 2.5 times that of BGO or 30-40% that of NaI(Tl), a density of 5.35 g/cm^3, is not hygroscopic, and was measured to have fast emission with a 15-30 ns decay constant as obtained in different studies. Figure I.7.1 shows absorption and luminescence of a 1 mm thick $YAlO_3$ crystal doped with 0.1% by weight of cerium [201].The measured luminescence band at 347 nm is attributed to a 5d - 4f transition in Ce^{3+}. The scintillation decay spectrum for ^{137}Cs gamma-ray excitation is shown for the same samples, with a single 27 ns exponential component. Single-exponentiality of the decay demonstrates the absence of quenching centers in the tested samples. In addition to the fast component of 31 ns (98%), a second slow component of 246 ns (2%) was also seen [202]. The dependence of the light output normalized to NaI(Tl) and the decay constant on cerium doping level is presented in figure I.7.2. Decay time depends only weakly on cerium amounts above the 0.2% point (by weight).

Yttrium aluminate was also reported in a recent preliminary study to be very radiation hard [146]. In figure I.7.3 the transmission spectra of a 4 mm thick $YAlO_3$ sample doped with 0.6 mol% cerium measured before and after a ^{60}Co gamma dose of 10^8Rad are shown. To increase crystal density a program was started to substitute yttrium with ytterbium or other isoelectronic cations [8].

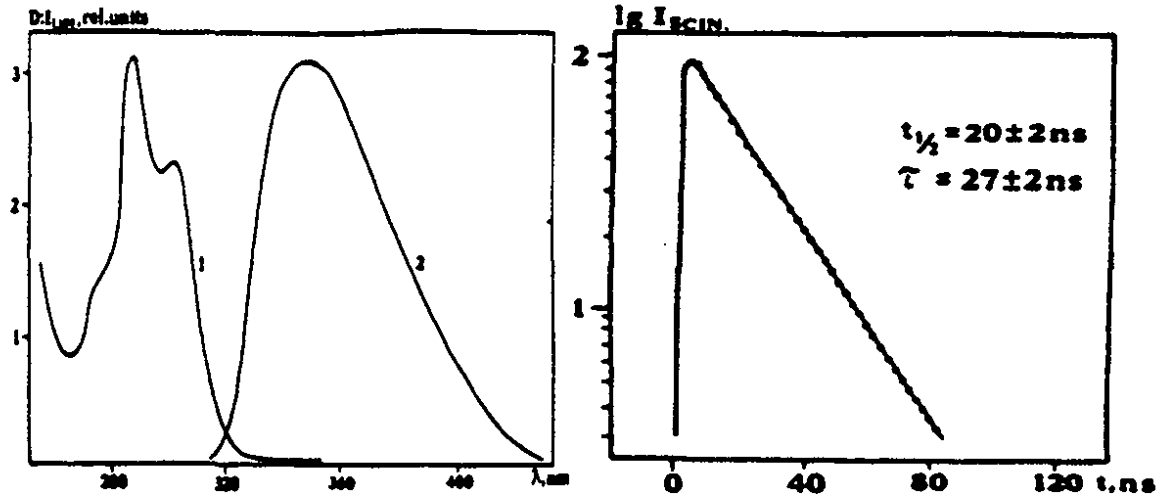

Figure I.7.1: Absorption (1) and luminescence (2) (left spectra) and scintillation decay curve (right spectrum, excited with gamma-rays) of $YAlO_3$:Ce. Measured @300 °K [201].

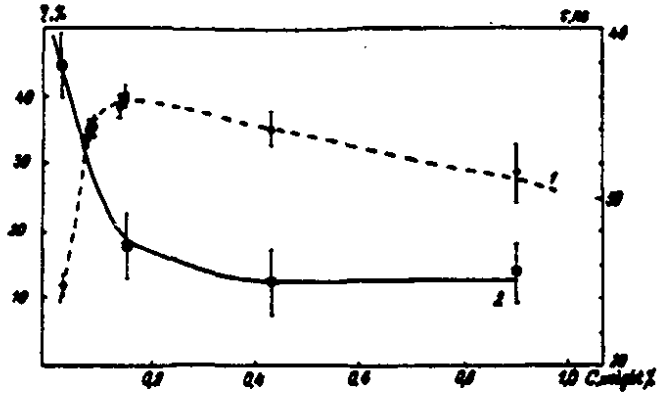

Figure I.7.2: Dependence of scintillation light output (1) and luminescence decay time (2) in $YAlO_3$:Ce on Ce activator doping level C, in % by weight, @ 300°K [201].

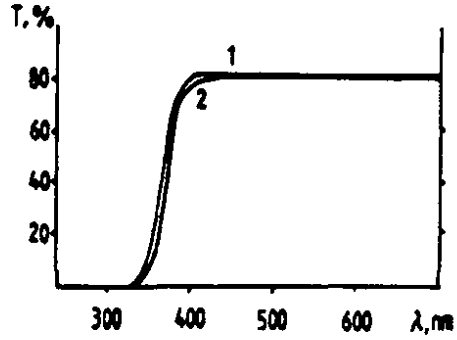

Figure I.7.3: Transmission of a 4 mm thick $YAlO_3$:Ce (0.6 mol%) sample before (1) and after (2) irradiation to a gamma dose of 10^8 Rad [146].

LaF_3

Scintillation properties of a Nd^{3+} doped LaF_3 VUV scintillator were studied recently [89, 203-205]. LaF_3 has a high density of 5.94 g/cm^3, is radiation hard and non-hygroscopic. The optical transmission extends down to a cut-off VUV wavelength at 125 nm. The emissions at 173 nm, 216 nm, and 245 nm (figure I.7.4) are caused by the 5d-4f transitions in Nd^{3+} .The 173 nm emission line has a 6.3 ns decay constant (figure I.7.5 [203], see also correction [204]) and is well matched to gas photocathodes such as TMAE or TEA [89, 203, 204].

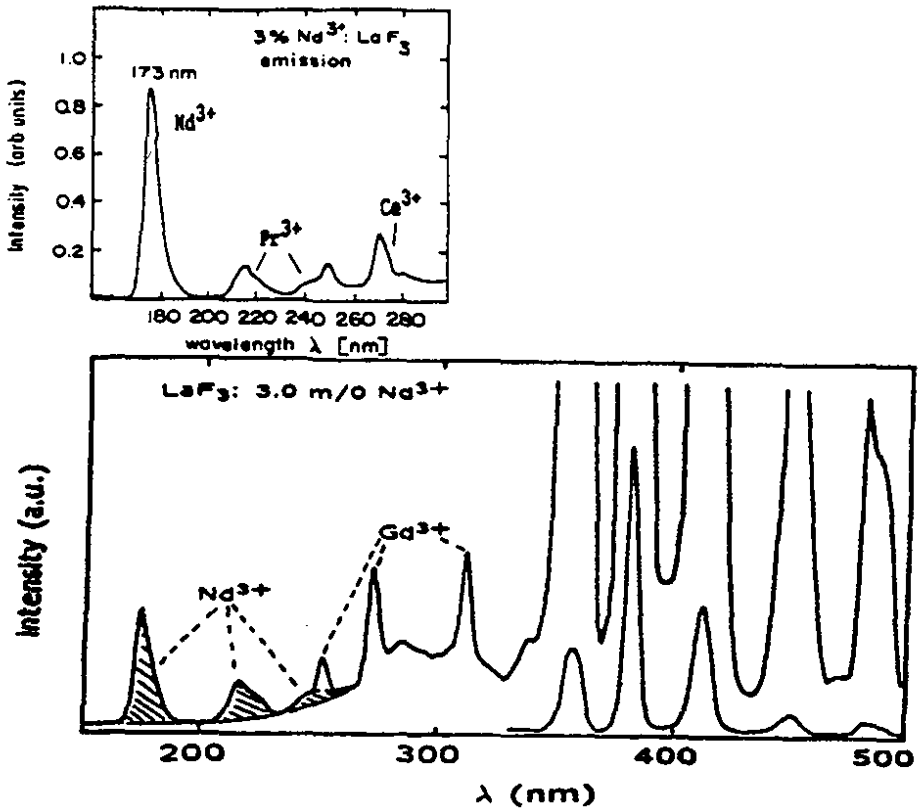

Figure I.7.4: Scintillation emission spectra of $LaF_3:Nd^{3+}$ (3 mol%) when excited with < 35 keV X-rays. (Upper spectrum from refs. [89, 203], see also correction [204]; lower spectrum from ref. [205]). Two intensity scales, different by a factor 25, were used in the lower spectrum in the region between 350nm and 500 nm.

The intensity of this band, originating from the fast allowed 5d - 4f dipole transition (of the same type as observed in the cerium-doped scintillators such as yttrium aluminate), increases with the rise (up to 12 mol%) of the Nd concentration. Presently available samples have contaminats such as Ce, Gd, and Pr, contributing to the emission spectrum and to absorption at wavelengths below 200 nm. At longer wavelengths there are also strong emission lines for 357 nm, 382 nm, 414 nm, and 448 nm from much slower (decay times of the order of milliseconds) 4f -4f transitions in Nd^{3+} (figure I.7.). As in the case of BaF_2, a selectively sensitive photodetector must be used to exploit the fast component only. An example is a PMT or a gas electron multiplier with a CsI photocathode. The samples used in a preliminary test with a TMAE gas photocathode have all shown a very low yield, at least a factor 10 lower than for BaF_2 [53]. It is possible that this poor performance was due to impurities in the samples. It was also reported that it is technically more difficult to grow LaF_3 crystals than BaF_2 crystals [53].

A similar crystal, $LiYF_4:Nd^{3+}$, has comparable light output to $LaF_3:Nd^{3+}$ with the 184 nm emission line corresponding to the 173 nm line in $LaF_3:Nd^{3+}$ [10].

Attempts with cerium-doped lanthanum fluoride have not resulted in a better, more efficient or appreciably faster scintillator than pure CeF_3 [206].

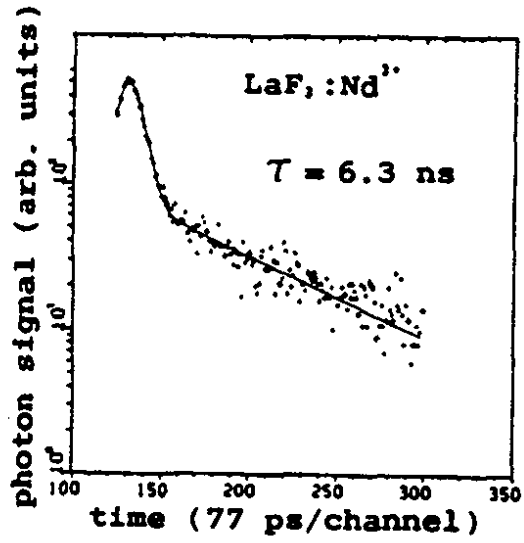

Figure I.7.5: Decay of the light pulse from $LaF_3:Nd^{3+}$ (3 mol%) [203]. The peak on the left is the prompt coincidence peak, not from LaF_3:Nd.

$KMgF_3$

$KMgF_3$ is a relatively light (3.1 g/cm^3) and efficient scintillator emitting fast scintillation centered at 170 nm [195] with a decay constant of under 1.5 ns. The intensity of its cross-luminescence light is almost twice that of BaF_2. Figure I.7.6 shows an overlay of $KMgF_3$ emission and quantum efficiencies of TEA and TMAE vapours [208-210] and the transmission of a 3.1 mm thick $KMgF_3$ crystal [10].

A solid CsI photocathode is also well matched with this emission (see section I.2.2). The tested crystals had detectable europium contamination. The report of a preliminary study in which a $KMgF_3$ crystal was coupled to a wire chamber [211] and a parallel-plate avalanche chamber (PPAC) with a TEA gaseous photocathode [212] demonstrated a sensitivity of only 4.5 and 9 photoelectrons per MeV of deposited energy in a crystal, respectively. In a comparative measurement with BaF_2 coupled to a TMAE gas photocathode in a PPAC the result was 30 photoelectrons for $KMgF_3$ versus 10 photoelectrons for BaF_2 [212]. A new $KLuF_4$ scintillator [208] exhibited a fast cross luminescence @165 nm much like $KMgF_3$, and was also coupled to a gas photodetector [10, 11, 208, 213]. $KLuF_4$ is however less efficient than $KMgF_3$, and is apparently difficult to produce in large quantities [194].

Cesium Fluoride

CsF is a unique fast inorganic crystal of a scintillation efficiency similar to that of pure CsI [156], only much faster. It has high stopping power and it is one of the few known scintillators in Table I without the slow decay constant in the region of many tens to hundreds of ns. The fast component has a decay constant of 3 ns [43] to 5 ns, as obtained in different studies. CsF has a light output of only about 5% of that of NaI(Tl) and is used in

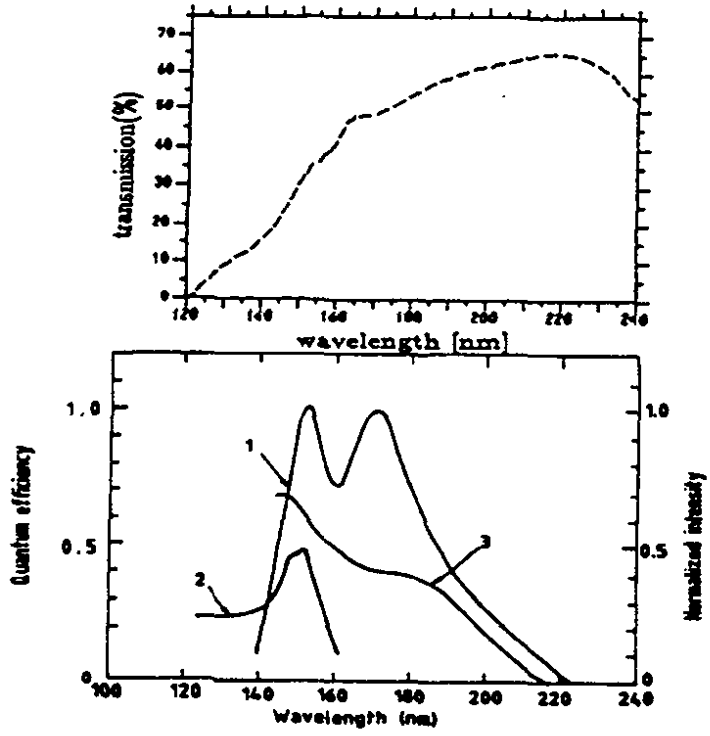

Figure I.7.6: Upper spectrum shows UV transmission of a 3.1 mm thick $KMgF_3$ sample not corrected for Fresnel reflections (adapted from ref. [10]). In the lower emission the spectrum of $KMgF_3$ (1) and the quantum efficiencies of TEA (2) and TMAE (3) vapors are shown (adapted from refs. 209, 210).

nuclear physics or PET [214] applications when count rates are very high and timing resolution is important. With its fast emission CsF was hoped to be a good substitute for BaF_2. It is however not only extremely hygroscopic (requiring hermetic packaging), but also, unfortunately, the few radiation damage tests performed gave only dismaying results, with a substantial damage seen already after a dose of 10 kRad [55]. It is however possible that this poor performance was totally due to impurities in the presently available samples and that this could be improved. In the high radiation dose applications CsF crystals would have to be encapsulated in containers with radiation-hard (quartz) windows.

BGO

BGO is the slowest of the various materials discussed here with its 300 ns decay constant. Until recently it was known to be sensitive to radiation, at least partly due to impurities which were present in the standard production-quality material. Bismuth germanate's main advantage is that it is a very dense scintillator (7.13 g/cm^3). Because of this it is used in PET cameras [215-218] and in particle physics. There is much experience in the production of large quantities of BGO crystals. About 11,500 monocrystals have been grown for the L3 experiment at CERN [219]. Even before, in 1985 the 360-crystal CUSB-II BGO calorimeter at Cornell became operational, marking the first use of BGO in an electromagnetic calorimeter [220, 221]. For high rate/high dose applications, however, BGO

is rather slow and its radiation resistance record is average. Several studies were done of the correlation between radiation damage of BGO and trace impurities in the crystal [222, 223]. Trace concentrations of Cr, Mn, Fe and Pb were found in samples showing substantial radiation damage, while other impurities had less effect. In a recent systematic study of long L3 crystals [224], a model was proposed to explain experimental results. The role of impurities, mainly iron, was shown in the formation of color centers, predominantly in the blue transmission region. Very serious damage was observed after gamma and electron doses of only 500-1000 Rad. Radiation damage saturated after a dose of about 10^4 Rad. Neither the fluorescence spectrum nor the efficiency of luminescent centers was modified [225]. The BGO samples in some studies spontaneously recovered already at room temperature. The accellerated suppression of color centers was obtained by a thermal bleaching treatment (@250 °C, for instance) [172, 223-225], or by an optical treatment in the visible range. Irradiation with a UV Xe lamp (320 nm) causes transmission damage similar to the electron or gamma-ray induced radiation damage. Large crystal-to-crystal variations were observed indicating different levels of color center producing impurities.

An attempt was made to develop crystals with better recovery properties by doping BGO with europium [224, 226-228]. The doped crystals had a much reduced initial damage and recovered faster. Europium allowed de-excitation of trapping centers. The radiation resistance was found to increase with europium doping. Part of the effect could be due to the fact that the fluorescence spectrum in doped samples is pushed to the longer wavelength around 600 nm (red). Only a negligible difference [227, 228] between doped and undoped crystals was observed in the total light yield, and in one case no differences were reported at all [224]. Unfortunately the europium doped crystals exhibited a very long (1.5 ms [228] - 3 ms [224]) afterglow emission due to the dopant's states. This observation thus questions the use of doped crystals for applications; even at medium counting rates.

In a very recent paper [229], a production of highly radiation resistant samples grown with a new version of the Bridgman technique was reported. The optical transmission of a 2.5 cm x 2.5 cm x 1 cm sample at a peak emission of 480 nm degraded by no more than 10% when irradiated with ^{60}Co gamma-rays to a dose of 1.03×10^8 Rad at a high dose rate of 720 kRad per hour (figure I.7.7). No correction for surface reflection was applied. The transmission decreased slightly and the crystals turned grayish already after a dose of 12 kRad (after 1 minute of irradiation!), but no further change took place up to the total dose of 103 MRad. No transmission recovery after irradiation was observed at room temperature. The annealing at 400 °C for two hours had led to a complete recovery of crystal transmittance. The samples did not exhibited the photochromic effect (yellowish discoloration) typically seen in regular BGO samples after being exposed to UV light or daylight. Figure I.7.7 also includes a comparison of the transmission losses observed in the small samples produced in that study [229] with the 1 cm x 1 cm x 2 cm samples produced for the L3 experiment at CERN [227]. The authors speculate that this dramatic improvement in radiation resistance is due to crystal regularization and lower concentration of non-stoichiometric defects in the crystals produced by the new technique. This observation may be applicable to many other crystal scintillators. It was also found that the new BGO samples grown for that study have increased radiation resistance to 10^7 Rads [146] (figure I.7.8). The authors have pointed out that the radiation limit they recorded for the

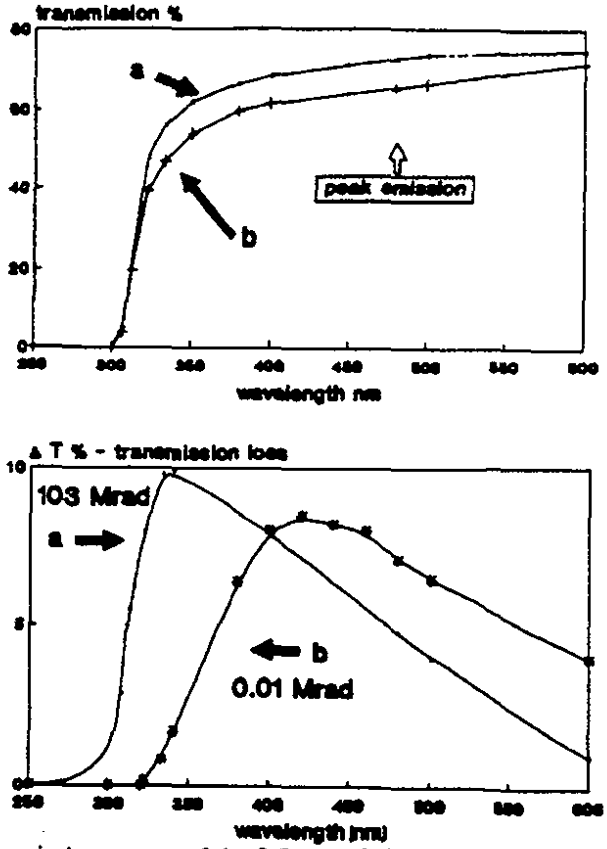

Figure I.7.7: Upper: the transmission curves of the 2.5 cm x 2.5 cm x 1 cm BGO crystal samples before (a) and after (b) gamma irradiation to a dose of 103 MRad; Lower: the comparison of transmission losses for the new samples (a) and the L3 1 cm x 1 cm x 2 cm thick samples [229].

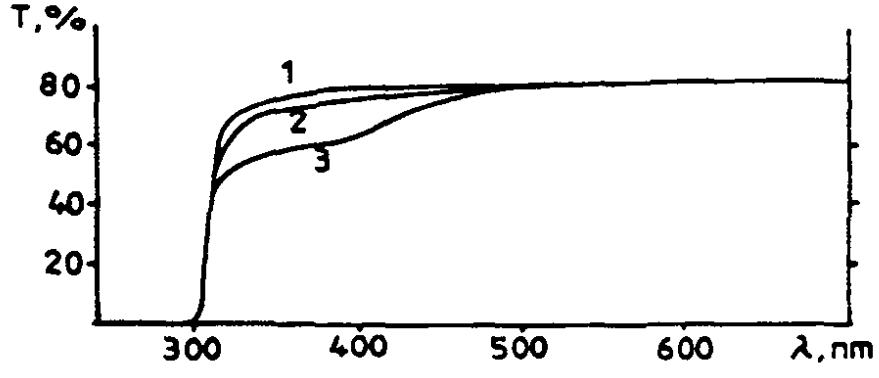

Figure I.7.8: Transmission spectra of the 5 mm thick BGO sample before (1) and after ^{60}Co gamma doses of 10^7 Rad (2) and 10^8 Rad (3) [146].

BGO samples was not final. Rather the technologically achieved level of radiation resistance in their work was due to limitations related to purity/price considerations. The BGO and other samples grown in that study had an impurity level of about 10^{-3}.

In summary, it appears that the radiation resistance of BGO could be improved and highly radiation resistant large crystals may be available. The main drawback, however, is

that an extremely long decay constant remains, preventing the compound's use in high rate applications.

Two new efficient scintillators with significantly fast emission were found during a recent survey of over 400 different crystals [12]: $BaCl_2$ and $CeCl_3$ (figure I.7.9). Neither of them, however, is a high density scintillator (ρ = 3.90 g/cm^3). Two more heavy scintillators, CuI (ρ = 5.62 g/cm^3) and Yb_2O_3 (ρ = 9.17 g/cm^3), were tested in the same study and exhibited very fast scintillation with a major decay component < 0.5 ns. Their light output, however, was rather low (equal to 7% and 1.3% that of BGO, respectively).

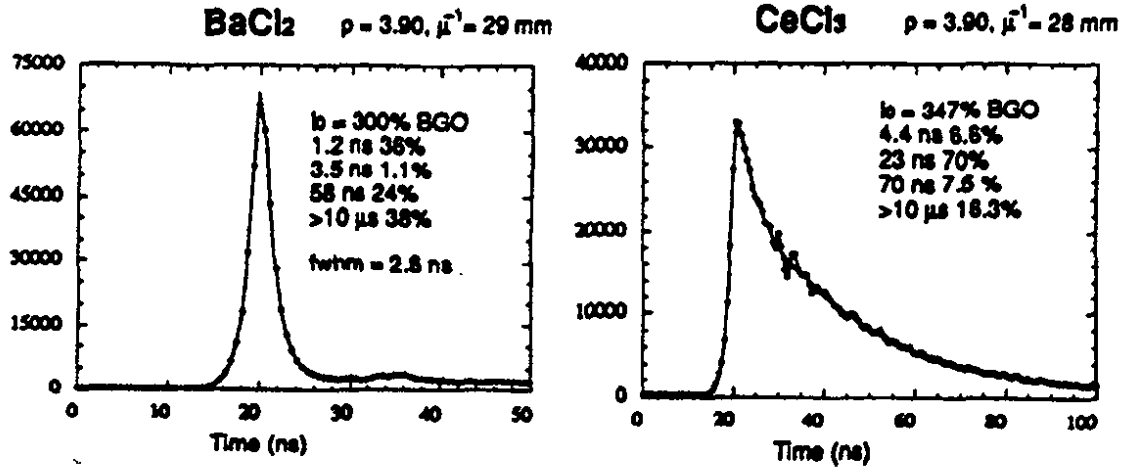

Figure I.7.9: Decay curves for two efficient scintillators, $BaCl_2$ and $CeCl_3$ [12], when excited with 0.5 ns pulses of 20 keV X-rays. Luminescence intensity is also given, as compared to BGO.

Scintillating Glasses

Even the fastest known scintillating glasses (doped with cerium oxide) are still relatively quite slow [230]. GS1 glass, for instance, has a decay time constant of the order of 55 ns [231]. Even worse, new measurements indicate the presence of a slow component extending up to 1 ms [232]. The light yield of cerium doped glasses increases with cerium content up to about 6%, but the attenuation of scintillation light also increases [233]. New scintillating glasses with improved light yield and homogeneity are constantly under development [234]. A new scintillating glass, KRS-6 [7], is currently under investigation. The radiation resistance of scintillating glasses is still not very good, despite the fact that they are much more radiation hard than lead glasses, and that their transmission properties are only moderately altered after a proton dose of 10^5 Rad [235]. Cerium doping greatly improves radiation resistance of glasses in general, and lead glasses in particular [236]. A typical doping level is 1-2 weight % of CeO_2. Irradiations with gamma-rays and reactor neutrons have shown that some of the optical windows made with cerium doped glasses can survive doses as high as 10^8 Rads and above [237]. The suppression of the radiation-induced discoloration is due to the Ce^{4+} ion, a powerful electron acceptor. Ce^{4+} serves to remove the radiation-created free electrons trapped in the glass, preventing the formation of

color centers. Radiation damage due to color centers can be annealed not only by heating, but also by the use of violet-blue light sources [238].

It was suggested [6, 8, 239] that heavy fluoride glasses can have characteristics similar to the crystalline fluorides. They are excellent hosts for rare earth and cerium doping may result in scintillating glasses superior to oxide glasses. Some glasses contain BaF_2 as the major constituent and are expected to show the same type of fast luminescence transition. They have increased radiation resistance as compared to other glasses. Additionally, fluoride glasses are excellent media for fiber fabrication. Fluoride fibers have low transmission losses in the wavelength region above 2 μs Scintillator research can profit from the available body of data on fluoride glasses. A sublimation technique, for instance, was developed to reduce impurities such as iron and copper in the fluoride fiber material [240]. This method may be applicable in the scintillating fluoride glass production.
The main anticipated difficulty is the selection of a proper host glass. The need is for a glass that would have a strong UV transparency to allow for transmission of short wavelength scintillation light. First cerium doped samples of heavy fluoride glasses were recently prepared in Europe, and a program of research is underway [8]. These materials are potentially quite interesting because of cost considerations for large detectors.

I.8. Summary

In short summary BaF_2 and CeF_3 as scintillators and PbF_2 as a Cherenkov radiator seem to be at the present time the most promising radiation resistant and fast materials for high intensity applications. The lack of a slow component, a conveniently located emission spectrum, and a higher density make CeF_3 a more promising candidate, but production feasibility of large good quality crystals has still to be demonstrated. Also, for some applications even a 25 ns decay constant can be considered "slow". Possible mass production of large (25-50 cm) good quality crystals of barium fluoride is actively investigated and, provided that a solution will soon be found, this crystal scintillator seems to be the most serious available choice for high rate applications in the future large detectors.

One can expect that the present vigorous research on high density, fast and radiation hard crystal scintillators will continue. It is quite possible that many new and improved practical materials will appear quite soon, and it would not be surprising if some of the scintillators listed in Table I will prove to be better choices. In a recent review Van Eijk [11] concluded that in the coming years the emphasis of scintillator research will be on the two groups of materials exhibiting either cross luminescence (fast scintillators) or materials with the 5d-4f transition luminescence (high light yield in the visible range). In general, developments in the technology of crystal production will lead to a marked improvement in the quality of crystals grown, dramatically reducing the level of impurities and defects. This in turn will permit the creation of efficient and fast crystal scintillators which will be able to survive the multi-MRad radiation doses to be encountered in the future high energy physics and nuclear physics experiments.

I.9. Acknowledgements

First , I would like to thank all the other authors-contributors to this instrumentation volume and especially the Editor, Dr Fabio Sauli, for their infinite patience in waiting for my late-coming contribution. Discussions with Dr Craig Woody from Brookhaven, who provided me with much information on BaF_2, CsI and PbF_2, proved to be particularly enlightening, and I am very thankful to Craig for his friendly help. Dr Ren-Yuan Zhu provided crucial information on the status of the BaF_2 GEM-SSC project by taking his time and continuously informing me about the latest technical developments. Finally, I would like to thank my daughter, Dorota, who spent several long days during the holiday season helping me with the manuscript.

As I was writing this review a constant flow of new material kept coming in, adding yet more data to the enormous library I was already using. I found myself having to fight the temptation to include them all. I would like to thank all those authors for sending in reports on their contributions to detector research and apologize to all those I did not have the time to include in my paper.

I.10. References

1. D. E. Groom, *Radiation Levels in SSC Detectors*, SSC-201, January, 1989; D. E. Groom, *Radiation Levels in SSC Detectors*, contribution to the *ECFA Study Week on Instrumentation for High-Luminosity Colliders*, Barcelona, 14-21 September 1989, CERN 89-10, ECFA 89-124; D. E. Groom et al., *Radiation Levels in the SSC Interaction Regions, Erratum*, SSCL-285, 19 July 1990.
2. G. R. Stevenson, *New Dose Calculations for LHC Detectors*, contribution to the *LHC Workshop*, Aachen, October 1990, CERN 90-10, ECFA 90-133, Vol. III, p. 565.
3. E. Lorenz, *Crystal Calorimeters for Future High Luminosity Hadron Colliders*, contribution to the *ECFA Study Week on Instrumentation for High-Luminosity Colliders*, Barcelona, 14-21 September 1989, CERN 89-10, ECFA 89-124, Vol. 2, p. 621.
4. J. Bensinger et al., *Electron Identification and Implications in SSC Detector Design*, SSCL-287, SDC-39, UCLA-HEP-90-004, May 1990.
5. D. Green, *Physics Requirements for LHC/SSC Calorimetry*, presented at the *Calorimetry and High Energy Physics Conference*, Capri, Italy, October 14-18, 1991, FERMILAB-Conf-91/281.
6. P. Lecoq and M. Schneegans, *A Fast and Radiation Hard Crystal Calorimeter for the LHC*, contribution to the *LHC Workshop*, Aachen, October 1990, CERN 90-10, ECFA 90-133, Vol.III, p. 374.
7. J. Colas et al., *Calorimetry at the LHC*, contribution to the *LHC Workshop*, Aachen, October 1990, CERN 90-10, ECFA 90-133, Vol.I, p. 370.
8. P. Lecoq et al., *Progress and Prospects in the Development of New Scintillators for Future High Energy Physics Experiments*, presented at the *5th Pisa Meeting on Advanced Detectors*, Isola d'Elba, June 1991, CERN-PPE/91-124, August 6, 1991.
9. P. Schotanus, *Recent Developments in Solid Scintillator Research, New Materials and*

Research Trends, presented at the *International Symposium LUMDETR '91*, October 9-12, 1991, Riga, Latvia.

10. P. Dorenbos et al., *Photon Yields And Decay Times of Cross Luminescence in Ionic Crystals*, presented at the *1991 IEEE Nuclear Science Symposium*, Santa Fe, New Mexico, November 5-9, 1991.
11. C. W. E. Van Eijk, *Fast Scintillators And Their Applications*, presented at the *International Symposium LUMDETR '91*, October 9-12, 1991, Riga, Latvia.
12. S. E. Derenzo et al., *X-Ray Fluorescence Measurements of 412 Inorganic Compounds*, presented at the *1991 IEEE Nuclear Science Symposium*, Santa Fe, New Mexico, November 5-9, 1991.
13. G. Finsel et al., *Nucl. Instr. and Meth.* **A290** (1990) 450.
14. R. DeSalvo, *Hybrid Photomultiplier Tubes*, CERN LAA/HC/89-004.
15. D. Winn et al., *Properties of Photodetectors for SSC Scintillating Calorimeters*, Proceedings of the *Symposium on Detector Research and Development for the Superconducting Super Collider*, 15-18 October, 1990, Fort Worth, Texas, World Scientific, 1991, p. 419.
16. R. DeSalvo et al., *First Results on the Hybrid Photocathode Tube*, CERN-LAA-HC/91-, CERN-PPE/91-.
17. A. M. Gorin te al., *Nucl. Instr. and Meth.* **A310** (1991) 251.
18. L. K. van Geest and K. W. J. Stoop, *Nucl. Instr. and Meth.* **A310** (1991) 261.
19. S. Nagamiya et al., *Construction of a Highly Segmented High-Resolution TOF System*, in Proc. *Fourth Workshop on Experiments and Detectors for a Relativistic Heavy Ion Collider*, Brookhaven, July 2-7 1990, BNL-52262, p. 433.
20. J. P. Vivien, *Boules et Chateaux de Cristal: Detecteurs Multicompteurs* $\gamma 4\pi$, report CRN/PN83-25, Strasbourg, 1983;
    F.A. Beck, in Proc. *Int. Conf. on Instrumentation for Heavy Ion Nuclear Research*, Oak Ridge, TN, USA, 22-25 Oct. 1984, ed. D. Shapira (Harwood Academic, 1985) p. 129.
21. K. Wisshak et al., *Nucl. Instr. and Meth.* **A292** (1990) 595;
    Nucl. Instr. and Meth. **A299** (1990) 60.
22. R. Novotny, *IEEE Trans. Nucl. Sci.* **NS-38** (1991)379;
    Neutral Meson Detection With the Photon Spectrometer TAPS, presented at the *1991 IEEE Nuclear Science Sumposium*, Santa Fe, New Mexico, November 5-9, 1991.
23. R-Y. Zhu, *Limits to the Precision of Electromagnetic Calorimeters*, invited talk at the *First International Conference on Calorimetry in High Energy Physics*, Fermilab, 29 October-1 November 1990, in Proceedings, p. 25, World Scientific 1991.
24. H. B. Newman, *Precision Electromagnetic Calorimeters* for *The Superconducting Supercollider*, Proceedings of the *Symposium on Detector Research and Development for The Superconducting Super Collider*, Fort Worth, October 15-18, 1990, in Proceedings, p. 15, World Scientific, 1991.
25. *A Precision* BaF_2 *Crystal Calorimeter for the Superconducting Super Collider, Research and Development Proposal and Progress Report*, The BaF_2 Collaboration, submitted to the SSC Laboratory, September 1991.
26. P. Schotanus et al., *Nucl. Instr. and Meth.* **A238** (1985) 564.
27. M. Suffert and G. Charpak, *Influence of the Temperature on the Response of the Fast*

Component of BaF_2 Scintillators coupled to a Photomultiplier or a Photosensitive Wire Chamber, CERN-EP Internal Report 86-03 (1986).
28. S. Kubota et al., *Phys. Stat. Sol. (b)* **139** (1987) 635.
29. H. Kobayashi et al., *Nucl. Instr. and Meth.* **A270** (1988) 106.
30. C. L. Melcher et al., *IEEE Trans. Nucl. Sci.* **NS-36** (1989) 1188.
31. K. Wisshak et al., *Nucl. Instr. and Meth.* **A259** (1987) 583.
32. D. F. Anderson and D. C. Lamb, *Nucl. Instr. and Meth.* **A260** (1987) 377.
33. Z. Y. Wei et al., *Nucl. Instr. and Meth.* **B61** (1991) 61.
34. C. Woody et al., *Radiation Damage in BaF_2 Crystals*, presented at the *IEEE 1991 Nuclear Science Symposium*, Santa Fe, New Mexico, November 5-9, 1991.
35. M. Laval et al., *Nucl. Instr. and Meth.* **206** (1983) 169.
36. M. Moszynski et al., *Nucl. Instr. and Meth.* **226** (1984) 534.
37. K. Ishii et al., *Nucl. Instr. and Meth.* **A253** (1986) 128.
38. P. Sperr, *Nucl. Instr. and Meth.* **A254** (1987) 635.
39. J. R. Votaw et al., *IEEE Trans. Nucl. Sci.* **NS-35** (1988) 712.
40. S. Kubota et al., *Nucl. Instr. and Meth.* **A242** (1986) 291.
41. P. Schotanus et al., *Nucl. Instr. and Meth.* **A259** (1987) 586.
42. C. Shi et al., *J. Lumin.* **40/41** (1988) 189.
43. S. Kubota et al., *Nucl. Instr. and Meth.* **A289** (1990) 253.
44. Yu. M. Aleksandrov et al., *Sov. Phys. Sol. State.* **26** (9) (1984) 1734.
45. Ya. A. Valbis et al., *JETP Lett.* **43** (4) (1985) 172.
46. P. A. Rodnyi et al., *J. of Luminescence* **47** (1991) 281.
47. P. Schotanus et al., *IEEE Trans. Nucl. Sci.* **NS-34** (1987) 272.
48. W. H. Wong et al., *IEEE Trans. Nucl. Sci.* **NS-34** (1984) 381.
49. C. I. Petridou and C. Woody, *Scintillation Properties of Barium Fluoride Crystals*, Technical Note E787-76, April 1985.
50. S. Majewski and D. Anderson, *Nucl. Instr. and Meth.* **A241** (1985) 76.
51. Y. C. Zhu et al., *Nucl. Instr. and Meth.* **A244** (1986) 577.
52. W. Klamra et al., *Nucl. Instr. and Meth.* **A254** (1987) 85.
53. P. Bruyndonckx et al., *Nucl. Instr. and Meth.* **A310** (1991) 107.
54. T. Francke and M. Suffert, *Nucl. Instr. and Meth.* **A276** (1989) 263.
55. S. Majewski and M. K. Bentley, *Nucl. Instr. and Meth.* **A260** (1987) 373.
56. B. K. Sinha and R. Bhattacharya, *Nucl. Instr. and Meth.* **A276** (1989) 237.
57. V. Yanovsky et al., *Nucl. Phys. B (Proc. Suppl.)* **23A** (1991) 347.
58. K. Wisshak and F. Kaeppeler, *Nucl. Instr. and Meth.* **227** (1984) 91.
59. K. Wisshak et al., *Nucl. Instr. and Meth.* **A251** (1986) 101.
60. G. Graham and H. Yamamoto, *Nucl. Instr. and Meth.* **A307** (1991) 240.
61. T. K. Lewellen et al., *Improving the Performance of the SP-3000 PET Detector Modules*, presented at the *1991 IEEE Nuclear Science Symposium*, Santa Fe, New Mexico, November 5-9, 1991.
62. M. Kobayashi et al., *Nucl. Instr. and Meth.* **A305** (1991) 401.
63. P. Schotanus and P. Dorenbos, *Some Aspects of the Application of* presented at the *X-th International Seminar on High Energy Physics Problems, Relativistic Nuclear Physics and Quantum Chromodynamics*, September 24-29, 1990, Dubna, Russia.
64. H. Yamamoto, *Resolution of EM Calorimeter Made of BaF_2 Crystal*, Proceedings of

the *First International Conference on Calorimetry in High Energy Physics*, Fermilab, 29 October-1 November 1990, World Scientific 1991, p. 286.
65. G. Tzanakos et al., *IEEE Trans. Nucl. Sci.* **NS-37** (1990) 1599.
66. D. F. Anderson et al., *Nucl. Instr. and Meth.* **217** (1983) 217;
Nucl. Instr. and Meth. **225**(1984)8;
Nucl. Instr. and Meth. **228**(1984)33.
67. D. C. Imrie et al., *Nucl. Instr. and Meth.* **A297** (1990) 179.
68. J. Seguinot et al., *Nucl. Instr. and Meth.* **A297** (1990) 133.
69. D. C. Imrie et al., *Nucl. Instr. and Meth.* **A310** (1991) 122.
70. G. Charpak et al., *Nucl. Instr. and Meth.* **A307** (1991) 63.
71. V. Dangendorf et al., *Nucl. Instr. and Meth.* **A308** (1991) 519.
72. D. F. Anderson et al., *Technical Memo on New Results on CsI Photocathodes: Enhancement and Aging*, Fermilab TM-1753, September 1991.
73. P. Fonte et al., *Nucl. Instr. and Meth.* **A310** (1991) 140.
74. V. Peskov and A. Zichichi, *A New Scintillator: $LiBaF_3$, Preliminary Tests*, presented at the *Workshop on New Technologies for Supercolliders*, Erice, Sicily, 15-20 September 1990, CERN-PPE/91-139, 3 June 1991.
75. S. Kwan and D. F. Anderson, *Nucl. Instr. and Meth.* **A309** (1991) 190.
76. G. Charpak et al, *Study of BaF_2 Calorimeters in Future Hadron Colliders*, presented at the *8th Workshop of the INFN-ELOISATRON Project on Perspectives for New Detectors in Future Supercolliders*, Erice, 17-24 October 1989, CERN-EP/90-41, CERN/LAA/EC/90-005, 4 April 1990.
77. E. Dafni, *Nucl. Instr. and Meth.* **A254** (1987) 54.
78. W. Klamra et al., *Nucl. Instr. and Meth.* **A265** (1988) 485.
79. V. Yanovsky and P. Kozma, *Nucl. Instr. and Meth.* **A276** (1989) 659.
80. P. Kozma and C. Hradecny, *Nucl. Instr. and Meth.* **A254** (1987) 639.
81. E. Lorenz et al., *Nucl. Instr. and Meth.* **A249** (1986) 235.
82. J. B. Czirr and E. Catalano, *Nucl. Instr. and Meth.* **143** (1977) 487.
83. R. C. Tailor et al., *IEEE Trans. Nucl. Sci.* **NS-33** (1986) 243.
84. C. L. Woody et al., *IEEE Trans. Nucl. Sci.* **NS-36** (1989) 536.
85. P. A. Rodnyi et al., *Spectra and Models of Luminescence of Barium-Based Fluorides*, Internal Report IAE-4963/11, I. V. Kurchatov Institute of Atomic Energy, Moscow, 1989.
86. R. Visser et al., *IEEE Trans. Nucl. Sci.* **NS-38** (1991) 178.
87. P. Dorenbos et al., *Nucl. Instr. and Meth.* **A310** (1991) 236.
88. P. Schotanus et al., *Nucl. Instr. and Meth.* **A281** (1989) 162.
89. P. Schotanus et al., *IEEE Trans. Nucl. Sci.* **NS-36** (1989) 132.
90. A. Lempicki et al., *Inorganic Scintillation Research*, Boston University, unpublished report, 1990.
91. T. Shimizu et al., *IEEE Trans. Nucl. Sci.* **NS-33** (1986) 370.
92. S. Kubota et al., *IEEE Trans. Nucl. Sci.* **NS-34** (1987) 438.
93. S. Kubota et al., *Nucl. Instr. and Meth.* **A270** (1988) 598.
94. S. Kubota et al., *Nucl. Instr. and Meth.* **A285** (1989) 436.
95. D. F. Heath and Paul A. Sacher, *Appl. Opt.* **5** (1966) 937.
96. M. Murashita et al., *Nucl. Instr. and Meth.* **A243** (1986) 67.
97. A. J. Caffrey et al., *IEEE Trans. Nucl. Sci.* **NS-33** (1986) 230.

98. A. Murakami et al., *Nucl . Instr. and Meth.* **A301** (1991) 435.
99. T. Murakami et al., *Nucl. Instr. and Meth.* **A253** (1986) 163.
100. F. Takasaki, *A Note on Radiation Damage to BaF_2 Crystals*, SSC-SR-1033, p. 299, June 1988.
101. R. Zhu, CalTech, *private communication.*
102. P. Schotanus et al., *Nucl. Instr. and Meth.* **A272** (1988) 917.
103. P. K. Chakraborty and K. V. Rao, J. *Mater. Sci.* **22** (1987) 587.
104. C. L. Woody, *A Report on Radiation Damage in Barium Fluoride to the GEM Collaboration*, unpublished, Brookhaven National Laboratory, December 4, 1991, and references quoted therein.
105. A. Badala et al., *Nucl. Instr. and Meth.* **A306** (1991) 283.
106. R. Novotny et al., *Nucl. Instr. and Meth.* **A262** (1987) 340.
107. C. Agodi et al., *Nucl. Instr. and Meth.* **A269** (1988) 595.
108. D. T. Baran and W. A. Kolasinski, *The Response of Barium Fluoride to Energetic Heavy Ions*, contribution to the *1990 IEEE Nuclear Science Symposium*, October 22-27, 1990, Crystal City VA, in Conference Record IEEE-90CH2975-1, Vol. 1, p.169.
109. H. J. Karwowski et al., *Nucl. Instr. and Meth.* **A245** (1986) 207.
110. T. Matulewicz et al., *Nucl. Instr. and Meth.* **A274** (1989) 501.
111. P. E. Koehler et al., *Nucl. Instr. and Meth.* **A265** (1988) 596.
112. W. Karle et al., *Nucl. Instr. and Meth.* **A271** (1988) 507.
113. T. Matulewicz et al., *Nucl. Instr. and Meth.* **A289** (1990) 194.
114. J. Clayton et al., *Nucl. Instr. and Meth.* **A305** (1991) 116.
115. R. Fonte et al., *Nucl. Instr. and Meth.* **A307** (1991) 80.
116. O. Schwalb et al., *Nucl. Instr. and Meth.* **A295** (1990) 191.
117. B. Herskind, *Nucl. Phys.* **A447** (1985) 395c.
118. The detector was prepared at the Niels Bohr Institute under J. J. Gaardhoje. (*Private communication* from M. Moszynski, Strasbourg.)
119. R-Y. Zhu, *Nucl. Instr. and Meth.* **A306** (1991) 145.
120. J. Bialkowski et al., *Nucl. Instr. and Meth.* **A287** (1990) 532.
121. S. I. Ziegler et al., *IEEE Trans. Nucl. Sci.* **37** (1990) 574.
122. Z. H. Cho et al., *IEEE Trans. Nucl. Sci.* **NS-37** (1990) 842.
123. M. M. Ter-Pogossian et al., *IEEE Trans. Med. Imaging.* **MI-1**(1982), no. 3.
124. T. K. Lewellen et al., *IEEE Trans. Nucl. Sci.* **NS-35** (1988) 665.
125. B. Mazoyer et al., *IEEE Trans. Nucl. Sci.* **NS-37** (1990) 778.
126. A. N. Bice et al., *IEEE Trans. Nucl. Sci.* **NS-37** (1990) 696.
127. P. Schotanus et al., *Nucl. Instr. and Meth.* **A269** (1988) 377.
128. P. Mine et al., *Nucl. Instr. and Meth.* **A269** (1988) 385.
129. J. E. Bateman et al., *Nucl. Instr. and Meth.* **A283** (1989) 436.
130. R. W. Hollander et al., *Nucl. Instr. and Meth.* **A283** (1989) 448.
131. J. Suckling et al., *IEEE Trans. Nucl. Sci.* **NS-38** (1991) 703.
132. J. Suckling et al., *Nucl. Instr. and Meth.* **A310** (1991) 465.
133. K. Wells et al., *Current Status of the ICR/RAL BaF_2-TMAE Positron Camera*, presented at the *1991 IEEE Nuclear Science Symposium*, Santa Fe, New Mexico, November 5-9, 1991.
134. B. Guerard et al., *Nucl. Instr. and Meth.* **A310** (1991) 116.

135. C. L. Melcher and J. S. Schweitzer, *IEEE Trans. Nucl. Sci.* **NS-35** (1988) 876.
136. D. F. Anderson, *IEEE Trans. Nucl. Sci.* **NS-36** (1989) 137.
137. D. F. Anderson, *Nucl. Instr. and Meth.* **A287** (1990) 606.
138. L. E. Elias et al., *Phys Rev.* **8** (1973) 4989.
139. Yu. M. Aleksandrov et al., *Solid State Phys.* **29** (1987) 1896.
140. S. Kubota et al., *Mechanism of Luminescence from CeF_2 Excited by VUV Photons and Ionizing Charged Particles*, in *Radiation Detectors And Their Uses*, KEK Report 89-5, July 1989, p. 104.
141. W. W. Moses and S. E. Derenzo, *IEEE Trans. Nucl. Sci.* **NS-36** (1989) 173.
142. W. W. Moses and S. E. Derenzo, *Nucl. Instr. and Meth.* **A299** (1990) 51.
143. A. J. Wojtowicz et al., *Cerium Compounds as Scintillators*, contribution to the *1991 IEEE Nuclear Science Symposium*, Santa Fe, New Mexico, November 5-9, 1991.
144. M. Kobayashi et al., *Cerium Fluoride, a Highly Radiation-Resistive Scintillator*, KEK Preprint 90-140, November 1990, submitted to *Nucl. Instr. and Meth.*
145. M. Kobayashi et al., *R&D on Compact, Fast and Radiation-Hard Materials for Total Absorption EM-Calorimeters*, Presented at the Workshop *"Physics at UNK"*, Serpukhov, USSR, September 25-28, 1990, KEK Preprint 90-130.
146. G. I. Britvich et al., *Nucl. Instr. and Meth.* **A308** (1991) 509.
147. H. Ishibashi, *Nucl. Instr. and Meth.* **A294** (1990) 271.
148. T. Utsu and S. Akiyama, *J. of Crystal Growth* **109** (1991) 385.
149. M. Kobayashi et al., *Nucl. Instr. and Meth.* **A306** (1991) 139.
150. M. Kobayashi et al., *Nucl. Instr. and Meth.* **B61** (1991) 491.
151. H. Ishibashi et al., *IEEE Trans. Nucl. Sci.* **NS-36** (1989) 170.
152. K. Takagi and T. Fukuzawa, *Appl. Phys. Lett.* **42** (1983) 43.
153. C. L. Melcher et al., *IEEE Trans. Nucl. Sci.* **NS-38** (1991) 506.
154. C. L. Melcher et al.,*IEEE Trans. Nucl. Sci.* **NS-37** (1990) 161.
155. S. Kubota et al., *Nucl. Instr. and Meth.* **A268** (1988) 275.
156. B. K. Utts and S. E. Spagno, *IEEE Trans. Nucl. Sci.* **NS-37** (1990) 134.
157. C. L. Woody et al., *IEEE Trans. Nucl. Sci.* **NS-37** (1990) 492.
158. P. Schotanus et al., *IEEE Trans. Nucl. Sci.* **NS-37** (1990) 177.
159. S. Keszthelyi-Landori et al., *Nucl. Instr. and Meth.* **A303** (1991) 374.
160. R. B. Murray and F. J. Keller, *Phys. Rev.* **137** (1965) A942.
161. J. B. Birks, *The Theory And Practice of Scintillation Counting*, (Pergamon, New York, 1964).
162. T. Towyama et al., *J. Phys. Soc. Japan.* **24** (1968) 1133.
163. E. Blucher et al., *Nucl. Instr. and Meth.* **A249** (1986) 201.
164. E. Nordberg, *Performance of the CLEO II CsI Calorimeter*, presented at the *Workshop on Physics and Detecetors for KEK Assymetric B-Factory*, April 15-18, 1991.
165. *Proposal For a High Resolution Spectrometer For Neutral Mesons*, Los Alamos, December 1989.
166. W. G. Gong et al., *Nucl. Instr. and Meth.* **A287** (1990) 639.
167. C. L. Woody et al., *Radiation Damage in Undoped CsI and CsI(Tl)*, presented at the *1991 IEEE Nuclear Science Symposium*, Santa Fe, New Mexico, November 5-9, 1991.
168. J. A. Kierstead et al., *Progress Report on Generic R&D on Undoped Cesium Iodide*,

unpublished, Brookhaven National Laboratory, December 19, 1990.
169. M. Kobayashi and S. Sakuragi, *Nucl. Instr. and Meth.* **A254** (1987) 275.
170. O. Barnouin et al., *Nucl. Instr. and Meth.* **A299** (1990) 382.
171. D. Renker, *Radiation Damage of CsI(Tl) Crystals*, in the proceedings of the *ECFA Study Week on Instrumentation for High-Luminosity Hadron Colliders*, CERN 89-10, ECFA 89-124, November 1989, p. 601.
172. G. J. Bobbink et al., *Nucl. Instr. and Meth.* **227** (1984) 470.
173. Ch. Bieler et al., *Nucl. Instr. and Meth.* **A234** (1985) 435.
174. S. Schloegl et al., *Nucl. Instr. and Meth.* **A242** (1985) 89.
175. R. T. Williams, *SPIE radiation Effects in Optical Materials* **541** (1985) 25.
176. C. M. Rozsa et al., *Measurements of CsI (pure) Performance*, in proceedings of the *ECFA Study Week on Instrumentation for High-Luminosity Hadron Colliders*, CERN 89-10, ECFA 89-124, November 1989, p. 599.
177. T. Browder and M. Witherel, *Limits on Backgrounds for Detectors at a B-Factory*, report CLNS 90-1019.
178. J. Kirkby, *The Tau-Charm Factory*, CERN-EP/89-140.
179. R. S. Hayano et al., *Two-Arm Electron/Photon/Hadron Spectrometer, TALES Collaboration, Letter of Intent*, KEK Preprint 90-163, December 1990.
180. A. Hershcovitch et al., *Proposal to Develop a High Resolution Electromagnetic Calorimeter for RHIC Using Undoped Cesium Iodide Crystals*, unpublished, BNL, September 9, 1991;
Crystal Development for EM Calorimetry at RHIC, A Progress Report on R&D on Undoped Cesium Iodide and Lead Fluoride, unpublished, BNL, October 11, 1991.
181. A. V. Gektin et al., *Nucl. Instr. and Meth.* **A294** (1990) 591.
182. D. Renker, PSI, Villigen, *private communication* via D. Pocanic, University of Virginia.
183. P. Schotanus and A. M. Minville, *Scintillation Characteristics of CsI(Br)*, Internal Report, Quartz and Silice Holland B. V., QSH-910501, 1991.
184. E. B. Dally and R. Hofstadter, *Rev. Sci. Instr.* **39** (1968) 658;
IEEE Trans. Nucl. Sci. **NS-15**(1968)76.
185. D. F. Anderson, *Technical Memo on PbF_2 as a Cherenkov Radiator for EM Calorimetry*, Fermilab TM-1602, June 26, 1989.
186. G. Blasse, *IEEE Trans. Nucl. Sci.* **NS-38** (1991) 30.
187. D. F. Anderson and E. J. Ramberg, *Recent Developments in High Speed, Non-Sampling Electromagnetic Calorimetry*, contribution to the *V-th International Conference on Instrumentation for Colliding Beam Physics*, Novosibirsk, Russia, March 15-21, 1990, Fermilab-Conf-90/46;
E. J. Ramberg, *PbF_2 for High-Rate, High-Energy Calorimetry*, contribution to the *First International Conference on Calorimetry in High Energy Physics*, Fermilab, Batavia, 29 October - 1 November, 1990, in Proceedings p. 268.
188. D. F. Anderson et al., *Nucl. Instr. and Meth.* **A290** (1990) 385.
189. C. Woody, Brookhaven, *private communication.*
190. J. A. Kierstead et al., *Progress Report on Generic R&D on Undoped Cesium Iodide and Lead Fluoride*, unpublished, Brookhaven National Laboratory, October 10, 1991.
191. G. T. Bartha et al., *Nucl. Instr. and Meth.* **A275** (1989) 59.
192. Y. Yoshimura et al., *Nucl. Instr. and Meth.* **126** (1975) 541.

193. S. E. Derenzo et al., *IEEE Trans. Nucl. Sci.* **NS-37** (1990) 203.
194. G. Charpak et al., *New Developments in Calorimetry Based on VUV Scintillators Coupled to Photosensitive Gaseous Detectors,* contribution to the *ECFA Study Week on Instrumentation for High-Luminosity Colliders*, Barcelona, 14-21 September 1989, CERN 89-10, ECFA 89-124, 593.
195. J. A. Valbis et al., *Opt. Spectrosc. (USSR)* **64** (1988) 1196 (in Russian); *Solid State Commun.* **67**(1988)183.
196. V. Peskov and A. Zichichi, *A New Scintillator: $LiBaF_3$, Preliminary Results*, CERN-PPE/91-139, 3 June 1991.
197. P. Schotanus et al., *Detection of CdS(Te) Scintillation Light With Silicon Photodiodes*, presented at the *1991 IEEE Nuclear Science Symposium*, Santa Fe, New Mexico, November 5-9, 1991.
198. C. L. Melcher and J.S. Schweizer, *Cerium-Doped Lutetium Oxyorthosilicate: A Fast, Efficient New Scintillator*, presented at the *1991 IEEE Nuclear Science Symposium*, Santa Fe, New Mexico, November 5-9, 1991.
199. F. W. K. Firk, *Nucl. Instr. and Meth.* **A297** (1990) 532.
200. W. W. Moses et al., *Scintillation Properties of Lead Sulfate*, presented at the *1991 IEEE Nuclear Science Symposium*, Santa Fe, New Mexico, November 5-9, 1991.
201. V. G. Baryshevsky et al., *Nucl. Instr. and Meth.* **B58** (1991) 291.
202. S. I. Ziegler et al., *Characterisitcs of the New $YAlO_3$ Compared to BGO and GSO*, presented at the *1991 IEEE Nuclear Science Symposium*, Santa Fe, New Mexico, November 5-9, 1991.
203. P, Schotanus et al., *Nucl. Instr. and Meth.* **A272** (1988) 913.
204. P. Schotanus et al., *Nucl. Instr. and Meth.* **A284** (1989) 531.
205. P. Dorenbos et al., *IEEE Trans. Nucl. Sci.* **NS-37** (1990) 119.
206. W. W. Moses and S.E. Derenzo, *Nucl. Instr. and Meth.* **A299** (1990) 51.
207. W. W. Moses and S.E. Derenzo, *IEEE Trans. Nucl. Sci.* **NS-37** (1990)96; W. W. Moses et al., *IEEE Trans. Nucl. Sci.* **NS-38** (1991) 648.
208. A. F. Buzulutskov et al., *Nucl. Instr. and Meth.* **A288** (1990) 659.
209. G. Charpak et al., *New Scintillators for Photosensitive Gaseous Detectors*, presented at the *Symposium on Particle Identification at High-Luminosity Hadron Colliders*, 5-7 April, 1989, Fermi National Accelerator Laboratory, Batavia, USA, also CERN-EP/89-66.
210. G. Charpak et al., *BaF_2 Calorimeters With Photosensitive Gaseous Chambers*, contribution to the *ECFA Study Week on Instrumentation for High-Luminosity Colliders*, Barcelona, 14-21 September 1989, CERN 89-10, ECFA 89-124, Vol. 2, p. 588.
211. A. F. Buzulutskov et al., *Nucl. Instr. and Meth.* **A281** (1989) 99.
212. A. F. Buzulutskov et al., *Nucl. Instr. and Meth.* **A292** (1990) 546.
213. V. N. Makhov and N. M. Khaidukov, *Sov. Phys. Solid. State.* **32** (11) (1990) 1978.
214. N. A. Mullani et al., *IEEE Trans. Nucl. Sci.* **NS-27** (1980) 572.
215. T. J. Spinks et al., *IEEE Trans. Nucl. Sci.* **NS-35** (1988) 721.
216. H. Iida et al., *IEEE Trans. Nucl. Sci.* **NS-36** (1989) 1006.
217. J. E. Litton et al., *IEEE Trans. Nucl. Sci.* **NS-37** (1990) 743.
218. R. Lecomte et al., *IEEE Trans. Nucl. Sci.* **NS-37** (1990) 805.
219. R. Sumner, *Nucl. Instr. and Meth.* **A265** (1988) 252.

220. P. M. Tuts, *Nucl. Instr. and Meth.* **A265** (1988) 243.
221. R. D. Schamberger, *Nucl. Instr. and Meth.* **A309** (1991) 450.
222. R. Y. Zhu et al., Caltech preprint CALT-68-1392 (1985).
223. R. Y. Zhu et al., *Nucl. Instr. and Meth.* **A302** (1991) 69.
224. P. Lecoq et al., *Nucl. Instr. and Meth.* **A300** (1991) 240.
225. C. Laviron and P. Lecoq, *Nucl. Instr. and Meth.* **227** (1984) 45.
226. M. Chemarin et al., *Tests on Doped BGO Crystals*, L3-655 (1989).
227. Z. W. Yin et al., *Nucl. Instr. and Meth.* **A275** (1989) 273.
228. Z. Y. Wei et al., *Nucl. Instr. and Meth.* **A297** (1990) 163.
229. V. V. Yanovsky et al., *Nucl. Instr. and Meth.* **A309** (1991) 596.
230. A. D. Bross, *IEEE Trans. Nucl. Sci.* **NS-33** (1986) 144.
231. M. Atkinson et al., *Nucl. Instr. and Meth.* **A254** (1987) 500.
232. C. Angelini et al., *Nucl. Instr. and Meth.* **182** (1989) 50.
233. S. Brollo et al., *Nucl. Instr. and Meth.* **A293** (1990) 601.
234. U. Buchner et al., *Nucl. Instr. and Meth.* **A272** (1988) 695.
235. D. E. Wagoner et al., *IEEE Trans. Nucl. Sci.* **NS-31** (1984) 53;
Nucl. Instr. and Meth. **A238** (1985) 315.
236. M. R. Adams et al., *Nucl. Instr. and Meth.* **A238** (1985) 333.
237. B. McGrath et al., *Nucl. Instr. and Meth.* **135** (1976) 93.
238. P. Pavan et al., *Nucl. Instr. and Meth.* **B61** (1991) 487.
239. A. Lempicki et al., *BaF_2 and CsF Doped Scintillating Glasses*, unpublished report, Boston University, 1991.
240. S. Mitachi et al., *J. Appl. Phys. (Japan)* **22** (1983) L537.

FAST SCINTILLATORS FOR HIGH RADIATION LEVELS

Part II

Plastic and Liquid Organic Scintillators

Part II: Plastic and Liquid Organic Scintillators

II.1 Outline

We begin with a fairly detailed outline of the scintillation mechanism in organic (plastic and liquid) scintillators. An understanding of the fundamental phenomena will allow one to design an appropriate scintillator suitable for the high rate, high radiation areas of the hadron colliders. Questions concerning fast timing capability, light output, energy resolution, etc., are answered with modern scintillators. The principle problem remains that of sufficient radiation tolerance. Hence, most of the article will concentrate on the problem of a creating a radiation-resistant scintillator that also meets the other requirements. As will be seen, the achievement of radiation tolerance can result in the loss in one or more other capabilities. We begin the discussion of the radiation problem by reviewing what radiation levels will most likely exist at the colliders. From there the discussion will proceed to the effects of radiation upon scintillators with particular reference to the optical changes in the base material. This section will also include discussion of the key parameters affecting the level of damage detected. A section detailing the experimental results will follow which explores various attempts at improving the radiation tolerance of scintillators while minimizing any degradation to other useful characteristics. From there, we apply the present knowledge to planned detectors. A specific discussion of liquid scintillator research is followed by an outline of present research activities which are underway exploring some of the more detector-specific issues. A final concluding section closes the article.

II.2 The Scintillation Phenomenon

Scintillation is an exercise in applied photochemistry. It is useful to review the photochemical properties of the benzene molecule, as it forms the basis for all scintillation phenomena in organic plastics and liquids. Benzene contains six carbon and six hydrogen atoms. The carbon atoms have a ground state configuration of $1s^2 2s^2 2p^2$, but for binding, the configuration is $1s^2 2s 2p^3$, so that there are four valence electrons. Three of the valence electrons are hybridized into the trigonal (sp^2) configuration (figure 1). The electron wave functions are at angles of 120° to each other in a plane, giving the the benzene ring its planar hexagonal structure.

These three electrons form σ bonds, meaning that one has an electron pair (one from each adjoining carbon atom) shared in the area centered on a line joining the carbon atoms. The fourth valence electron (in a p-orbital) is a π electron, so that the bonding of the carbon atoms occurs by having the p-orbitals overlap in a

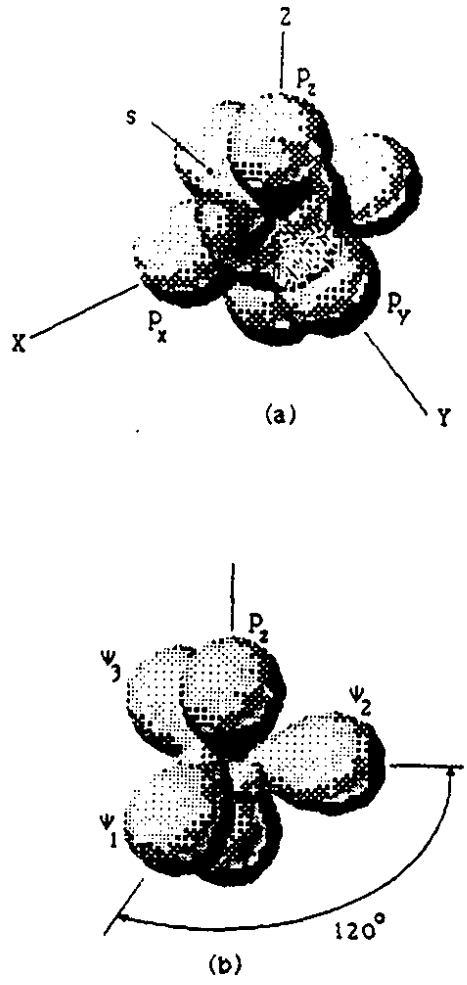

FIGURE 1: (a) Representation of the angular electronic wave function for the 2s and 2p states. (b) The hybridized sp^2 wavefunctions. Adapted from reference [17].

parallel fashion. A pair of electrons occupies the space both below and above the line joining the two carbon atoms. The double bonds of the benzene molecule are composed of one σ and one π bond. There are therefore only three double bonds within the benzene ring. It is known that each $C - C$ bond is equivalent, so the benzene molecule is considered to have a resonance hybrid structure whereby these three double bonds are shared equally among the six atoms. This is demonstrated in figure 2, along with the usual representation of a benzene ring drawn with a circle inside to reflect the π electron cloud resonance.

The π electrons form the basis for the scintillation mechanism. The π electron cloud is quantized into a series of singlet (S_{ij}) and triplet (T_{ij}) levels where $i = 0, 1, 2, ...$ denotes the electron energy level and $j = 0, 1, 2, ...$ denotes the vibrational sub-level. Figure 3 displays a representation of these energy levels. The fundamental luminescent properties arise from excitation of the molecule from the ground π states into the excited singlet and triplet states. Through non-radiative processes, there is de-excitation to the S_1 levels followed by a fast radiative transition to the ground S_0 states. This is known as *fluorescence*, and operates on a time scale of nanoseconds. It is also possible for an excited S_1 state to pass to an excited triplet T_1 state followed by a slow ($\approx 10^{-4}$ s) radiative decay to the ground state. Due to the difference in relative energy levels, this decay is at a longer wavelength than the fast fluorescent component. This phenomenon is known as *phosphorescence*. Finally it is also possible for a triplet T_1 state to pass to an excited singlet S_1 state followed by a fast radiative transition to the ground state. This is known as *delayed fluorescence* since it has the same spectral characteristics as the dominant fluorescent component. However since the transition probability for the triplet-singlet exchange is small, the time scale for the radiative transition is dominated by the initial spin flip process ($\approx 10^{-6}$ s). In liquid scintillators, it is probably the chief component of the tail in the scintillation decay time. It is also probably a major factor for plastic scintillators as well, but the fact of having a solid matrix complicates the extrication of all processes that contribute to the tail of the scintillation decay curve.

Given the presented information, one would deduce that the measured absorption would appear as in figure 4(a), when in fact they look more like figure 4(c). The sharp line spectrum of figure 4(a) corresponds to molecules at a very low pressure vapor phase. In a condensed phase, the fundamental energy levels can be split into many unresolved vibrational, rotational, and collisional substates (figures 4(b) and (c)). In addition, the absorption and emission spectra are split into different wavelength regimes by changes in interatomic spacing after excitation of the electronic

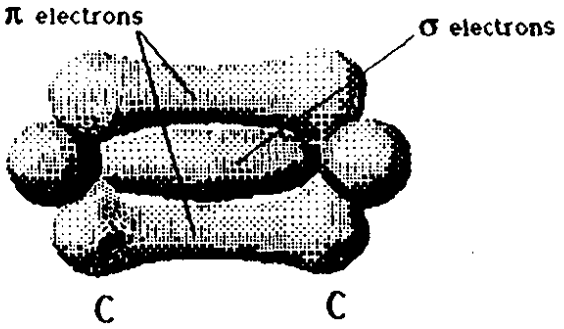

A

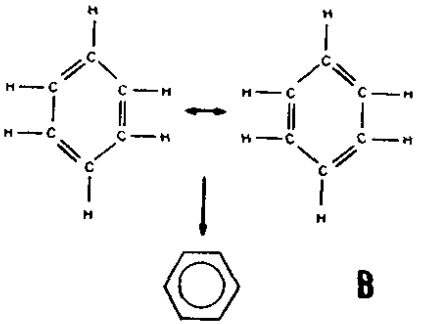

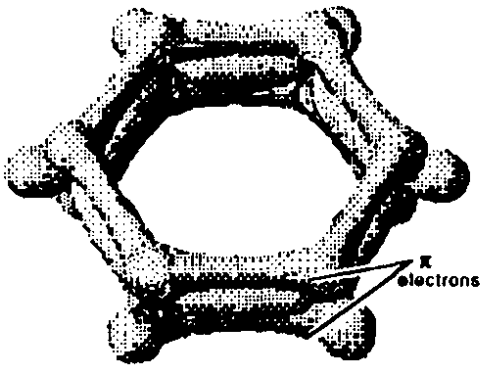

FIGURE 2: (a) Representation of the electron clouds which form the σ and π bonds in the benzene molecule. (b) The usual representation of the benzene molecule. The circle inside the bottom figure represents the π electron cloud. Adapted from reference [17].

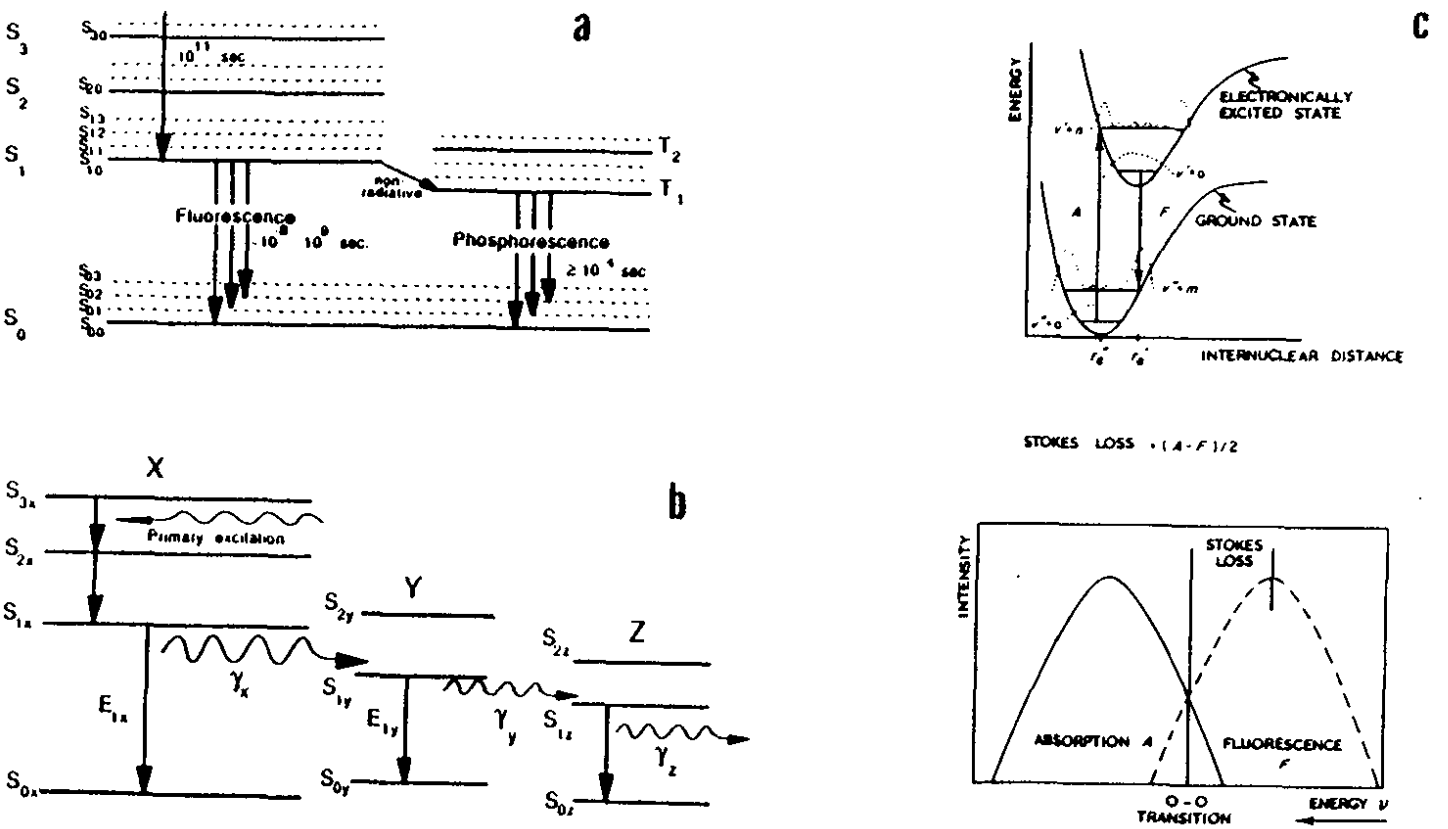

FIGURE 3: (a) The p electron energy levels. (b) An energy level representation of energy transfer in a scintillator composed of a solvent (X) plus two waveshifters (Y & Z). At higher concentrations (10^{-2} M), the dominant mode of energy transfer between X and Y becomes the non-radiative dipole-dipole interaction instead of the radiative mode shown in the figure. (c) Illustration of the how the Frank-Condon principle creates a shift between fluorescent absorption and emission. *Note the definition of the Stokes shift.* Figures 3(a) and (b) are adapted from reference [17]. Figure 3(c) is adapted from reference [19].

states. This is demonstrated in figure 3(c) for a diatomic molecule. Electronic transitions take place on a time scale that precludes any significant change in interatomic spacing during these transitions (the Frank-Condon principle). However, in the excited state, the equilibrium interatomic spacing is larger than in the ground state. Hence, the final radiative de-excitation transition goes to a substate above the ground state (followed by non-radiative transitions to the ground state). The net result is a separation between the absorption and emission spectra, a shift from shorter to longer wavelengths. This shift is expressed quantitatively as the *Stokes shift* or *Stokes loss* (figure 3(c)).

Practical organic scintillators are formed from using a solvent doped with a high concentration of primary fluor and a much lower concentration of a secondary fluor. The solvent acts as the initial energy dump. Not surprisingly, the most efficient solvents all have a benzene molecule incorporated within their structure (see appendix II.A). If we consider the action of a charged particle (say, a 1 MeV electron) passing through the scintillator, the primary excitation processes can be said to be (a) excitation of the π singlet states, (b) ionization of the π electrons, (c) excitation of other electron groups (such as the σ electrons), and (d) ionization of other electrons. The first process is mainly responsible for the fast fluorescent component. The second process followed by ion recombination seems to be responsible for any triplet states (as well as some singlet states) produced and probably leads to some if not all of the slow component in the scintillation process. Any excitation via the third process is dissipated thermally. The fourth mode of excitation seems to be the fundamental cause of radiation damage to the material.

Although the solvent is an inherent scintillation material, it has low quantum yields in terms of the energy output in the fast fluorescent component. For example, toluene is considered a highly efficient material for a solvent, but only yields 9% of the input energy in useful emission. Furthermore, the resultant emission spectrum (peaking at about 320 nm) is well below the region where the most common and cheapest photomultipliers detect light with the highest efficiency. One needs to transfer the useful excitation energy to some molecule that will efficiently transfer it into easily detectable light. A first step to this goal is taken by dissolving an appropriate amount of a fluorescent material that (a) is sufficiently soluble in the solvent, (b) has a high quantum yield (close to 1.0), and (c) has an absorption spectrum which overlaps as well as possible with the emission spectrum of the solvent. This last requirement brings us to the matter of energy transfer among the molecules.

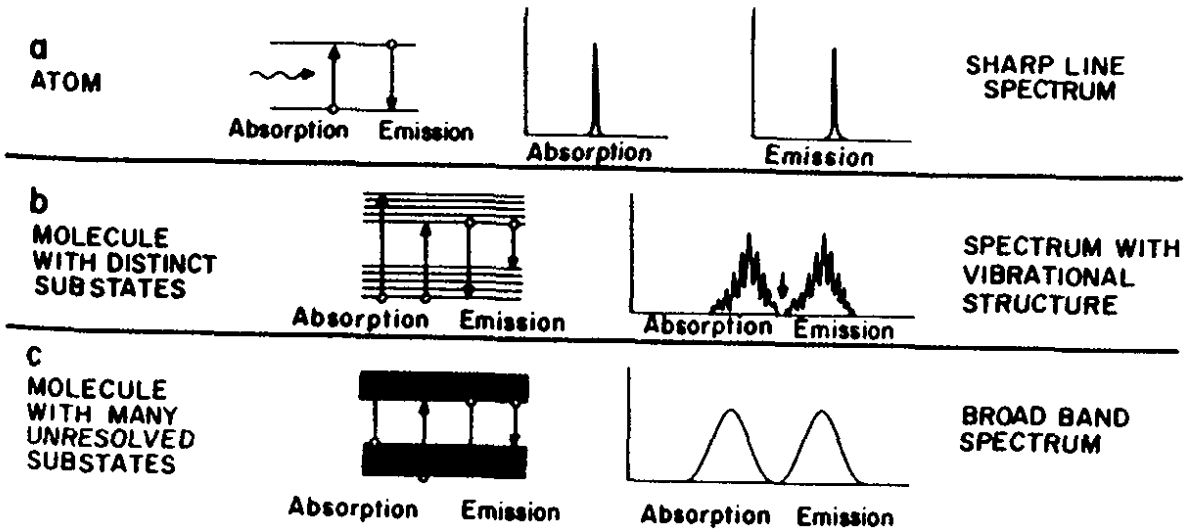

FIGURE 4: (a) Emission and absorption lineshapes for atoms at low pressure in a vapor phase. (b) The spectra for rigid molecules at low pressure in a vapor state. One can see how the formation of vibrational substates and the action of the internuclear potential (see figure 3(c)) creates Stokes shifted, broadened lineshapes. (c) Absorption and emission for typical molecules in a solvent with many unresolved substates. Adapted from reference [134].

Energy transfer from the solvent to the solute is achieved by several means: (i) radiative transfer from the solvent to the solute, (ii) a non-radiative dipole-dipole exchange known as *Förster transfer*, (iii) non-radiative transfer from excited solvent to neighbouring ground state solvent molecules (and thence to the solute by either (i) or (ii)), and (iv) collisional exchange of energy via diffusion of excited solvent molecules. The last is only operational in liquids. Process (iii) is necessary for increasing the probability for transfers to the solute via (i) and (ii). In plastics, the excited sites are *segmers*, the fundamental repeated part of the polymeric chain. The energy is transferred via electron exchange, a process whose transition probability decreases exponentially with distance between the segmers. Process (i) must be proportional to the overlap between the absorption spectrum of the solute and the emission of the solvent. It turns out that process (ii) is also proportional to this spectral overlap despite the fact that the process is non-radiative. Unlike the electron exchange process, the transition probability decreases as R^{-6} (which follows from the fact of it being a dipole-dipole interaction), where R is the distance between the excited *donor* molecule and the ground state *acceptor* molecule. At low concentrations of the solute, $\approx 10^{-4}$ M, energy transfer from the solvent to the solute will be radiative. As the concentration of the solute is increased, the probability for non-radiative Förster transfer will increase until it is the dominant mode ($\approx 10^{-2}$ M). Hence light output is maximized in the scintillator by maximizing the concentration of the solute (within the solubility limit of the solute). Equivalently, one can also use a lower concentration of a fluor with an unusually high molar extinction coefficient ϵ. This quantity is a measure of the peak amplitude of the absorption spectrum.

In practice, one has to add a secondary fluor that will absorb the emission of the primary fluor and shift the output to a sufficiently longer wavelength. Figure 5 is an example of how one matches fluor absorption and emission spectra in order to produce a green-emitting scintillator. The common primaries, such as PTP and BPBD,* can only emit at a peak wavelength of about 360 nm which would result in a macroscopic attenuation length of a few centimeters. This is due to the combined effect of (a) absorption by the solvent, and (b) self-absorption by the primary fluor of its own emission. Although the tail of the absorption spectrum is several orders of magnitude smaller than at the peak, this residual is sufficient to absorb the emission over a macroscopic scale and hence creates a boundary condition on the required

* Appendix II.A is a glossary containing the common abbreviations for fluors and solvents plus their full name and a schematic of the molecule.

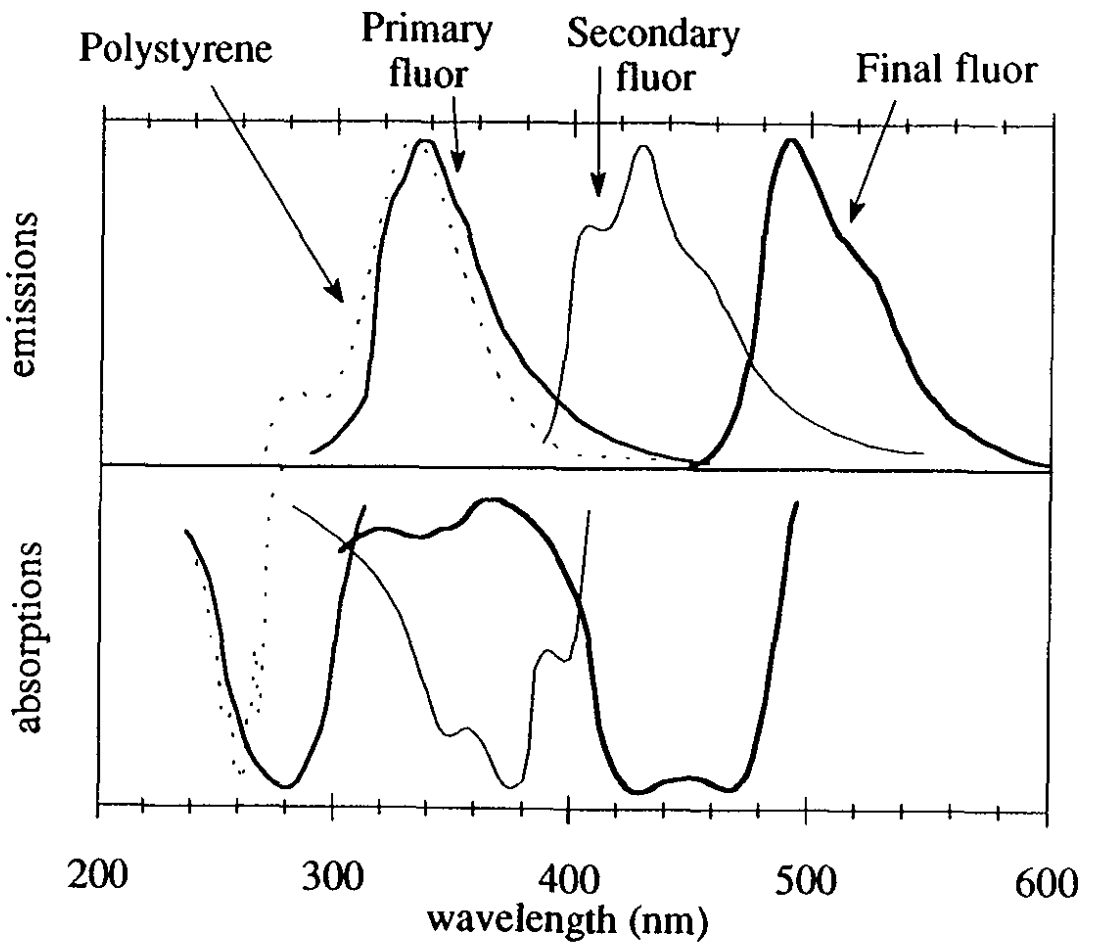

FIGURE 5: Illustration of how the matching of absorption and emission spectra create a green-emitting scintillator. Adapted from reference [135].

concentrations of the fluors. In the case of the primary, the low quantum yield of the solvent requires that the primary fluor be present at a high concentration in order to facilitate efficient energy transfer via the non-radiative dipole-dipole interaction. Unfortunately, the shift to the longer wavelength is not sufficient to avoid severe absorption by the solvent and the primary solute. By adding a small concentration of an appropriate secondary fluor, the primary emission is radiatively transferred to the secondary, and the final emission (the peak being in the region of 400-440 nm), avoids absorption in the system. The small concentration limits the self-absorption by the secondary to an acceptable level while maximizing light output. Bulk attenuation lengths of 3 to 4 meters are possible although the actual measured attenuation length can be highly dependent upon the shape and size of the scintillator as well as the nature of the boundary conditions for the sample such as the surface quality of a plastic sample, or the use of reflective surfaces.

Liquid scintillators are produced in a straightforward method by dissolving the fluors in the solvent. However, care must be taken in maintaining high purity standards for all the ingredients. For example, water vapor will create a murky solution if allowed to dissolve in the scintillator. Most importantly, dissolved oxygen will quench the scintillation process. That is, the normal radiative fluorescent transition will be quenched by having the excited molecule transfer energy by non-radiative means to the oxygen. Although the careful use of quenchers is used to decrease the decay time of selected scintillation formulations, in general, the presence of a quenching molecule will severely decrease the light output (typically 30% in liquids) and should be assiduously avoided. Hence liquid scintillators are stored in inert, dry nitrogen atmospheres.

Plastic scintillators are produced by a much more elaborate procedure. Simple melting of the plastic followed by doping with the desired fluors does not produce an efficient scintillator. Although there are variations on the technique, the basic method goes as follows [1]:

The basic liquid monomer, styrene, has a polymerization inhibitor (tert-butylcatechol) removed by column filtration. The styrene is purified by vacuum distillation using a rotary evaporator. Storage of the product is possible (in a freezer) for up to two months. The desired fluors are dissolved into the liquid styrene with the solution placed in silylated glass containers.

Silylation is a process whereby the glass container is cleaned and then coated to allow for easier removal of the finished plastic sample. Concentrated nitric and sulfuric acid is used to thoroughly clean the glass followed by rinsing with distilled

water and drying in air. The container is then immersed for several hours in a 30% solution of dichlorodimethylsilane/chloroform, and then rinsed in turn with chloroform, methanol, and distilled water followed by a final drying.

The doped styrene solution undergoes three freeze-thaw-pump cycles (using liquid nitrogen) to remove dissolved gases before having the polymerization process begun in a heated silicone bath. The heat bath has the following temperature profile: (i) 2 h @ 90° C, (ii) 24 h @ 110° C, (iii) 48 h @ 125° C, (iv) 12 h @ 140° C, (v) ramp down at 10° C/h to 90° C. At 125° C, the containers are backfilled with nitrogen gas to prevent boiling. The stage at 140° C is used to minimize the residual amount of monomer. After the heating cycle is completed, the samples are temperature quenched in liquid nitrogen to prevent the formation of vacuum bubbles (which occur if the cooling is allowed to take place slowly to room temperature), and to facilitate the easy removal of the finished scintillator. The finished forms can be machine cut and polished to the desired specification.

This is more or less the method used to make cast sheets as well as cylindrical preforms used in fiber production. In the former, polymerization takes place between flat sheets of glass in order to maintain good surface quality. Diamond mill sawing can be used to cut the sheets while maintaining high surface quality at the cut surface. For fibers, the finished cylindrical preform is placed snugly inside a tube of acrylic which will become the cladding for the fiber. A combination of heat and pressure is used to bond the surfaces together, and the heated preform is then drawn into the finished fiber. Fiber diameters can be as large as 3 or 4 mm but 0.5 to 1.0 mm is more typical. Special techniques can be used to produce extremely thin fibers of 30 μm diameter. (Essentially, the initial fibers are gathered together into a "fiber preform" and then redrawn into the much smaller diameter fiber.) Needless to say, there are many "tricks-of-the-trade" used in the production of a scintillating fiber. Although good fibers can be produced as of the time of this writing, many subtleties are under active investigation.

II.3 Radiation Damage to Organic Scintillators

II.3.1 Expected Radiation Levels

Traditionally, the question of radiation-induced damage to organic scintillators has been a moot point as the detectors only had to endure dosages well below the threshold of damage ($\approx 10^3$ Gy) observed in tests of small samples [2]. However, experiments utilizing very high particle fluxes [3] and the planned construction of the SSC and LHC hadron colliders have brought to the forefront the question of

whether organic scintillators will be suitable for the new hostile environment that will exist at these facilities [4-7]. This section is an updated review [8,9] of this subject with an emphasis on those studies most pertinent to the present problem.

We begin with a brief overview of the radiation problem expected for the proposed SDC detector at the SSC [10]. Most of this discussion is based upon a recent article by Groom [11] which includes an important correction to an error in a previous publication on the subject [4].

In terms of the direct dose from a flux of charged particles from the interaction region (for a design luminosity of 10^{33} $cm^{-2}s^{-1}$), one finds that the delivered dose to an absorber whose thickness is much thinner than one nuclear interaction length (e.g., a plastic scintillating fiber ribbon with 1 mm diameter fibers) scales as the inverse square of the radial distance (in a cylindrical geometry) from the beamline. At one meter from the beamline, the expected dose is 40 Gy/yr. (Low momentum tracks that repeatedly transverse the material—*"loopers"*—may increase the dose by another factor of two.) Central tracking detector designs that utilize plastic scintillating fiber cover a radial region from about 0.6 meters to 1.6 meters [10]. Therefore, we are dealing with yearly doses of about 15 (outer radius) to 110 Gy (inner radius) per year at the lower luminosity option. Using the conversion factor of 1 Gy $\equiv$ 100 rads, we have 1.5 krad to 11 krad. Since the higher luminosity option of 10^{34} $cm^{-2}s^{-1}$ is considered a priority item, the total ten year dosage at that level would be 0.15 to 1.1 Mrad. This latter number will impose a serious problem for standard scintillators.

Calorimeters, especially electromagnetic calorimeters, face a much more serious environment. Figure 6 displays an estimate of the expected doses at the electromagnetic shower maximum for the scintillator in a Pb/scintillator calorimeter design. The numbers correspond to the yearly dose at the low luminosity option (10^{33}) and in parentheses, the ten year accumulated dose at the high luminosity option (10^{34}). The dose increases rapidly in the forward regions to catastrophic levels. Most of the research on increasing radiation resistance of scintillators has been concentrated on the development of plastic capable of withstanding these forward doses. Liquid scintillator is being considered for use in the extreme forward regions since it may be possible to develop a circulation system to replenish damaged scintillator, or to develop a modular design for removal of damaged sections.

Some question has been raised as to how the level of damage varies as a function of the type of irradiation particle. Specifically, this reduces to the question of whether the scintillator suffers only damage from ionization in the material, or

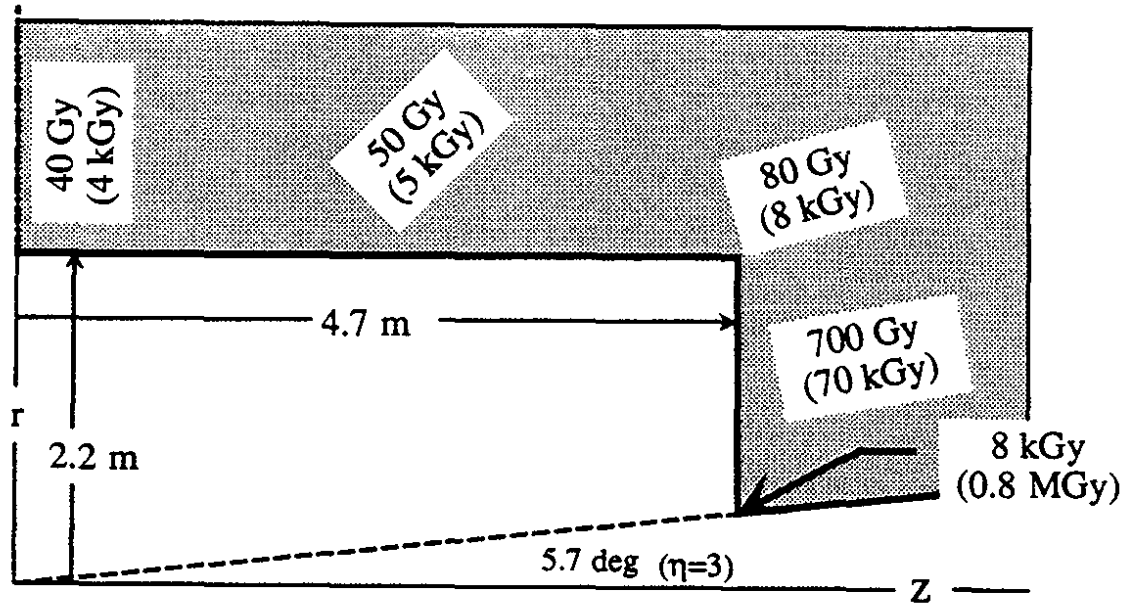

FIGURE 6: Estimates of the ionizing dose at electromagnetic shower maximum in the SDC detector at SSC design luminosity for one year, and in parentheses, at ten times the design luminosity for ten years. These doses are for the scintillator. Adapted from reference [11].

are there additional effects such as the well-known ones suffered by solid state devices when irradiated with high energy neutrons. The current wisdom [11] seems to indicate that neutrons will have no special effect and with the expected fluences ($< 10^{13}$ cm^{-2}yr^{-1}), may be safely ignored. Some data comparing gamma and neutron irradiations does exist [12] in which "gamma-only" irradiations are compared to "60% γ+ 40% n" equivalent irradiations. It suggests that neutron and gamma irradiations are equivalent, although it makes use of fluence-to-dose conversion factors that some investigators [11] have doubts regarding their validity. In any case, this area is still actively under investigation [13], and so it may be that damage results will have to be quoted in terms of (a) damage achieved by a given *dose* of gammas and/or charged particles, and (b) damage achieved by a given *fluence* of neutrons with a given energy spectrum.

II.3.2 Plastic Scintillators

Figure 7 illustrates the essential effect of ionizing radiation upon a plastic scintillator: (1) the increase in attenuation of the signal, and (2) the loss in *intrinsic* scintillation output. The first seems to be due mostly to the creation of color centers in the base plastic, but additional color centers can be created through the destruction of some fluorescent molecules as well as any additional dopants used in the manufacture of the scintillator. Although one would think that the loss in intrinsic scintillation would be due to destruction of fluorescent molecules, the current research indicates that most of this effect is actually due to the creation of color centers in the plastic that compete with the scintillation mechanism [14]. More about this will be said later.

Before discussing radiation damage phenomenology in detail, we will review the scintillation mechanism, as some salient features of scintillation are critical for understanding the sources of the optical effects and for composing a strategy for alleviating the effects of radiation damage. In that regard, this discussion will only include the relevant aspects (or more accurately, those that seem most relevant at present) to the problem of alleviating the effects of radiation. The interested reader can revel in the wonders of the classic tome by Birks [15] which provides myriad details of the scintillation phenomenon. Other useful discussions may also be found in Pla-Dalmau [1], Brooks [16], White [17], Davis [18], Flournoy [19], Bowen [20], and Bross [21].

The modern scintillators use either polystyrene (PS) or the related polyvinyltoluene (PVT) as the base material. A crucial aspect of these substances is that they

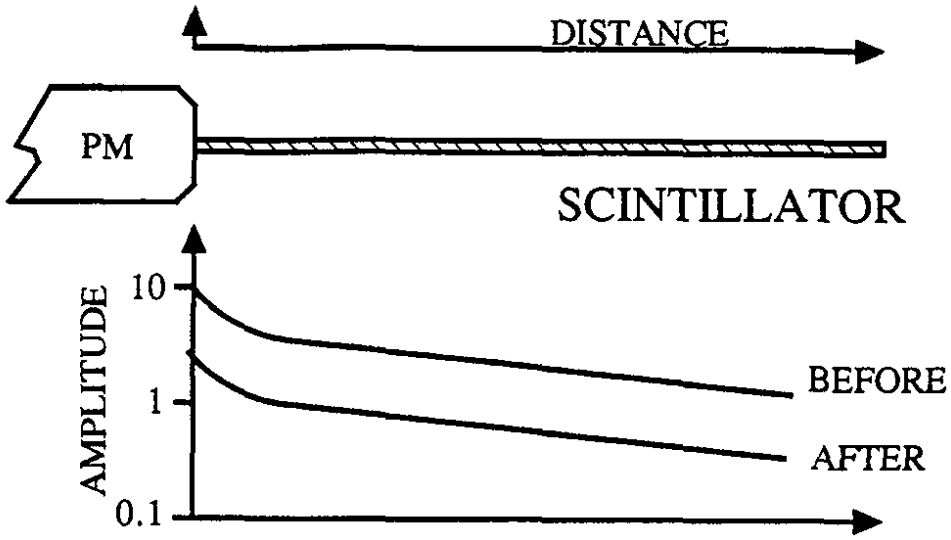

CASE 1: DAMAGE TO LOCAL SCINTILLATION YIELD ONLY

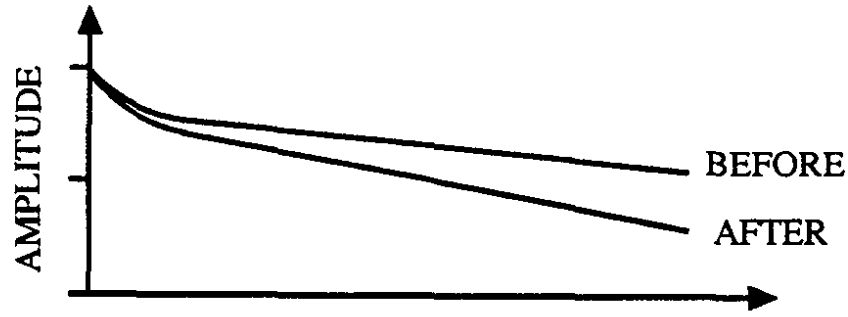

CASE 2: DAMAGE TO TRANSMISSION ONLY

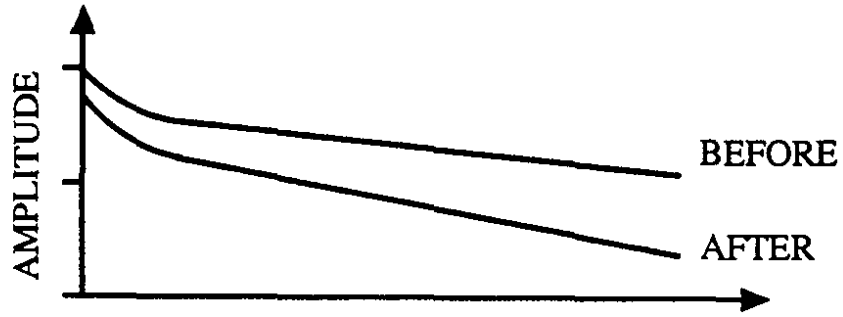

CASE 3: TYPICAL DAMAGE OBSERVED IN EXPERIMENTAL CONDITIONS

FIGURE 7: Effect of radiation damage upon optical performance of scintillators. Adapted from ref. [8].

are (albeit very weak) fluorescent emitters in their own right, with their absorption bands in the deep UV (240-280 nm), and an emission spectrum in the region of 290-370 nm (peaking at 320-330 nm) [22]. By using a suitable fluorescent dopant, that is, one with (a) high solubility in the plastic, (b) high quantum yield and (c) an absorption band that overlaps the emission spectrum of the plastic, one can effectively shift the final output to a longer wavelength (typically peaking at 350-370 nm). Typical fluors are PTP and BPBD. At low concentrations (10^{-4} moles/liter), the mode of energy transfer between the base plastic and the fluor is radiative. However, at higher concentrations (10^{-2} moles/liter), the energy is transferred via a non-radiative, resonant dipole-dipole interaction known as *Förster transfer* [23]. The ultimate light output is limited by (1) solubility limits of the fluor in the plastic, and (2) the self-absorption of the fluor's own light due to the overlap of the absorption and emission spectra of the dopant. (It is important to take note of this non-radiative transfer mode as the relevant consequence of irradiation of a plastic scintillator is the creation of absorptive color centers which interfere with *radiative* transfer.) Unfortunately, the final emission is not sufficiently blue-shifted from the UV. First, the plastic has enough absorptive power at these wavelengths to produce a scintillator with a small attenuation length. Secondly, the most common photomultipliers have a spectral response peaking in the region of 400-450 nm. Finally, at these concentrations, self-absorption by the fluor will severely limit the attenuation length. To deal with these limitations, a secondary dopant is added, this one with an absorptive band matching the emission of the primary. Examples are POPOP, bis-MSB and TPB. The final emission peaks in the region of 420-450 nm, which brings it into the range of peak response of the phototubes and lessens the effect of absorption by the plastic base. The concentration of the secondary is deliberately kept small to minimize self-absorption effects. Hence the dominant mode of energy transfer is necessarily radiative. This has important consequences in terms of the effect of irradiation on the scintillator.

For acrylic-based scintillators, this model has to be modified slightly as the acrylic material does not fluoresce. Instead, a large concentration (several percent by weight) of naphthalene is used to act as the initial energy "dump" whereupon the naphthalene transfers the energy to the primary fluor, and so on.

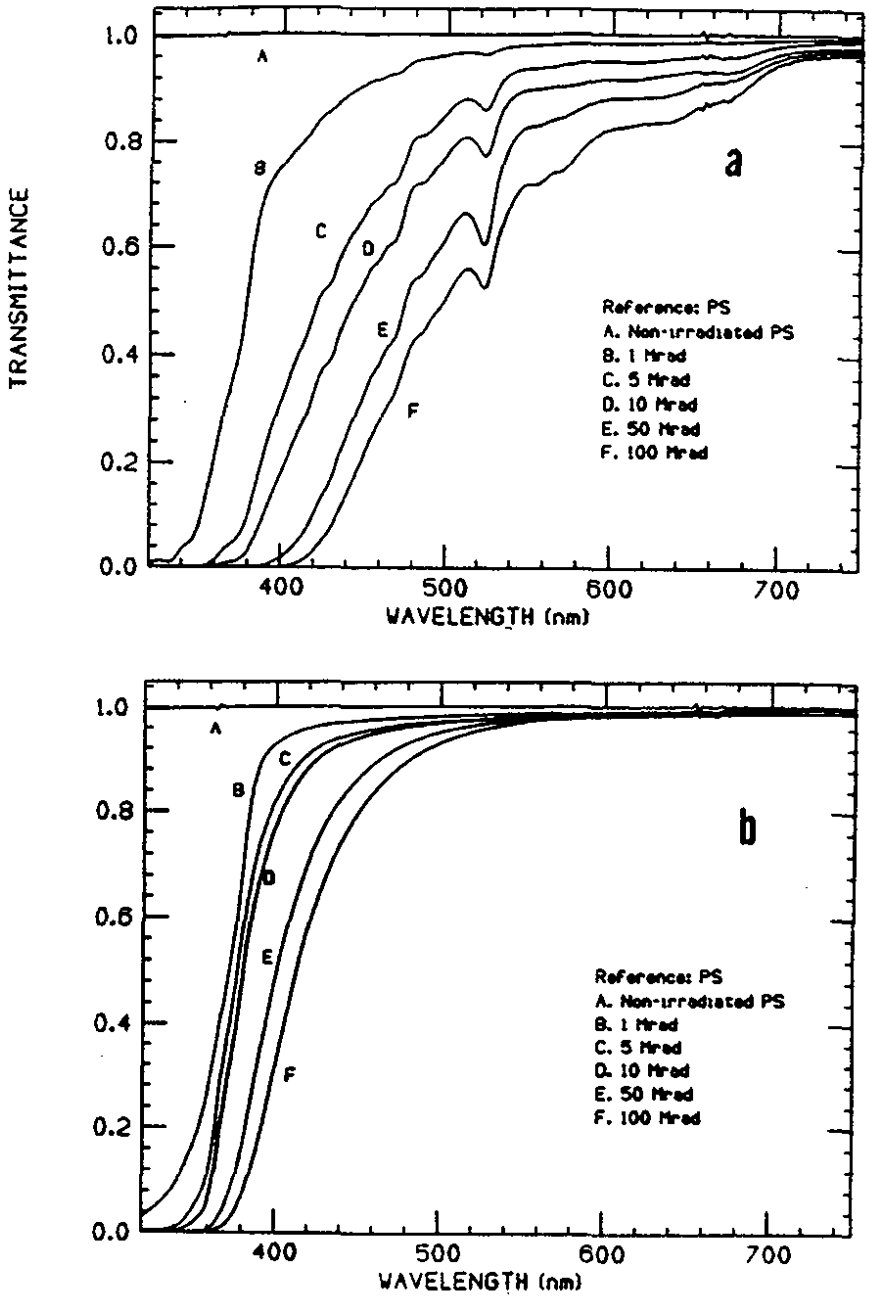

FIGURE 8: Examples of transmission damage in undoped polystyrene after several high dose rate irradiations. Figure 8(a) displays the damage immediately after the irradiations while (b) displays the residual damage after annealing in air. The significant levels of damage in the UV strongly affect the radiative transfer between the primary and secondary fluors. A key question is whether the final post-anneal damage is equivalent to the effects of a very low dose rate irradiation (see figures 15 & 16). Adapted from reference [14].

II.3.3 Damage Mechanisms

If one ignores any effect of irradiation upon the fluorescent molecules themselves, then one can examine the changes in light output solely as an effect due to the increased absorption induced in the base plastic. As figure 8 shows, the primary effect of radiation upon a sample of polystyrene is to add additional absortion centers in the UV and blue region, thereby creating an absorption "edge" which moves into the blue and yellow monotonically as a function of increasing dose (although strictly speaking, there is also some absorption in the green and red, but at a much smaller level). Since the mode of transfer between the base plastic and the primary fluor is non-radiative, this absorptive edge has *no* effect upon the initial energy transfer. However, as the edge moves into the longer UV, it interferes with the radiative transfer between the primary and secondary. (An alternate view of this is expressed in terms of the *transfer length* [24] needed to transfer $1 - e^{-1} \equiv 63\%$ of the initial energy from the *donor* (the primary) to the *acceptor* (the secondary) molecule. For the typical concentrations used, the non-radiative mode has a transfer length ranging from 10-20 μm while the radiative mode is an order of magnitude larger.) Hence, barring any damage to the fluors and other additives, *the loss in light output can be solely explained in terms of absorptive changes in the base plastic leading to severe interference with the generation of the scintillation light.* In terms of the phenomena shown in figure 7, the strong increase in absorption in the UV leads to the drop in intrinsic light output while the much smaller but nonetheless significant increase of absorption in the blue and green results in the observed attenuation changes.

This idea was originally proposed from the results of experiments with the irradiation of liquid scintillators [25], and has been verified recently for typical plastic scintillators [14]. A qualitative verification of this model was seen in a study [26,63] in which the concentrations of the primary and secondary fluors were varied in order to ascertain the effect of fluor concentration upon the radiation resistance of the scintillators. Indeed, variations in the concentration of the primary fluor were found to have the most effect while the concentration of the secondary had no significant role. It is important to note that this does not mean that fluors cannot be damaged, nor that damaged fluors cannot contribute to formation of color centers. However, the commonly used ones do seem to bear up better than initially expected [27]. There are also cases of interesting new fluors that have turned out to be highly susceptible to irradiation, in particular when they are dissolved in a polystyrene base. These will be discussed later.

A critical result of this model is the proposed method of alleviating the problem. Ideally, one should use a highly soluble, highly efficient, radiation-resistant fluor whose absorption band spans the emission band of the plastic and whose emission is as red as possible (i.e., a large Stokes shift fluor), in effect creating what one researcher has termed an *intrinsic scintillator* [1,21]. At an appropriate concentration, the mode of transfer will be dominantly non-radiative, hence immune to the most severe optical changes occurring in the plastic. Finally the output will be shifted to sufficiently long wavelengths to avoid the secondary absorption effects. This ideal has to be modified by several observations: (1) as figure 9 shows, polystyrene has an absorption curve which falls until about 600 nm, hence the emission should preferably be in the range of 500 to 600 nm, (2) fast and efficient photodetectors with suitable quantum efficiency at those wavelengths are still only a research curiosity (although the research is very active!) [29-32], (3) longer wavelength fluors tend to get slower [19,22], and hence lose a critical feature for high energy physics applications (although the new "G" series of fluors from Bicron seem to be a breakthrough in being fast (2-4 ns decay times), efficient, green-emitting (> 470 nm) waveshifters [33]).

The chemical mechanism for the damage to the polymer base is not completely understood although the general categories of reactions are known [1,20]. The most likely cause of the color centers is probably due to the presence of the *tertiary benzylic* hydrogen atom in polystyrene (and PVT) [34]. Figure 10 displays the reaction chain. This type of hydrogen atom, because of its placement in the molecule, is particularly susceptible to reactions with radicals formed from the irradiation of the polymer. This leads to the formation of polyenyl free radical chains whose absorption bands are a function of their length (for $n = 1$, $\lambda_{max}^{abs} = 260$ nm, while at $n = 5$, $\lambda_{max}^{abs} = 400$ nm). The recovery phenomenon seen after a high dose rate irradiation would be the slow (due to the large viscosity of polystyrene) recombination of these polyenyl radicals into short chains of polyenes within the main polymer backbone. The polyenes have their absorption bands at substantially shorter wavelengths (e.g., for $n = 1$: $\lambda_{max}^{abs} = 185$ nm, for $n = 5$: $\lambda_{max}^{abs} = 340$ nm). The polyenes would presumably be the source for the residual damage levels recorded after the initial annealing is completed. As likely as this model is (because it is based upon well-established chemistry), detailed and careful experimental studies will still be necessary to verify or refute it.

The most important parameters relating to radiation damage seem to be (a) dose, (b) dose rate, (c) atmosphere (i.e., presence of oxygen) before, during, and

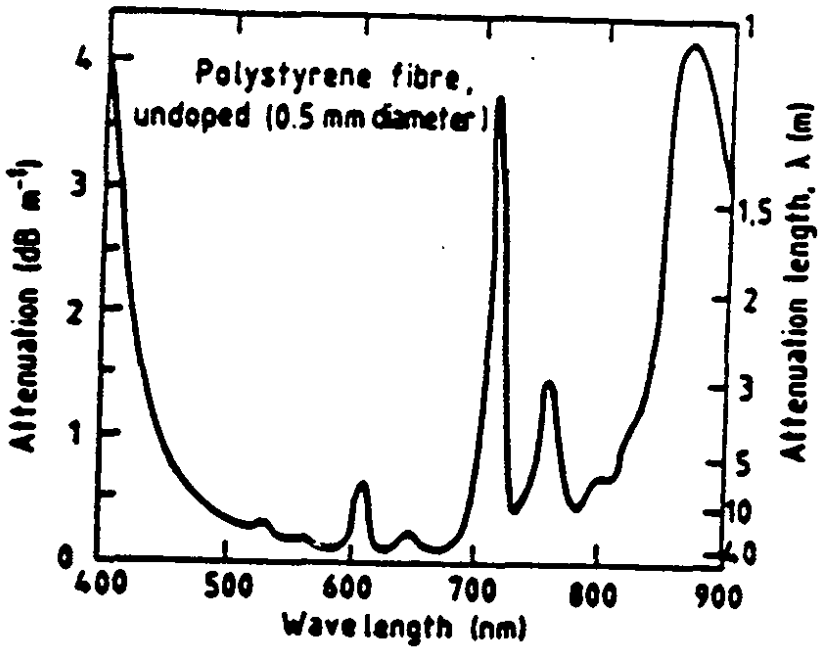

FIGURE 9: Absorption data for a 0.5 mm diameter undoped polystyrene fiber. Adapted from reference [28].

after irradiation, (d) fluorescent dopants, (e) other additives (particularly antioxidants) used in scintillator production, (f) temperature (including localized heating due to high rate irradiation), (g) size and shape of sample, and (h) type of plastic base material. It should be noted, as will be evident in the discussion to follow, that these parameters cannot necessarily be dealt with independently of one another (for example, dose rate and atmosphere).

The more visible effects of dose seem to become noticeable only after at least 10^2 Gy [2,35-38] for samples with small dimensions (several cm^3). In such small samples, there usually seems to be a threshold effect, in that below some level, no damage is seen. In terms of the above model, this seems understandable. As the accumulated dose increases, the absorptive edge moves steadily towards the more visible wavelengths. As this edge overlaps with the region where the primary waveshifts radiatively to the secondary, the plastic will absorb the light intended for the secondary. Hence one would expect a threshold where the light output would be expected to start rapidly dropping. In realistically large samples, one can hypothesize that on a logarithmic dose scale, light output would slowly decrease at low dosages. Above, say 10^3 Gy, would follow a region of rapidly decreasing light output. Whether there is saturation at high doses (> 1 MGy) is still an open question (although there is some evidence for this [39]).

Dose rate as a parameter has become of critical concern. There has been a variety of evidence to indicate that experiments must be sensitive to this parameter in order to correctly evaluate the validity of their results for actual experimental situations where a given dose may be spread out over a year or longer. Figure 8 illustrates the effect of using an unrealistic high dose rate. In this case, samples of polystyrene are irradiated by a ^{60}Co gamma source at a high rate to levels of 10-500 kGy. Figure 8(a) shows the transmission spectra immediately after these irradiations. However, the samples are seen to anneal over a period of time (several days to weeks), especially in air (figure 8(b)). Indeed this "bleaching" [40] of the sample can be seen as the yellow discoloration disappears from the surface towards the interior (figure 11). This process has been studied in some detail [40,41]. It is most rapid in the presence of oxygen, and the rate of bleaching is consistent with the diffusion of oxygen into the plastic. In addition, the rate of the annealing edge slows down as a function of dose and seems to reach a minimum rate above some dose ($\approx$ 80 kGy).

An annealing effect has also been verified to occur even in vacuum although at a much slower rate than at room temperature. An increase of the ambient

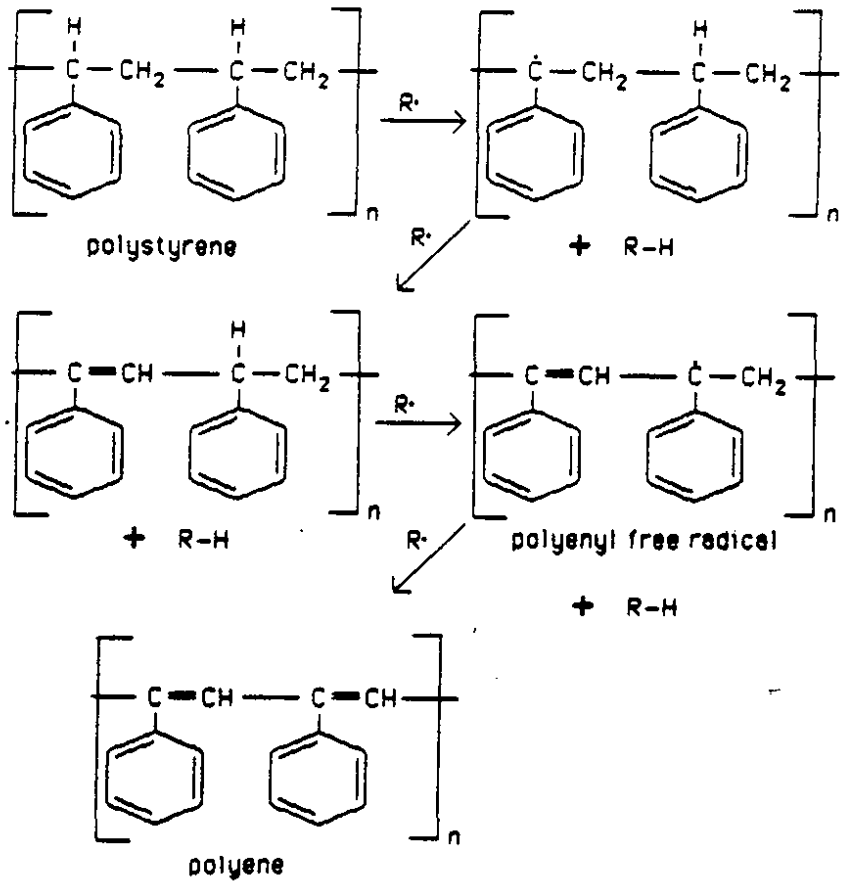

FIGURE 10: A likely candidate for the mechanism by which color centers are formed in polystyrene (and the related polyvinyltoluene). Adapted from reference [34].

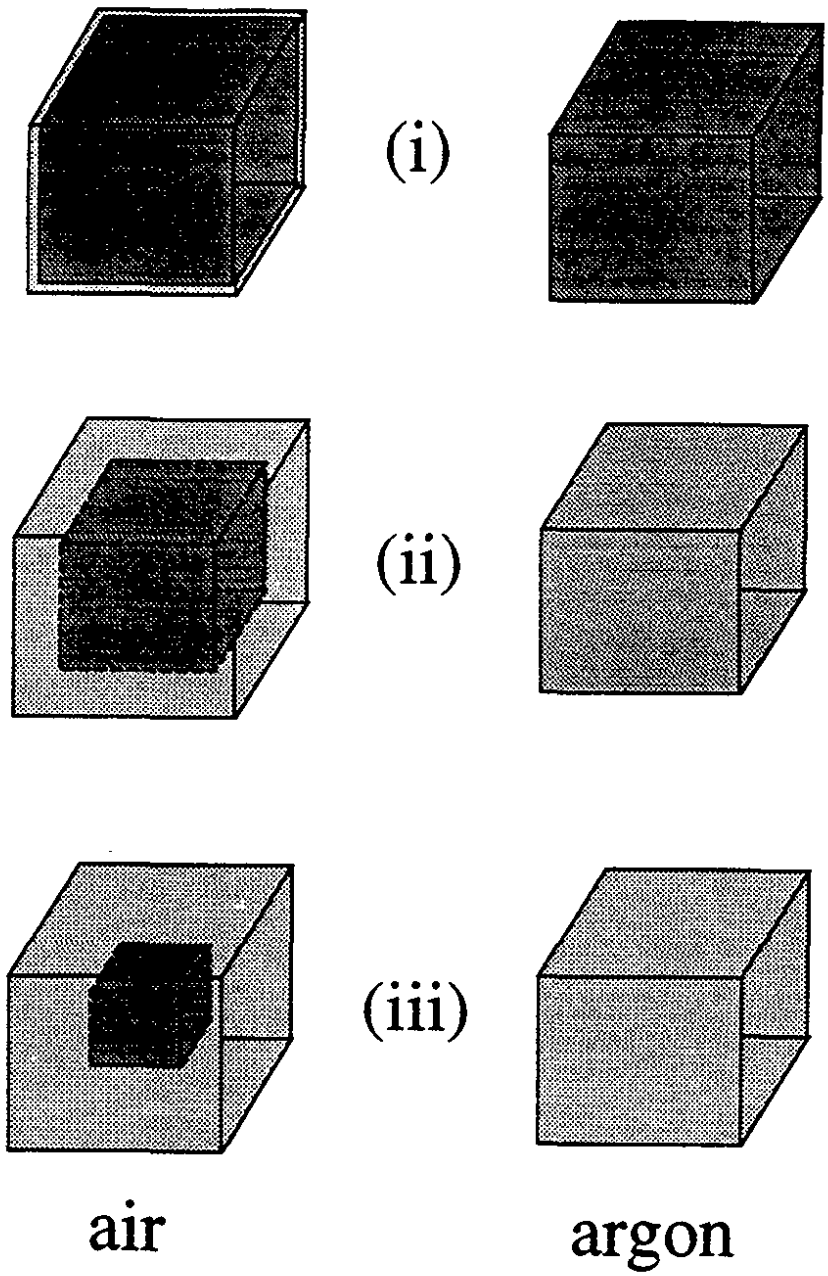

FIGURE 11: A pictorial representation of post-irradiation annealing in polystyrene cubes after a high dose rate irradiation. In air, oxygen diffusion drives the bleaching process at a rapid rate while in an oxygen-free atmosphere (e.g., argon), color center relaxation takes place slowly throughout the volume of the material. In air, the time scale from (i) to (iii) can be a matter of days while in argon the relevant time scale can be several months.

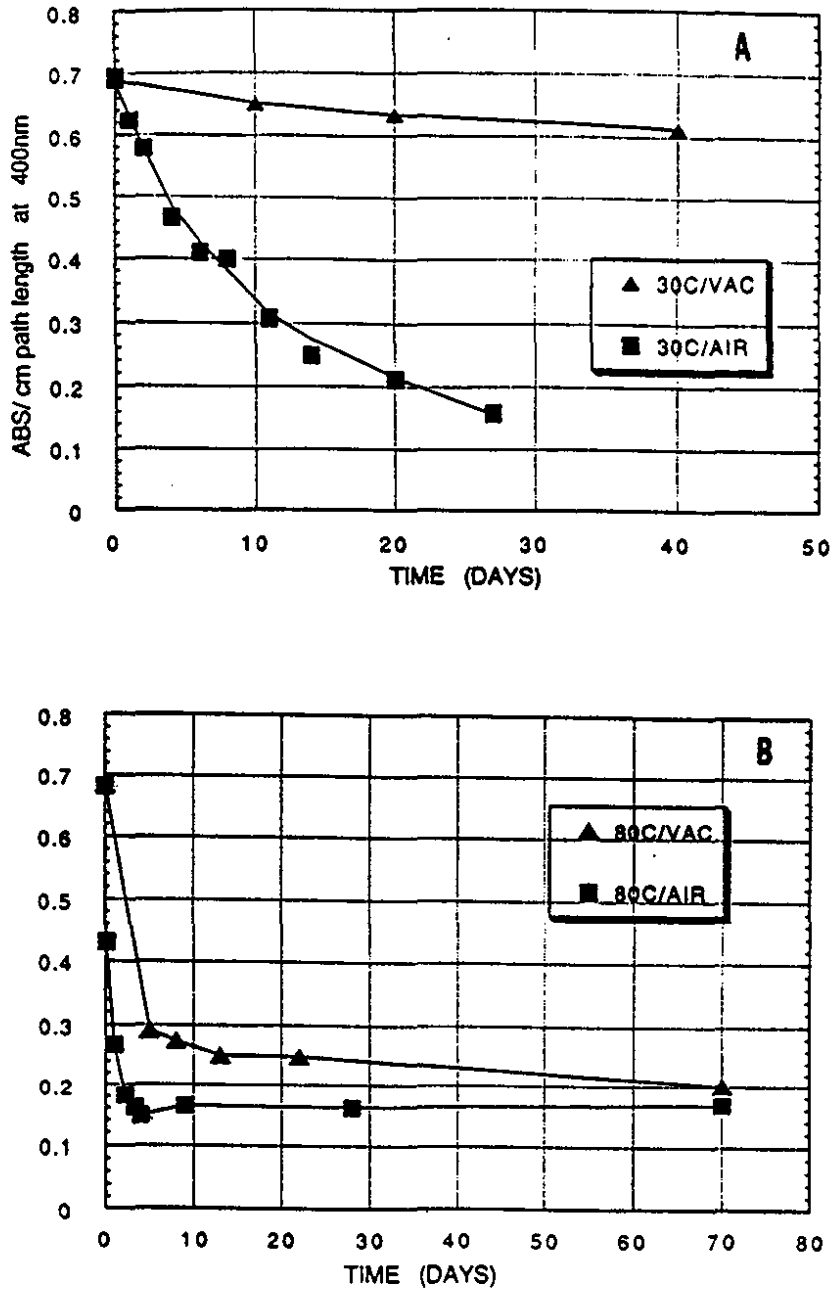

FIGURE 12: (a) Annealing of circular disks (0.25" thick x 0.612" diameter) of polystyrene in air and vacuum at room temperature after a high rate irradiation in vacuum to 15 Mrad. (b) Annealing of similar samples but at a substantially higher ambient temperature. Adapted from reference [41].

temperature ($50-80°C$) can increase this rate greatly [36,41] (figure 12). Unlike the foregoing case, the annealing takes place uniformly throughout the plastic. There is also a residual level of damage remaining after the completion of annealing. This residual level is larger as a function of the delivered dose.

The question that arises is whether this level of damage is the same as would occur if the same dose was delivered at a "realistic" rate (say over a period of at least a year). Very low dose rate experiments (< 10 Gy/hr) are now in progress and the full results are expected in the fall of 1991 and into 1992 [7,38,42]. As of this writing, some preliminary but nonetheless important results are available. These will be discussed later. First, we will review the indications given by previous studies.

One of the most relevant studies was performed by a sub-group of the ZEUS collaboration [40,43,44] upon polystyrene-based scintillators and acrylic-based wavelength shifters (WLS). In the case of the polystyrene-based scintillators, it was found that for a range of 30 Gy/hr to 10^4 Gy/hr, the level of damage was the same for a given dose (25 kGy) *if complete annealing was allowed to take place* (figure 13(a)). More importantly, online annealing was seen to take place (in air) since at the lower dose rates, less damage was observed immediately after irradiation than if the same dose was delivered at a much higher rate (figure 13(b)). In fact, the experimenters were able to find a dose rate (45 Gy/hr) for their thickness of scintillators (2.6 mm) for which they determined that the annealing formed an equilibrium with the permanent color center formation. On the other hand, they also reported [44] that for SCSN-38 [45] polystyrene-based scintillator, the loss in intrinsic light loss was twice as large for those samples irradiated in dry air as for those irradiated in an oxygen-free argon atmosphere. This seems to be indicative of a possible deleterious effect of oxygen during irradiation.

For acrylic, however, the effects are quantitatively different. A study [46] of acrylic-based scintillator used in a uranium/scintillator sampling calorimeter found that high rate tests underestimated the level of damage seen at a much smaller dose rate (in this case, due to the radioactive decay of the uranium absorber). In addition, this damage was greatly enhanced in the presence of oxygen. Figure 14 illustrates this result. The previously mentioned ZEUS group also noted that the annealing was much slower with the acrylic-based wavelength shifters. The high level of damage seen in these was attributed to the smaller diffusion coefficient for oxygen in acrylic (10 times lower than in polystyrene) and to the much higher levels of color center formation (a factor of 60) per unit dose compared to the polystyrene

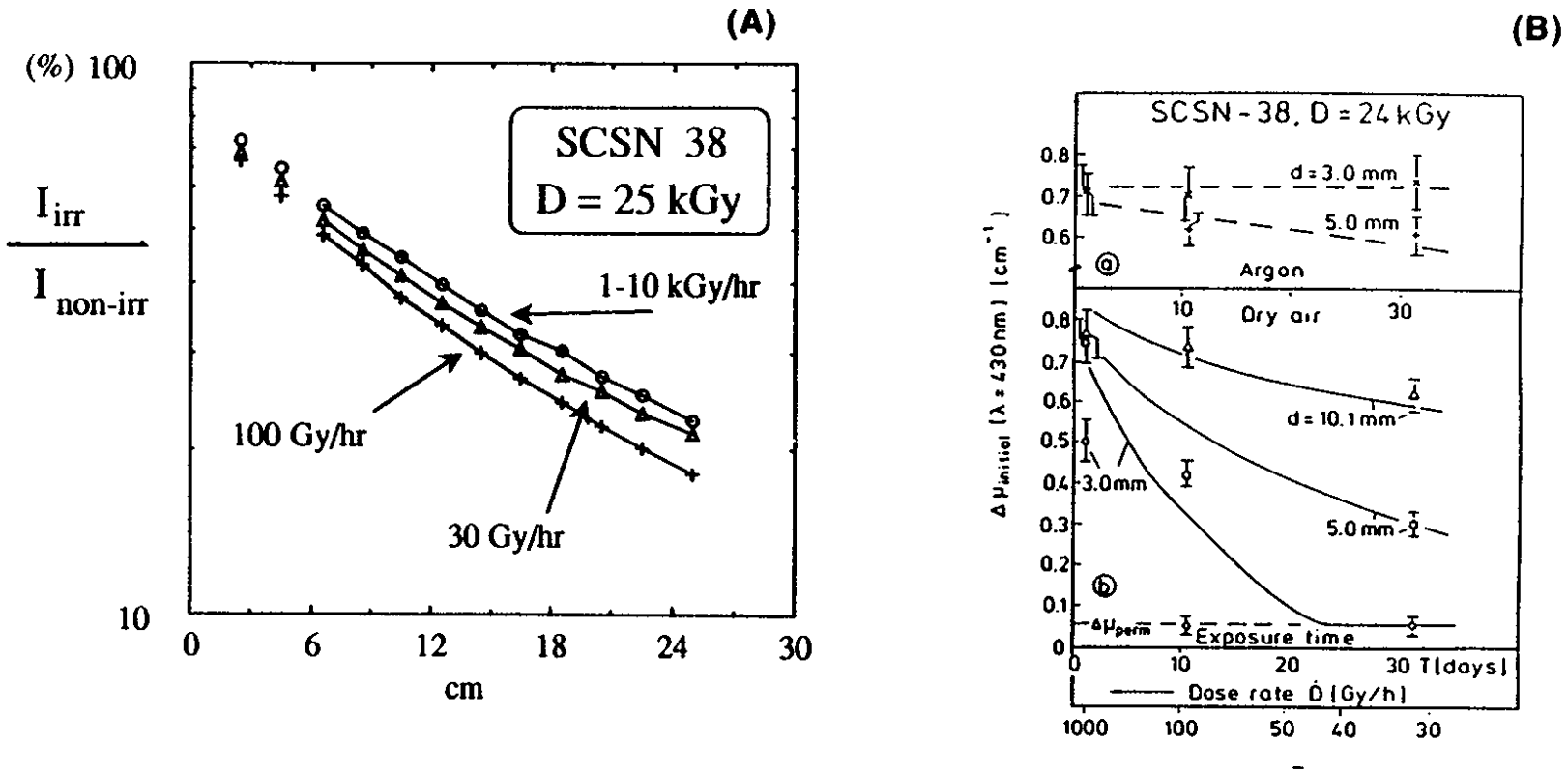

FIGURE 13: (a) Apparent dose rate independence in polystyrene-based scintillator irradiated and annealed in air. The level of transmission damage was found to be identical as long as complete annealing was allowed to take place. Adapted from reference [43]. (b) Demonstration of online annealing effect of oxygen during irradiation. The ordinate is a measure of the change in absorption through the scintillator sample. Adapted from reference [44].

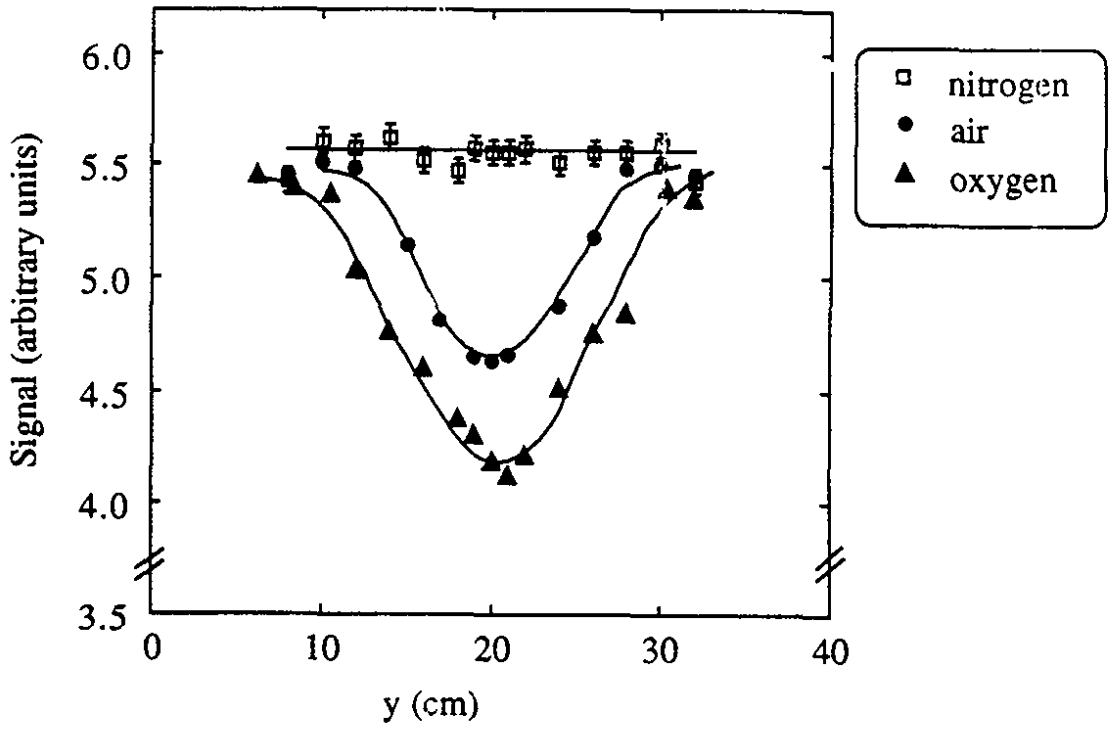

FIGURE 14: A demonstration of the destructive effect of oxygen during a low dose rate irradiation upon an acrylic based scintillator. A similar test at a high rate showed no such dependency upon atmosphere during irradiation. Adapted from reference [46].

scintillators [44].

In some of the initial studies on damage to plastic scintillator [2,36], a significant difference was found in the relative pulse height spectra obtained from small samples of scintillators depending upon whether an alpha (surface excitation) or a gamma (volume excitation) source was used. Specifically, the alpha particle induced spectrum seemed to have a much smaller relative amplitude. It was conjectured [2] that this was an indication of extra damage induced at the surface of the sample by the action of diffusing oxygen during irradiation. There are now some indications that this was indeed the case [47]. In irradiating 1 in^3 samples of polystyrene at 500 Gy/hr to 160 kGy, additional absorption was observed in a small layer ($\approx$ 2 mm thick) at the surface of the sample *after* annealing in air was allowed. The size of this layer is consistent with the extent of oxygen diffusion during the irradiation (in air). More importantly, this observation is indicative of a dose rate dependence for the irradiation of polystyrene (in an oxygen bearing atmosphere). The first implication is that polystyrene-based scintillators will exhibit additional permanent damage induced by the diffusing oxygen. The annealing by the oxygen is seen after the irradiation is completed. An important question arises: if the scintillator is kept out of contact with atmospheric oxygen (which is likely to some extent in some of the applications), will the radiation-induced color centers have time to relax under the more gentle conditions of an actual experiment as opposed to the high rate test conditions in which a relatively large concentration of color centers is created during the irradiation? Some early results from a ongoing low dose rate experiment (< 10 Gy/hr) seem to provide a (positive) answer to this question. We proceed to a brief discussion of this experiment.

II.3.4 Recent Low Dose Rate Results

As has been already mentioned, some results of a low dose rate (5.5 Gy/hr to 5 kGy) irradiation of a wide variety of scintillating fibers are now available. The study is a continuance of an earlier attempt at low dose rate irradiations [42]. All fibers are 1.5 meters in length and 1 mm in diameter. The irradiation is accomplished by a line source of depleted ^{60}Co. Figure 15 displays some typical data from the irradiation. The first 30 cm of fiber is shielded by a lead annulus in order that a measure of intrinsic light loss can be made at the point where the fiber becomes unshielded. The lead is thick enough to provide a factor of 200 less dose in the shielded region. The fibers are split into two groups: one irradiated in a flowing dry air atmosphere, and the other in flowing argon. Moreover, each of these two groups

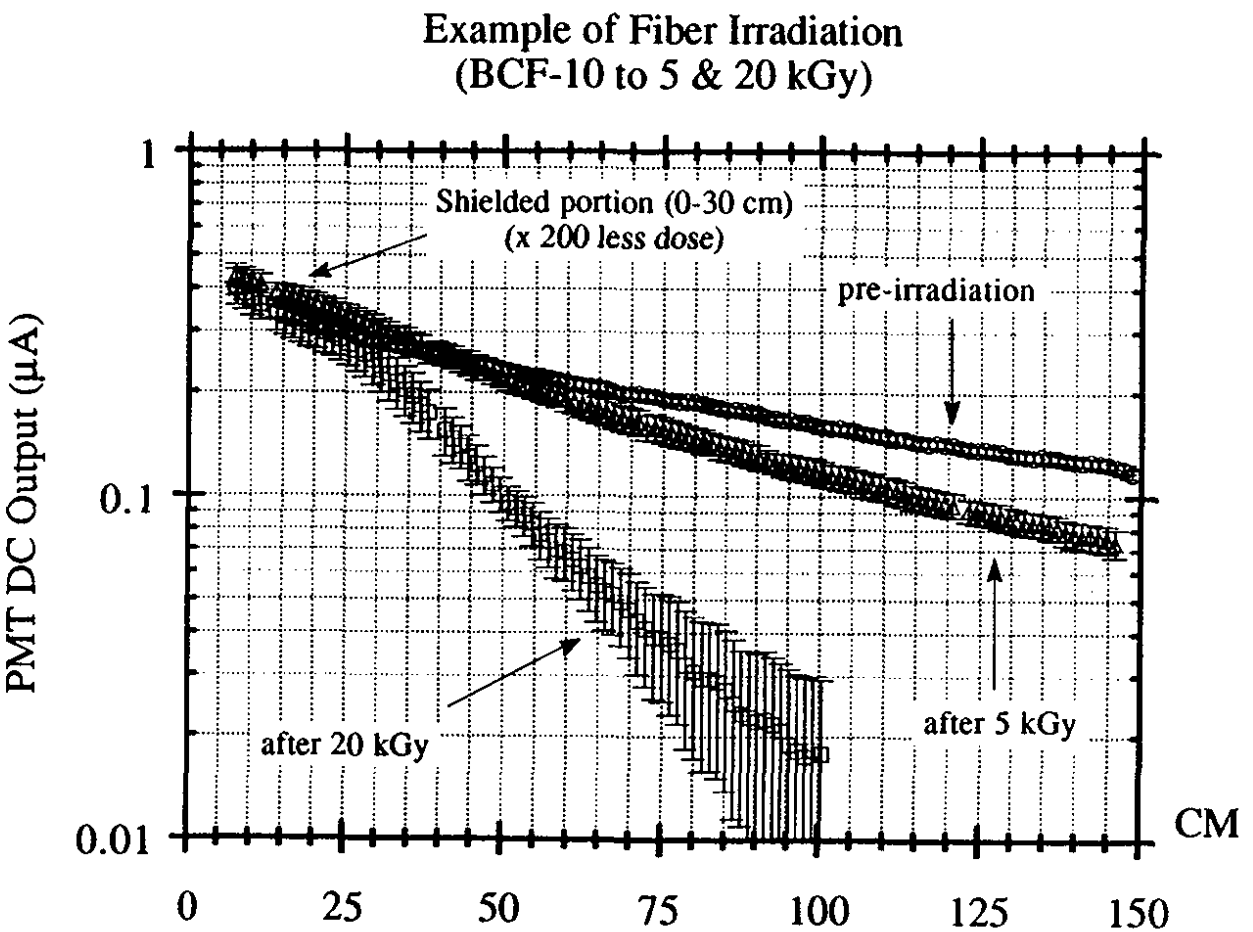

FIGURE 15: Typical data from a low dose rate (< 10 Gy/hr) irradiation of selected scintillating fibers.

is split into another two groups: one irradiated at 5.5 Gy/hr to 5 kGy, and the other at 7 Gy/hr to 20 kGy. There are 3 samples of each fiber in each of the four sets (12 samples of each fiber type in total) in order to obtain a measure of fiber to fiber variation. A first report on the transmission changes in the fibers has been reported elsewhere [141]. The preliminary results are clear: those fibers irradiated slowly (in order to allow complete oxygen diffusion into the material) in air suffer significantly more transmission damage than those irradiated in the oxygen-free (argon) atmosphere. Figure 16 is a display of the change in transmission character of two types of fiber: a blue-emitting (BCF-10) and green-emitting (3HF-doped) fiber after the 5 kGy irradiation. The importance of this result is twofold. First, since high rate irradiations do not allow sufficient time for diffusion of oxygen into the material, the post-anneal results from such irradiations should be equivalent to a low rate irradiation in an inert atmosphere. (Part of this low rate experiment will include such a comparison.) Hence, in realistic (i.e., low dose rate) situations where oxygen will be present, high rate irradiations will *underestimate* the amount of damage to be expected. Secondly, it may be worthwhile to circulate an inert gas (e.g., nitrogen) around a scintillation detector to minimize the level of radiation damage. Further studies of data include (a) measuring the intrinsic loss in light output, (b) comparing and contrasting the effect of a fluorinated acrylic cladding versus the standard PMMA cladding, (c) using optical filters, and (d) repeating the study for the 20 kGy sample set. The optical filters serve three purposes: (1) since only a bialkali photomultiplier tube is being utilized, the optical filters allow one to simulate (to some degree) the response of green and red-enhanced photodetectors, (2) the extent of damage as a function of wavelength can be ascertained, and (3) since some detectors, particularly fiber tracking systems, will use several meters of light pipe fiber for readout, the filters can simulate the effect of natural filtration of the scintillation light by these readout fibers.

II.3.5 Promising New Fluors

An "ideal" fluor should have the following characteristics: (1) high radiation tolerance, (2) high solubility, (3) large Stokes shift ($> 10,000$ cm^{-1}), (4) high quantum yield, (5) good Förster overlap with the base plastic, (6) low self-absorption, (7) large extinction coefficient, and (8) fast decay time (< 5 ns). (It is assumed that all such properties are valid when the dopant is dissolved in the typical scintillator bases.) The first large Stokes shift fluors to be tested were PMP [48-52], HBT [21], and 3HF [1,36,53,54]. Standard scintillators use a two-fluor system to emit in a

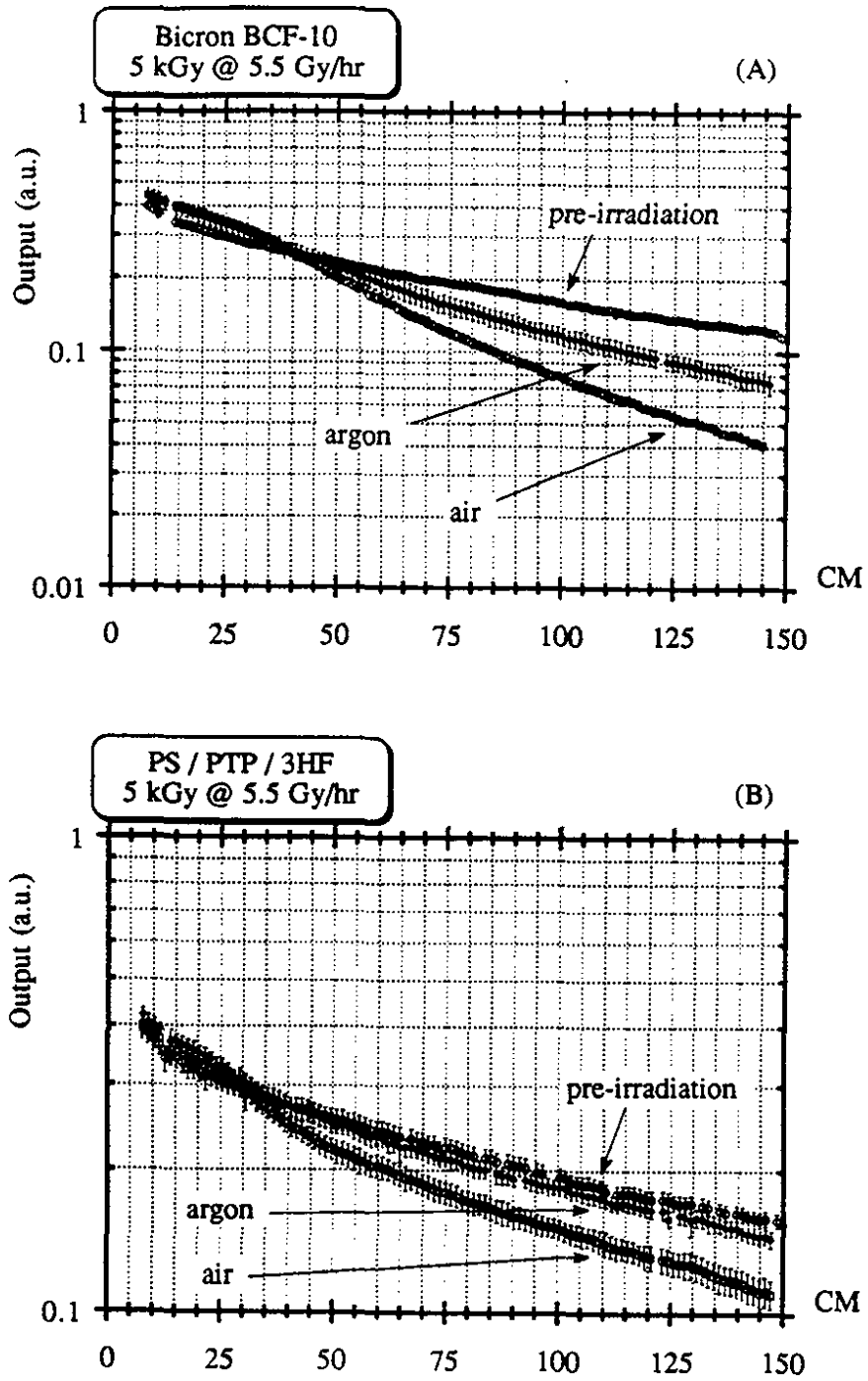

FIGURE 16: Some samples of data from a low dose rate irradiation of selected scintillating fibers (1 mm ϕ) in air and argon. The figures refer to (a) a blue and (b) a green-emitting fiber.

wavelength region of 420-440 nm. PMP is a large Stokes shift fluor that, in one step, emits at a peak wavelength of 425 nm. It was developed as a replacement for the standard two-fluor system for very thin optical fibers (< 50 μm diameter) in which the typical transfer length (> 100 μm) of primary emission to secondary absorption would result in a large loss in scintillation efficiency. The use of a large Stokes shift fluor at a high concentration results in a sufficiently small transfer length (≈ 10 μm) from base to fluor [24]. It has all the ideal properties except that of radiation resistance [7,27,55,56]. Some variants on this molecule have been synthesized which seem to have a better radiation tolerance [7] but seem to lack in some other qualities in comparison to the original PMP molecule such as self-absorption and quantum yield [57].

3HF was originally used as a method of producing a long attenuation length scintillator [58] with a peak emission at 530 nm. However the properties which allowed this also implied that a more radiation tolerant scintillator could be produced. These original [36,53,54] studies tested trial scintillators made of both PS/3HF and PS/PTP/3HF in a small sample size for their radiation tolerance. Better light output was found with the PTP/3HF combination, and so this is the presently used formulation in commercially available versions of the scintillator. This fluor has some drawbacks: (a) poor quantum yield (31%±5%) [1], (b) a poor overlap with the polystyrene emission band [58] (it is now used as secondary with PTP as a primary in order to obtain maximum light output), (c) a somewhat long (but not unacceptable) decay time (8 ns), and (d) is chemically labile [59]. In fact, it was at first rejected for use in a later study [21] because of processing problems in the production of the scintillator leading to discoloration of the samples. Another fluor with similar properties (but without the processing problems), HBT, was substituted. Unfortunately, it was found to have unacceptable levels of sensitivity to radiation [1]. In contrast 3HF is quite tolerant to being irradiated. Furthermore, the problems with 3HF can be overcome by (a) careful purification of the fluor, and (b) changing the temperature cycle for the scintillator polymerization process [1]. So despite some drawbacks to 3HF, it is still the chief component in any radiation-tolerant scintillators currently produced.

3HF has also been used to demonstrate how one could deal with the losses in intrinsic scintillation output [60-63]. This is accomplished by increasing the concentration of the fluor in the material. Figure 17 displays the result of irradiating several fibers doped with varying amounts of 3HF (and a fixed concentration of the primary PTP). For this irradiation, a portion of the fiber was shielded by a lead

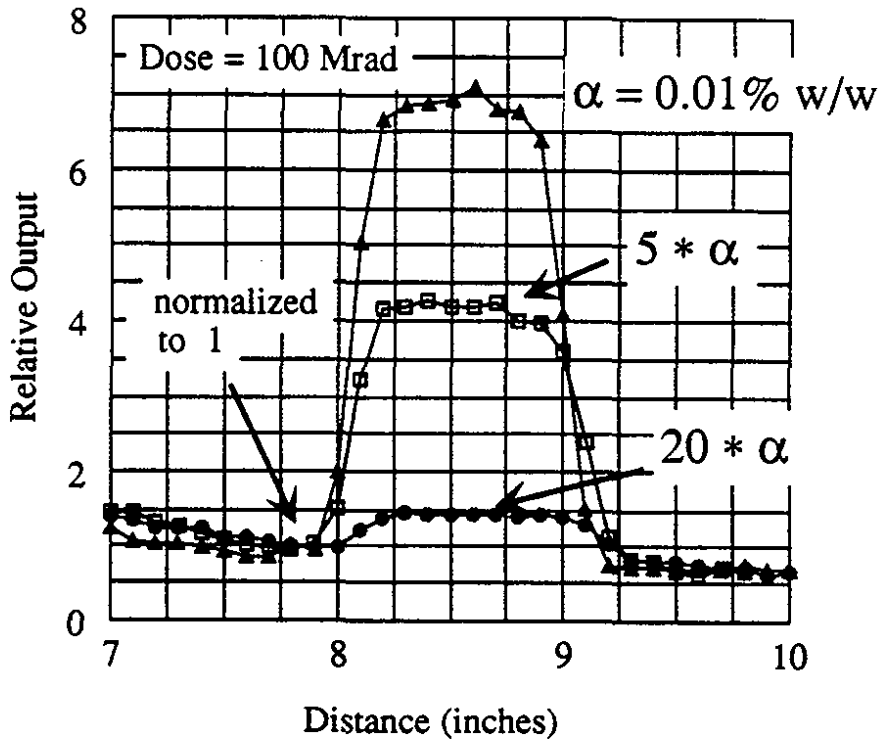

FIGURE 17: Effect of 3HF concentration upon intrinsic scintillation loss in a PS/PTP/3HF fiber. The larger the step size, the larger the loss in intrinsic light output. The use of increased concentrations of secondary fluors may minimize radiation damage in electromagnetic calorimeters. Adapted from reference [61].

sheet during the irradiation by a 3 MeV electron beam. The size of the step in light output between the shielded and unshielded portions indicates the relative amount of light loss—the larger the step size, the larger the loss [43]. Figure 17 shows that as the concentration of 3HF is increased, the intrinsic light yield is less damaged. The concentration effect may be useful for minimizing the effects of damage in electromagnetic calorimeters where loss in intrinsic output is the greatest concern [63-66]. (It is interesting to note that this concentration effect was originally reported over 35 years ago [39] in a study of the effects of radiation upon the light output of various polystyrene-based scintillators.)

The cause of this effect is likely due to a peculiarity in the way the absorption spectrum of 3HF overlaps the emission spectra of polystyrene and PTP. In one study of the effect of fluor concentration upon radiation resistance, only the concentration of the *primary* had any significant effect upon post-irradiation recovery [26]. In terms of the "hidden absorption" model [14] described above, this seems comprehensible. However, 3HF has a rather unique feature: while its absorption band does overlap the emission band of the common primary fluor PTP [22,58], it also overlaps the emission band of polystyrene. Hence, as the concentration of 3HF is increased, there is a growing probability of non-radiative energy transfer taking place between the plastic base and the fluor (and perhaps even with the primary). In a standard scintillator, the secondary (at the typical concentrations) can only interact radiatively with the primary fluor. By allowing for an alternate route of energy transfer, it is possible for the PS/PTP/3HF scintillator to have increased resistance to intrinsic light losses. (Finally, since the concentration of the fluor is affecting the rate of the energy transfer process, it is possible that the decay time of the scintillator may be significantly improved. An experimental test could prove worthwhile.)

It should be pointed out that there are a variety of efforts in progress to make acceptable substitutes for 3HF [1,27,34,67-69] (in terms of decay time, quantum yield, Stokes shift, Förster overlap with polystyrene, and radiation resistance). Bicron Corporation has produced two green-emitting scintillators based on large Stokes shift technology that are brighter and faster than PTP/3HF. Unfortunately, as with PMP, these fluors are radiation-soft. However, they may have a useful application as fast, bright waveshifter fluors for sampling calorimeters that do not face radiation problems [84].

One can formulate scintillators for two idealized cases:

(1) An intrinsic scintillator [1,21] doped with a single large Stokes shift fluor emit-

ting above 500 nm combining the positive aspects of PMP (solubility, low self-absorption, speed, quantum yield) and those of 3HF (emission above 500 nm, radiation resistance).

(2) A two-step scintillator doped with two fluors, at least one of which must have a large Stokes shift: (i) a large Stokes shift primary emitting at 420-450 nm, and (ii) a secondary waveshifter with an emission preferably above 500 nm. This system may be useful for calorimeter systems that utilize active scintillator elements read out by waveshifter fibers. More about this will be said later.

II.3.6 Radiation Tolerant Bases

Another approach to improving radiation tolerance would be to find or synthesize a more radiation-tolerant plastic base. A study done some years ago [70] indicated that of the related materials polystyrene (PS), polyvinyltoluene (PVT), and polyvinylxylene (PVX), the order of radiation resistivity goes as PVX > PVT > PS. PVT is a well-known material for bulk scintillators, but it cannot be readily used in fiber form (which is of high interest at present). Although it may be the most radiation resistant, PVX seems to have some serious shortcomings, among them being the difficulty of polymerization and toxicity of the raw material. An initially hopeful candidate was polymethylphenylsiloxane [20,71-76]. This material has excellent optical qualities, one of them being radiation resistance. However, the solubilities of the standard fluors are extremely poor in it. This has resulted in the synthesis of a variety of oligophenylene fluors [20,34,68,71-73] which could be dissolved in sufficient quantities in this material. A result of this research is that some of these fluors may now form the basis of highly resistant *polystyrene*-based scintillators [67]. Efforts were also made to modify the structure of the siloxane material in order to improve its mechanical qualities as it tends to form elastomers [77,78]. Unfortunately, this seems to have resulted in serious degradation in the optical quality of the material. (Incomplete polymerization resulted in the formation of crystalline Rayleigh scattering centers giving the material inherently poor attenuation properties.)

Bicron has also produced an improved base material (RH-1) (not related to the aforementioned polysiloxane) which has undergone some promising preliminary tests of its radiation hardness when used as a base for blue-emitting scintillator [61,62]. It may be that a combination of this material (or a suitable improvement over it) doped with the new large Stokes shift fluors may produce the most radiation resistant plastic scintillator.

Additives are undergoing active study for two reasons: (1) their possible role in increasing the absorptive damage, and (2) the possibility of using them as active radical "eaters" that would prevent the formation of color centers. A group at Sandia National Laboratories [27] is actively researching this topic at present.

It may turn out that temperature will be a critical parameter both in understanding and alleviating radiation damage. It may also explain some accounts of significant amounts of radiation damage in scintillators that were thought to have a higher tolerance [37,38]. It has already been pointed out how temperature may have affected the quality of 3HF-doped polystyrene [1]. Johnson [79] has reported that standard plastic scintillators, pre-heated before irradiation, consistently suffered greater levels of residual (post-anneal) damage as compared to "room temperature" (25°C) scintillators. Coincident with this is a continuing study of radiation damage in polystyrene [41], which has shown that the rate of recovery of the plastic after irradiation can be highly accelerated in a vacuum to a point where the rate of recovery is not much lower than in air (figure 12). There is also an indication that the presence of oxygen during irradiation at an elevated temperature (50°C) can increase the levels of damage seen as compared to those observed with the same atmosphere but at normal room temperature [36]. Taken together with the low dose rate results, this could indicate that for maximum radiation protection, one should (a) *minimize* exposure to oxygen during irradiation (which could be the default with scintillator imbedded in some structure such as lead), and (b) maintain a slightly elevated temperature so as to allow for annealing in anaerobic conditions.

II.4 Applying this Knowledge to Scintillator-based Detectors

II.4.1 Plastic Scintillators

The use of scintillator in the form of optical fibers is of great interest for some detectors proposed for the SSC and LHC as well as at current facilities [3,28,48,80-110]. Even in cases where bulk scintillator is proposed, optical waveshifting and light guide fiber is proposed as the method of transporting the output to the photodetectors [111]. Figure 18 displays the structure of such a fiber. They are of the "step-index" variety with a core made of doped polystyrene (refractive index n=1.60) clad with acrylic (n=1.49). The typical diameters are 0.5-1.5 mm and are either circular or square in cross section. The question arises as to whether the radiation softness of the acrylic will degrade the performance of the fiber even though the polystyrene-based scintillator core is sufficiently radiation hard. To appreciate this point better, it is best to discuss some aspects of measuring the optical

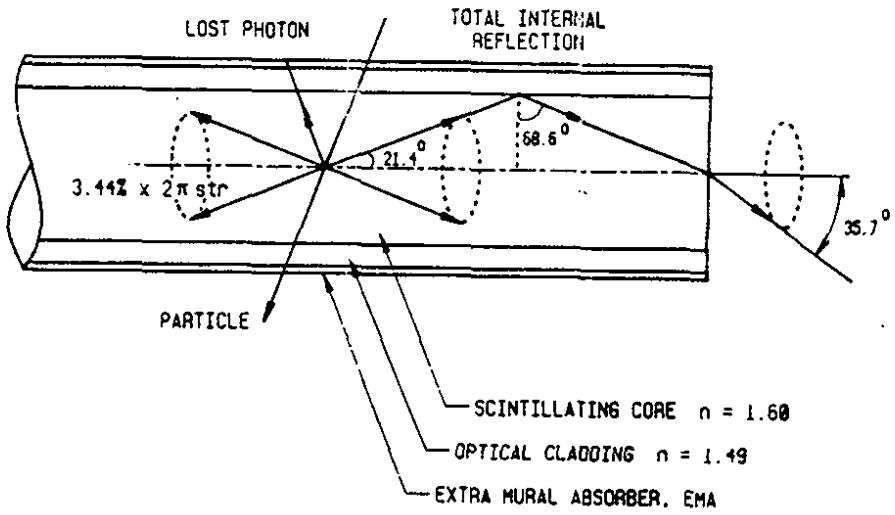

FIGURE 18: *Schematic representation of a typical scintillating fiber. Adapted from* reference [133].

characteristics of these scintillating fibers.

Figure 19 shows the light output (dc current from a bialkali phototube) detected as a source (continuous X-ray tube) is moved along the fiber. It has been found [101] that most of the light detected within the first 50 cm was due to light propagating down the cladding. This light was sharply attenuated as a function of distance. However, it added a large component to the detected signal near the readout end of the fiber. In addition, the authors claimed that this light was significantly affected by repeated handling of the fiber. Hence it was impossible to obtain consistently repeatable results. It became evident that this component should be filtered out from the detected signal. This filtering of the cladding light is necessary for another reason. If the cladding grows optically more opaque than the core for a given dose, then the cladding light will be optically attenuated to a greater degree than the core light and hence the output signal will vary to a much greater degree than if the cladding light had been eliminated in the first place [12]. The absorption of the cladding light can be accomplished by coating the fiber with an extra-mural absorber (EMA) for a short distance near the readout end of the fiber. Even with the removal of this component, an additional component can be seen. At this point, it is important to note the effect of the photodetector. After the cladding light has been eliminated, the photodetector's response as a function of wavelength determines the shape of the attenuation curve. With a blue-sensitive bialkali tube, this extra component seems due to the shorter wavelengths that are attenuated fairly rapidly within the fiber (see figure 20). By use of a filter (or equivalently a red-enhanced photodetector such as the Burle 8852 or Hamamatsu R1333), the effect of these shorter wavelengths can be removed and a significantly higher attenuation length measured [61,112,113]. Equivalently, the use of a sufficiently long piece of clear (undoped) fiber can be used to filter out both the cladding light and the shorter wavelengths [30].

A key component in the attenuation behavior of the fiber is the quality of the fiber-cladding interface, that is, the effective reflection coefficient must differ from 1.0 by only a small fraction ($< 10^{-3}$) [18,115]. With respect to radiation studies, although the cladding plays no active role in the transmission of light (and in fact this cladding light should be eliminated as an extraneous noise element), there is the question of whether the interface is maintained as well after irradiation, especially a low dose rate one. At the time of this writing, a low rate test (< 10 Gy/hr) is in progress with both acrylic and fluorinated acrylic clad fibers to determine if the cladding has some effect [42,142]. The preliminary data indicates that there

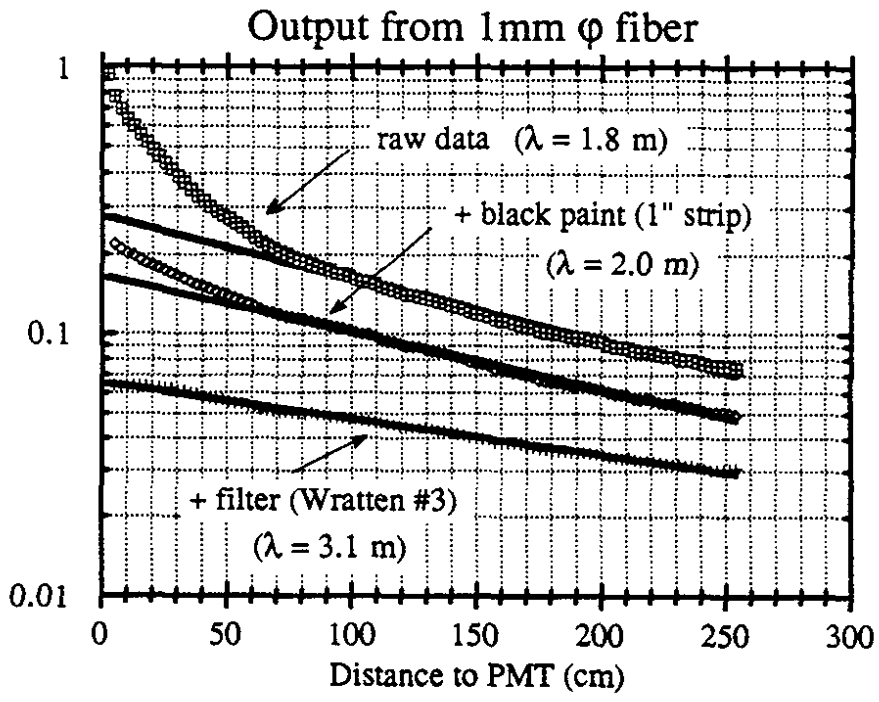

FIGURE 19: Typical attenuation behavior for a 1 mm fiber (SCSF-38). Cladding light creates a large but highly attenuated component near the readout end. Improved attenuation behavior can be achieved by absorbing this light with EMA and by optical filtering. In proposed tracking detectors, long lengths (several meters) of readout lightpipe fiber will have the same combined effect.

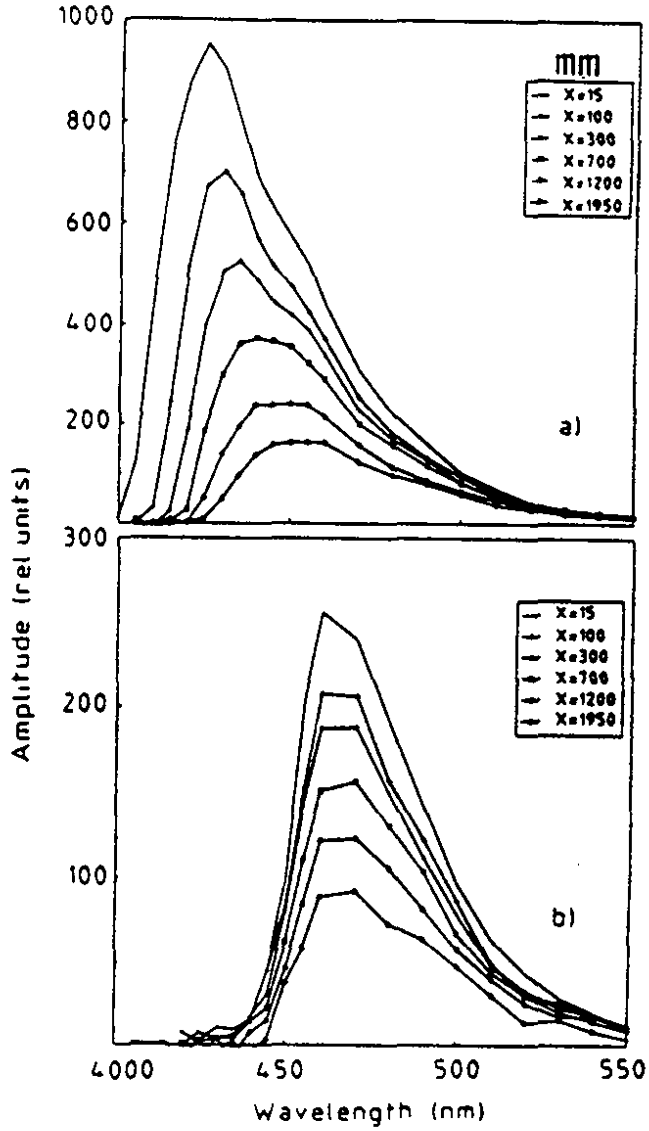

FIGURE 20: Attenuation of the fluorescent emission of fiber used in the UA2 experiment. The use of an optical filter (Wratten #3) reduces the total light output but improves the attenuation behavior. Adapted from reference [112].

is no advantage to the alternate cladding. In addition, two atmospheres (air and argon) are being used to see (a) if oxygen is necessary for online annealing or will the color centers anneal on their own, and (b) can oxygen cause problems with the cladding and polystyrene core as noted above [41,47]. As noted previously, it seems clear that the presence of oxygen during irradiation at such a low dose rate leads to increased transmission damage over fibers irradiated in an essentially oxygen-free atmosphere.

For proposed tracking detectors utilizing scintillating fibers, both the amount of intrinsic scintillation output and attenuation length could be crucial to their performance since trackers will depend upon maximal detection of photons at the readout end of the detector. The large size of such a detector (several meters in length) will make the detection efficiency sensitive to any attenuation changes and loss in intrinsic light output. Fortunately, their position in the barrel region of the detector will allow them to escape the highest dose levels.

On the other hand, the electromagnetic calorimeters, particularly in the forward regions, will suffer the highest dose levels ($>$ 10 kGy annually) due to the copious production of $\pi^0 \rightarrow \gamma\gamma$ decays which shower in the calorimeter. For *electromagnetic* showers, most of the deposited energy is concentrated within a relatively short longitudinal range within the calorimeter. Monte Carlo studies [64] have indicated that the loss in scintillation output will have the most effect upon the measured energy resolution. Attenuation changes will have little influence upon the measurement. In contrast, attenuation changes will be critical for *hadronic* calorimetry since the showers are spread over a much larger volume. In fact, maximal attenuation lengths are needed for such calorimeters to achieve their expected energy resolution. Hence changes in attenuation can drastically alter their performance. Another aspect comes from the fact that the source of the irradiation will likely have a different energy spectrum than the source of the interesting physics. Hence a true test of the performance should be based on testing the capability of the detector to "resolve" the physics of, say $>$ 10 GeV particles after being irradiated with a 1 GeV beam [64].

Another proposed calorimeter uses small scintillation tiles read out by green waveshifter fibers [111]. The smallness of the tiles prevents the effects of attenuation from having too large an effect upon performance, while at the same time, the use of a green dye in the readout fiber minimizes attenuation. This system is currently undergoing development for the Solenoidal Detector Collaboration [10].

With regard to this approach, some recent results [67] on new scintillation

dyes may provide a useful guide. Very encouraging results were obtained with scintillators utilizing the modified oligophenylenes (synthesized originally for the aforementioned polysiloxane research) as the primary, and standard waveshifters such as BBQ and K27 as the secondary. It is conceivable to think of the scintillator plates doped with O415A or O408 emitting (very efficiently) fluorescent light in the blue region. This could be absorbed and re-emitted at 470 or 500 nm (peak) by either of the two waveshifter fluors. *It is important to note that the scintillators formed from using only the sexiphenyl primaries are not only as bright as standard blue scintillators, but are also the most radiation-resistant plastic scintillators recorded in the literature (for small size samples).* Table 1 lists the results of high rate irradiations from the study [67]. The primary limitation on the use of these oligophenylenes is the present high cost of synthesis of these fluors. Nonetheless, the exceptionable performance of these sexiphenyl scintillators warrants immediate further investigation of their properties when used in larger scintillator sheets and fibers. (These oligophenylenes are also unique in having exceptionally high extinction coefficients, and so smaller concentrations are required to maximize the probability of non-radiative Förster transfer.)

II.4.2 Liquid Scintillators

Although liquids have traditionally had some problems associated with them (handling, toxicity, leakage), they have the potential of offering maximal radiation tolerance (over plastics) for extremely high radiation areas such as the forward regions ($\eta > 3$) of SSC and LHC detectors. In principle, one could conceive of circulating the fluid so as to replace the damaged material in the worst case scenario. There has not been as large an effort devoted to liquids, but the initial results indicate that serious consideration should be given to using liquids as the sampling medium in forward calorimeters [25,116-118]. In addition, liquids are being tested for high resolution tracking applications [56,119-123,136,139,140].

Unlike plastics, no annealing phenomenon is seen with liquids [25]. This may indicate that annealable color centers cannot form in a liquid state. Hence it is possible that liquids may very well display dose rate independence which will facilitate easier testing.

Some inital tests of 3HF in a liquid base [25] showed little or no change after a 50 kGy irradiation (in a small sample). More recently, 1-phenylnaphthalene (1PN) has been tested as a more radiation-resistant base for a synthesized fluor MOPOM (to replace PMP) [56,122]. Even after 100 kGy, the light output dropped by only a

SCINTILLATOR[a]	λ[b] (nm)	Light Yield				Ratio[d]
		Before	After	After 13 days[c]	After 53 days[c]	
MOPOM	420	0.90	0.05	0.48	0.56	0.62
MOPOM + 0.01% BBQ	470	1.08	0.15	0.72	0.81	0.75
MOPOM + 0.02% BBQ	470	1.09	0.18	0.78	0.86	0.79
MOPOM + 0.01% K27	500	1.08	0.31	0.85	0.94	0.87
MOPOM + 0.02% K27	500	1.08	0.31	0.85	0.96	0.88
O415A	415	1.05	0.56	0.90	1.00	0.96
O415A + 0.01% BBQ	470	1.15	0.48	0.98	1.10	0.96
O415A + 0.02% BBQ	470	1.16	0.39	1.01	1.13	0.97
O415A + 0.01% K27	500	1.10	0.65	0.99	1.09	0.99
O415A + 0.02% K27	500	1.13	0.60	1.00	1.11	0.99
O408	410	1.00	0.55	0.86	0.94	0.94
O408 + 0.02% BBQ	470	1.16	0.39	0.99	1.13	0.97
O408 + 0.02% K27	500	1.10	0.65	1.01	1.11	1.01
DAT	375	0.83	0.18	0.52	0.53	0.64
DAT + 0.01% DMPOPOP	430	0.98	0.35	0.80	0.85	0.87
DAT + 0.01% 3HF	530	0.97	0.46	0.72	0.78	0.81
PTP	360	0.96	0.24	0.47	0.48	0.50
PTP + 0.01% DMPOPOP[e]	430	1.00	0.58	0.81		

[a] Fluor concentrations are by weight with the concentrations of the primaries at 1% (except for PTP and DAT which are at 1.25%).

[b] Wavelength of peak emission.

[c] First 10 days in oxygen and the remainder of the recovery time was in air.

[d] The ratio is defined as *(After 53 days) / (Before)*.

[e] Defined as the reference scintillator.

TABLE 1: The results of irradiating new fluor combinations doped in polystyrene to a total dose of 100 kGy. MOPOM is a fluor originally synthesized as a more radiation tolerant version of PMP. In a liquid base (1-phenyl-naphthalene), MOPOM was significantly more radiation resistant than PMP [56,122]. The oligophenylenes (O415A, O408, DAT) were originally synthesized as soluble fluors for polysiloxane-based scintillators [20,34,68,71-73]. Note in particular the exceptional performance of the sexiphenyls (O415A, O408). Such combinations may be worthy of study for tile/fiber calorimeters [111]. (The molecular formulae for the new fluors may be found in appendix II.A.) Adapted from reference [67].

few percent. This bodes well for the idea of a highly resistive liquid scintillator.

Currently, tests are underway [116,117] to test liquid scintillator calorimeter modules. These consist of hexagonal lead tubes with a central hole that allows for the insertion of glass capillary (1 mm ϕ) tubes that are filled with the liquid. Some initial tests of the effect of the "cladding" (in this case, glass) have indicated that browning of the glass does not affect the output of the scintillator. However there are concerns as to whether the glass interface can be made smooth enough (paralleling the concern in plastic fibers). Traditionally, teflon is used as the low index of refraction cladding material. Concerns about its mechanical stability under irradiation have prompted tests of replacement material such as HALAR [124] and VITON [118]. Other related fluoropolymers that should be investigated include PEEK [125] and KYNAR [126]. Developmental work is also taking place with a liquid version of the tile/fiber type of calorimeter [127] (where the scintillator tiles are replaced with liquid cells).

There is also work on using 20 μm glass capillaries filled with liquid scintillator being performed at CERN [121], in this case with PMP in 1-methylnaphthalene (1MN) or isopropyl-biphenyl (IPB), although there are plans to test the fluor MOPOM later [128]. An important accomplishment of this group (CHARM II) has been to produce very thin capillary glass capillary tubes [129] with an excellent inner surface. For thin tubes, the propagating light must suffer a large number of reflections, hence the quality of the inner surface is critical to the performance of this detector. Experimental studies with 49 μm, 180 μm, and 900 μm diameter capillaries filled with 3HF-doped IBP indicated that attenuation lengths above 1 meter were possible for this scintillator (although it should be noted that a *small* concentration of dye was used in this study to minimize self-absorption by the fluor). In a related study [139], attenuation lengths with realistic concentrations of fluors indicated attenuation lengths of 30-40 cm for capillaries. However, the point is made: attenuation in thin capillaries is limited by the bulk attenuation character of the scintillator, and *not* by the absorptive properties of the capillary itself. In recent beam tests [136], a liquid scintillator tracker with 20 μm diameter capillaries gave equivalent position resolution (15 μm) to plastic fibers of 30 μm diameter, while reducing crosstalk via the inclusion of EMA among the capillaries. (For plastic fibers, no EMA has been found which does not diffuse into the material.)

Some data on radiation resistance seems indicative of good radiation tolerance for *tracking* applications [140]. Glass capillaries of 100 μm diameter were filled with a scintillator 1MN + R6 (peak emission at 480 nm). After 130 kGy, the attenuation

length was reduced by 40%, and after 300 kGy, by over 60%. Comparing this with some data on 1 mm diameter plastic scintillating fibers [131], a blue-emitting fiber (RH-1) suffers a change of 75% in attenuation after 100 kGy, while a green-emitting fiber (SCSF-Y7) suffers a similar drop after only 30 kGy. A 3HF-doped fiber lost about 12% in attenuation after 30 kGy.

At the present time, the technique of using liquid scintillator seems highly promising and worthy of further development.

II.5 State of the Art

The most up-to-date information on the radiation resistance of scintillating fibers is found in data by the SPACAL [12,130], CEBAF [61,62], and FSU [131] groups. The latter two are continuing on from general studies of radiation damage in organic scintillators to more systematic tests of plastic scintillating fibers. Among these are (1) the effects of very low dose rates and the presence/absence of atmospheric oxygen (see figures 15 and 16), (2) the effect of different adhesives † ¶ (and a search for a suitable one that won't degrade the performance of the fiber), (3) defining a relationship between high and low dose rate tests,‡ (4) testing new scintillator formulations, and (5) checking for variations within and between batches of a single formulation. The FSU group is also participating in studies of radiation-hard liquid scintillators [117] and in radiation tests for the SDC tile/fiber calorimeter project [10,111]. Both the CEBAF and FSU groups have also collaborated with the University of Illinois at Urbana-Champaign (UIUC) group (responsible for the JETSET electromagnetic calorimeter [105]) in performing some very preliminary radiation tolerance evaluations of a Pb/PSF (lead/plastic scintillating fiber) calorimeter [63]. This same UIUC group has performed some tests with the lead-eutectic design of

---

† A. Para, E. Skup, and G. Yasuda of Fermilab are carrying out an extensive survey of the effects of a wide selection of adhesives upon plastic scintillating fibers before and after irradiation.

¶ A group from Japan has recently published a report [137] on the transmission changes to various optical glues after doses of up to 10^6 Gy. Among the results, we note that the standard optical cement NE581 [138] shows no degradation above 400 nm after a 10^6 Gy exposure from an intense ^{60}Co source for a sample thickness of 10 μm.

‡ A group lead by N. Giokaris at Fermilab is also engaged in current tests comparing scintillators irradiated at high (12 kGy/hr) and low (1 Gy/hr) dose rates to identical doses.

Boston University [83,132]. (These lead-eutectic modules are a modification of an earlier design by a European group [95,96].) The most important result of these studies was the need for further careful evaluations of the fibers when used in a specific calorimeter design.

It should be noted that only now are truly systematic studies taking place which will delineate the appropriate characteristics needed for good detector performance. The previous studies have been needed to provide the conceptual basis upon which specific tests of specific parameters can take place. (Presumably some of that conceptual basis has been presented in this report.) For example, the previously mentioned calorimeter tests first uncovered the possibility of temperature severely affecting the radiation tolerance of the scintillator. This occured because there had been evidence that the usual glue used in the construction of the calorimeter (BC600 [33]) was found to adversely affect the performance of the scintillator (presumably because the glue "attacked" the cladding during irradiation). In this case, the glue was replaced by a radiation-hard and chemically inert polymethylsiloxane. However the latter required some moderate heating to cure it. The performance of the "pre-heated" Pb/PSF sandwich seemed extremely poor after irradiation as compared to irradiations of the fiber alone (RH-1 [33]).

The SPACAL group [12,130] has also verified that a glue (Araldite F) used in an earlier SPACAL prototype (as well as in the OMEGA and NA38 fiber calorimeters [3]), would also severely degrade the performance of the fiber under irradiation (SCSF-38 [45]). The SPACAL study has the unique feature of predicting the performance of the fiber when used in a calorimeter by utilizing a non-uniform dose profile that approximates the one created by electromagnetic showers in a calorimeter of the SPACAL design (that no longer uses any glue of any sort). Based on the experimental studies of the fibers and upon a Monte Carlo study of the SPACAL calorimeter, it is concluded that SCSF-81 [45] and a PS/PTP/3HF formulation should provide acceptable performance up to a 70 kGy dose absorbed in the peak of the dose profile. These fibers had the best combination of least intrinsic light loss and least change in attenuation. (Specifically, SCSF-81 had the least light output loss and the PTP/3HF formulation had the minimum change to attenuation. No attempt was made to utilize the aforementioned concentration effect [60-63] to minimize the light loss in the PTP/3HF formulation.) In terms of the consequence of the obtained results for a Pb/PSF calorimeter, the SPACAL group concludes that *for 4 years of* 10^{-34} $cm^{-2}s^{-1}$ *luminosity at the LHC, Pb/PSF calorimetry is feasible for a pseudorapidity* $\eta < 2.7$ *at a distance of 4 meters from the pp interaction vertex*

[130]. The group plans further irradiation tests, particularly Pb/PSF calorimeter modules with electron beams of the appropriate energies.

II.6 Concluding Remarks

The present series of systematic investigations, if continued, should allow us to solidify our understanding of the effects of radiation upon scintillator performance to the point that for a given radiation environment (i.e., dose rate, atmosphere, temperature, etc.) and detector configuration, it may be possible to estimate (or even compute) the optimal combination of plastic base, fluors and fluor concentrations. Within the next few years we will probably have a variety of bases, with different strengths and weaknesses, and a palette of fluors to choose from. Most importantly we should have the quantitative understanding necessary to select the combinations most suitable to the physics goal.

ACKNOWLEDGEMENTS

I would like to thank Dr. Kurtis Johnson of Florida State University for his critical appraisal and useful suggestions. I must also express my gratitude to Dr. Fabio Sauli of CERN for patiently awaiting the final version of this paper long after the original due date.

Appendix II.A

Glossary of common solvents and fluors

(A) Solvents

Plastics:

[1] PS polystyrene

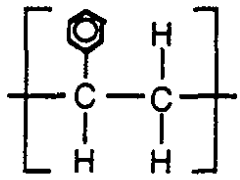

[2] PVT polyvinyltoluene

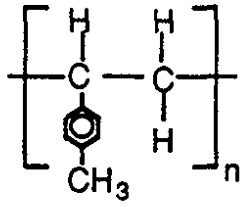

[3] PMMA polymethylmethacrylate

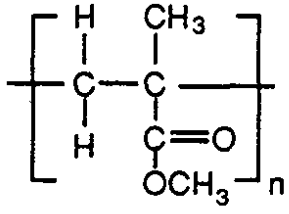

[4] PVX polyvinylxylene

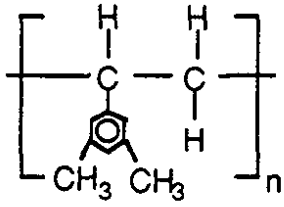

Liquid:

[5] Toluene

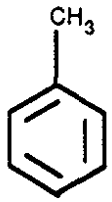

[6] 1MN 1-methyl-naphthalene

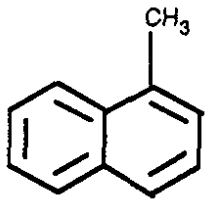

[7] 1PN 1-phenyl-naphthalene

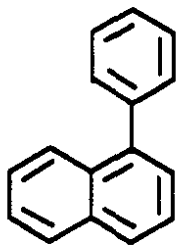

[8] pseudocumene

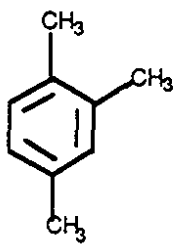

(B) Primary Fluors

[1] PTP para-terphenyl

[2] BPBD 2-(4-biphenyly)-5-(4-*tert*-butylphenyl)-1,3,4-oxadiazole

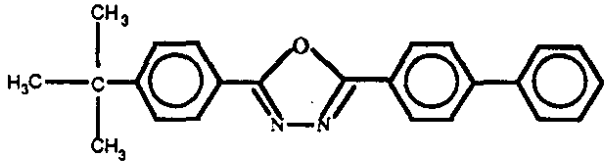

[3] PPO 2,5-diphenyloxazole

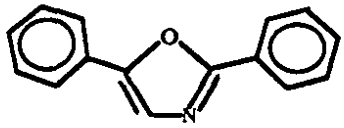

[4] PBD 2-(4-biphenylyl)-5-phenyl-1,3,4-oxadiazole

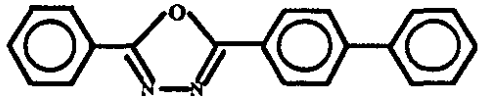

(C) Secondary Fluors

[1] POPOP *p*-bis[2-(5-phenyloxazolyl)]benzene

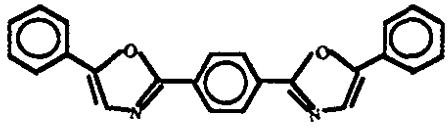

[2] bis-MSB *p*-bis(*o*-methylstyryl)benzene

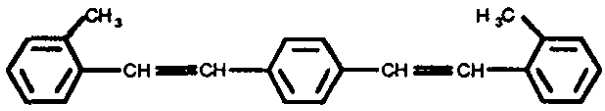

[3] TPB 1,1,4,4-tetraphenylbutadiene

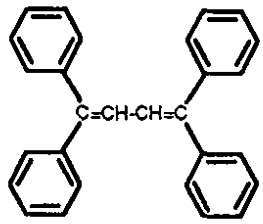

[4] BBQ 7H-benzimidazo[2,1-a]benz[de]isoquinoline-7-one

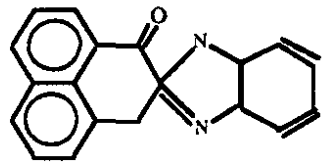

[5] Y7, K27 proprietary fluors

(D) Large Stoke Shift Fluors (>10,000 cm^{-1})

[1] 3HF 3-hydroxyflavone

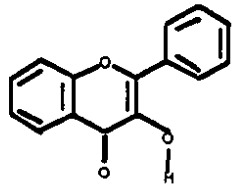

[2] HBT 2-(2'-hydroxyphenyl)-benzothiazole

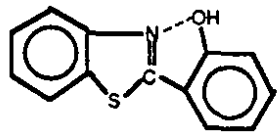

[3] BPD 2,2'-bipyridyl-3,3'-diol

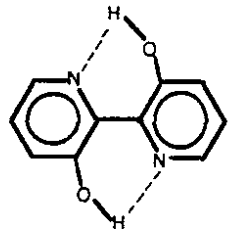

[4] PMP 1-phenyl-3-mesityl-2-pyrazoline

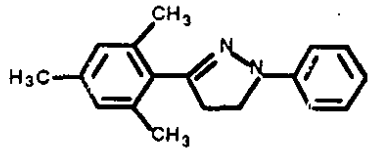

[5] MOPOM

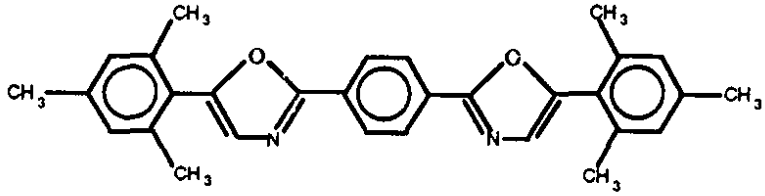

(E) Oligophenylenes

[1] DAT 4,4"-di-t-amyl-terphenyl

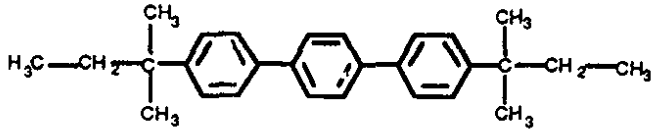

[2] O408 Oligo 408

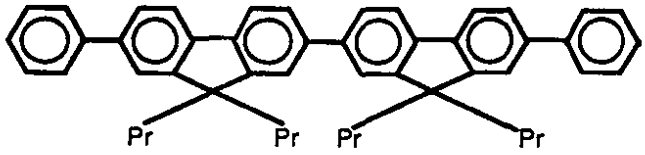

Pr = $CH_2CH_2CH_3$

[3] O415 Oligo 415

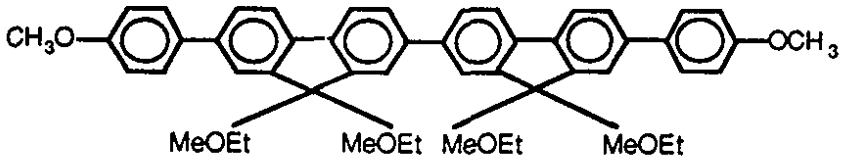

MeOEt = 2-methoxyethyl = $CH_2CH_2OCH_3$

References for Part II

[1] A. Pla-Dalmau, "Design of Fluorescent Compounds for Scintillation Detection," doctoral thesis, Northern Illinois University (1990).

[2] G. Marini et al., "Radiation Damage to Organic Scintillation Materials," CERN report 85-08 (1985).

[3] P. Sonderegger, *Nucl. Instr. Meth.* **A257** (1987) 523.

[4] D.E. Groom, "Radiation Levels in SSC Detectors," *Proceedings of the Summer Study on High Energy Physics in the 1990s*, ed. S. Jensen (World Scientific, Singapore, 1989) pp. 711-716.

[5] A. Van Ginneken, "Estimated Radiation Levels in SSC Detectors," *Radiation Effects at the SSC*, ed. G.D. Gilchriese, SSC report SR-1035 (LBL, Berkeley, 1988) pp. 409-428.

[6] H. Schönbacher, "Radiation Damage Studies for Detector Materials," *Proceedings of the ECFA Study Week on Instrumentation Technology for High Luminosity Hadron Colliders*, ed. E. Fernandez and G. Jarlskog, CERN report 89-10, pp. 129-151.

[7] H. Schönbacher and F. Wulf, "Radiation Hardness Studies for the LHC Detector Materials," *Proceedings of the Large Hadron Collider Workshop*, ed. D. Rein and G. Jarlskog, CERN report 90-10 (Vol. I, 1990) pp. 289-324.
G.R. Stevenson, "New Dose Calculations for LHC Detectors," *ibid.*, (Vol. III) pp. 566-583.

[8] S. Majewski, "Radiation Damage in Plastic Scintillators," *Proceedings of the Workshop on Calorimetry for the Supercollider*, ed. M.G.D. Gilchriese, (World Scientific, Singapore, 1990), pp. 451-485.

[9] C. Zorn, *IEEE Trans. Nucl. Sc.* **37** (1990) 504.

[10] Solenoidal Detector Collaboration, Expression of Interest to the SSC Laboratory (May 24, 1990).

[11] D.E. Groom, "Ionizing Radiation Environment in SSC Detectors," *Proceedings of the Workshop on Radiation Hardness of Plastic Scintillator*, ed. K.F. Johnson (March 19-21, 1990, Tallahassee, Florida, U.S.A.) pp. 69-75.

[12] A. Maio, "Effects of radiation damage on scintillating fibre calorimetry," *Proceedings of the Large Hadron Collider Workshop*, ed. G.Jarlskog and D. Rein, CERN report 90-10 (Vol. III, 1990) pp. 625-644.

[13] W.L. Dunn et al., "Radiation Damage Studies of Straw Tube and Scintillating Fiber Elements," *Proceedings of the Symposium on Detector Research and De-*

velopment for the Superconducting Super Collider, ed. T. Dombeck, V. Kelly, and G.P. Yost (World Scientific, Singapore, 1991) pp. 669-671.

[14] A.D. Bross and A. Pla-Dalmau, "Radiation-Induced Hidden Absorption Effects in Polystyrene Based Plastic Scintillator," *Proceedings of the ACS Symposium on Radiation Effects on Polymeric Materials*. ed. R.L. Clough and S.W. Shalaby (American Chemical Society, Washington, D.C., 1991) pp. 578-590.

[15] J.B. Birks, *The Theory and Practice of Scintillating Counting* (Pergamon, London, 1964).

[16] F.D. Brooks, *Nucl. Instr. Meth.* **162** (1979) 477.

[17] T.O. White, *Nucl. Instr. Meth.* **A273** (1988) 820.

[18] A.J. Davis et al., *Nucl. Instr. Meth.* **A276** (1989) 347.

[19] J.M. Flournoy, "An Introduction to Organic Scintillators," *Proceedings of the Workshop on Scintillating Fiber Development for the SSC*, November 14-16, 1988, Fermilab, Batavia, Illinois, U.S.A., pp. 507-529.

[20] M.K. Bowen, "Study of New Polysiloxane-based Scintillators," Master of Science thesis, University of Florida (1988).

[21] A.D. Bross, *Nucl. Instr. Meth.* **A295** (1990) 315.

[22] I.B. Berlman, *Handbook of Fluorescence Spectra of Aromatic Molecules*, 2nd edition (Academic Press, New York, 1971).

[23] T. Förster, *Ann. Phys.* **2** (1948) 55.

[24] P. Rebourgeard et al., *IEEE Trans. Nucl. Sc.* **36** (1989) 150.

[25] S. Majewski et al., "A Pilot Study of Radiation Damage in Liquid Scintillators," *Proceedings of the Workshop on Scintillating Fiber Development for the SSC*, November 14-16, 1988, Fermilab, Batavia, Illinois, U.S.A., pp. 801-817.

C. Zorn et al., "Development of Improved, Radiation-Resistant Plastic and Liquid Scintillators for the SSC," *Proceedings of the International Industrial Symposium on the Supercollider*, ed. M. McAshan (Plenum Press, New York, 1989) pp. 537-550.

C. Zorn et al., *IEEE Trans. Nucl. Sc.* **37** (1990) 487.

[26] S. Majewski et al., *Nucl. Instr. Meth.* **A281** (1989) 500.

[27] R.L. Clough et al., "Radiation Effects on Scintillating Fiber Optics for SSC," *Proceedings of the Workshop on Radiation Hardness of Plastic Scintillator*, ed. K.F. Johnson (March 19-21, 1990, Tallahassee, Florida, U.S.A.) pp. 15-27.

[28] H. Blumenfeld et al., *IEEE Trans. Nucl. Sc.* **33** (1986) 54.

[29] M.D. Petroff and M. Atac, "High Energy Particle Tracking using Scintillating Fibers and Solid State Photomultipliers," *Proceedings of the Workshop on*

Scintillating Fiber Development for the SSC, November 14-16, 1988, Fermilab, Batavia, Illinois, U.S.A., pp. 843-850.

R. Ruchti, "Scintillating Fiber Detectors," *Proceedings of the Symposium on Detector Research and Development for the Superconducting Super Collider.* ed. T. Dombeck, V. Kelly, and G.P. Yost (World Scientific, Singapore, 1991) pp. 90-99.

[30] B. Abbot et al., *IEEE Trans. Nucl. Sc.* **38** (1991) 441.

[31] M. Salomon and J. Kitching, *IEEE Trans. Nucl. Sc.* **38** (1991) 140.

[32] S. Reucroft et al., "Avalanche Photodiodes as Plastic Scintillating Fiber Readout Devices," *Proceedings of the Symposium on Detector Research and Development for the Superconducting Super Collider*, ed. T. Dombeck, V. Kelly, and G.P. Yost (World Scientific, Singapore, 1991) pp. 287-289.

[33] Bicron Corporation, Newbury, Ohio, U.S.A.

[34] J.M. Kauffman, "Design of Radiation Hard Fluors," *Proceedings of the Workshop on Scintillating Fiber Development for the SSC,* November 14-16, 1988, Fermilab, Batavia, Illinois, U.S.A., pp. 677-740.

[35] H. Schönbacher and W. Witzeling, *Nucl. Instr. Meth.* **165** (1979) 517.

[36] C. Zorn et al., *Nucl. Instr. Meth.* **A276** (1989) 58.

[37] C.S. Lindsey et al., *Nucl. Instr. Meth.* **A254** (1987) 212.

[38] N.D. Giokaris, "Radiation Damage of the CDF Beam-Beam Counters during the 1988-89 Fermilab Collider Run," *Proceedings of the Workshop on Radiation Hardness of Plastic Scintillator*, ed. K.F. Johnson (March 19-21, 1990, Tallahassee, Florida, U.S.A.) pp. 121-125.

M. Contreras and N.D. Giokaris, "Radiation Damage to SCSN23, SCSN81, and SCSN81+Y7 Scintillators," Fermilab CDF note 1341 (1991).

N.D. Giokaris, "BBC Inefficiencies: Evidence from the Data and Bench Measurements," Fermilab CDF note 1214 (1990).

[39] H. Hinrichs, *Z. Naturforsch.* **9a** (1954) 617.

[40] K. Wick et al., *Nucl. Instr. Meth.* **A277** (1989) 251.

[41] R.L. Clough and J.S. Wallace, "Radiation Effects on Organic Scintillators: Studies of Color Center Annealing," *Proceedings of the Symposium on Detector Research and Development for the Superconducting Super Collider*, ed. T. Dombeck, V. Kelly, and G.P. Yost (World Scientific, Singapore, 1991) pp. 661-665.

[42] C. Zorn et al., "Results of a Preliminary Low Dose Rate Irradiation of Selected Plastic Scintillating Fibers," *ibid.* pp. 666-668.

[43] U. Holm and K. Wick, *IEEE Trans. Nucl. Sc.* **36** (1989) 579.

[44] B. Bicken et al., *IEEE Trans. Nucl. Sc.* **38** (1991) 188.
A. Dannemann et al., "High and Low Dose rate Irradiations of Scintillators and Wavelength Shifters," *Proceedings of the Large Hadron Collider Workshop*, ed. G. Jarlskog and D. Rein, CERN report 90-10 (Vol. III, 1990) pp. 645-650.
K. Wick et al., *Nucl. Instr. Meth.* **B61** (1991) 472.

[45] Kuraray Corporation, Tokyo, Japan.

[46] Y. Sirois and R. Wigmans, *Nucl. Instr. Meth.* **A240** (1985) 262.

[47] J.S. Wallace, Sandia National Laboratories, private communication.

[48] C. D'Ambrosio et al., "Supercollider SCIFI Trackers," *Proceedings of the Workshop on Scintillating Fiber Development for the SSC*, November 14-16, 1988, Fermilab, Batavia, Illinois, U.S.A., pp. 613-640.

[49] P. Destruel et al., *Nucl. Instr. Meth.* **A276** (1989) 69.

[50] C. Angelini et al., *Nucl. Instr. Meth.* **A289** (1990) 342.

[51] C. Angelini et al., *Nucl. Instr. Meth.* **A289** (1990) 356.

[52] C. Angelini et al., *Nucl. Instr. Meth.* **A295** (1990) 299.

[53] C. Zorn et al., *Nucl. Instr. Meth.* **A271** (1988) 701.

[54] C. Zorn et al., *Nucl. Instr. Meth.* **A273** (1988) 108.

[55] S. Majewski et al., *Nucl. Instr. Meth.* **A281** (1989) 497.

[56] D. Puseljic et al., *IEEE Trans. Nucl. Sc.* **37** (1990) 139.

[57] C. D'Ambrosio et al., *Appl. Spect.* March-April issue (1991) 45.
C. D'Ambrosio et al., *Nucl. Instr. Meth.* **A307** (1991) 430.

[58] C.L. Renschler and L.A. Harrah, *Nucl. Instr. Meth.* **A235** (1985) 41.

[59] J.M. Flournoy, EG&G, private communication.

[60] S. Majewski et al., "Comparative Study of the Radiation Resistance of Selected Plastic Scintillating Fibers," *Proceedings of the ECFA Study Week on Instrumentation Technology for High Luminosity Hadron Colliders*, ed. E. Fernandez and G. Jarlskog, CERN report 89-10, pp. 129-151.

[61] C. Zorn, "Designing a Radiation Hard Plastic Scintillator for High Luminosity Hadron Colliders," *Proceedings of the Workshop on Radiation Hardness of Plastic Scintillator*, ed. K.F. Johnson (March 19-21, 1990, Tallahassee, Florida, U.S.A.) pp. 1-13.

[62] C. Zorn et al., *IEEE Trans. Nucl. Sc.* **38** (1991) 194.

[63] K.F. Johnson et al., *IEEE Trans. Nucl. Sc.* **37** (1990) 500.

[64] D. Acosta et al., "The Effects of Radiation Damage on a Scintillating Fiber Calorimeter," UC San Diego preprint (1989).

[65] J. Badier, "Electromagnetic Shower Resolution in a Scintillation Fiber Calorimeter," *Proceedings of the Workshop on Radiation Hardness of Plastic Scintillator*, ed. K.F. Johnson (March 19-21, 1990, Tallahassee, Florida, U.S.A.) pp. 77-84.

[66] J. Badier, "Radiation Damage and Resolution Loss in Scintillating Fiber Calorimeters," *Proceedings of the Large Hadron Collider Workshop*, ed. G. Jarlskog and D. Rein, CERN report 90-10 (Vol. III, 1990) pp. 661-665.

[67] A.D. Bross et al., "New Scintillation Materials for Fiber Tracking and Calorimetry," published in the Conference Record of the 1990 IEEE Nuclear Science Symposium (1990) pp. 132-136.

A.D. Bross et al., *Nucl. Instr. Meth.* **A307** (1991) 35.

[68] J.M. Kauffman and M.A. Aziz, "Progress on Design of Radiation-Hard Scintillators," *Proceedings of the Workshop on Radiation Hardness of Plastic Scintillator*, ed. K.F. Johnson (March 19-21, 1990, Tallahassee, Florida, U.S.A.) pp. 29-48.

[69] M. Kasha et al., "Molecular Electronic Criteria for Selection of Radiation-Hard Scintillators," *ibid.* pp. 49-60.

[70] V.D. Bezuglii and L.L. Nagornaya, *J. Nucl. Eng.* **19** (1965) 490.

[71] M. Bowen et al., *IEEE Trans. Nucl. Sc.* **36** (1989) 562.

[72] M. Bowen et al., *Nucl. Instr. Meth.* **A276** (1989) 391.

[73] M. Bowen et al., "Preliminary Results with a Polysiloxane-based, Radiation Resistant Plastic Scintillator," *Proceedings of the Workshop on Scintillating Fiber Development for the SSC*, November 14-16, 1988, Fermilab, Batavia, Illinois, U.S.A., pp. 785-797.

[74] V.M. Feygelman et al., *Nucl. Instr. Meth.* **A290** (1990) 131.

[75] V.M. Feygelman et al., *Nucl. Instr. Meth.* **A295** (1990) 94.

[76] J. Harmon and J. Walker, "Siloxane Scintillators," *Proceedings of the Workshop on Radiation Hardness of Plastic Scintillator*, ed. K.F. Johnson (March 19-21, 1990, Tallahassee, Florida, U.S.A.) pp. 61-68.

[77] J.P. Harmon and J.K. Walker, "A Review of Polymeric Scintillator Materials for Use at the SSC," *Proceedings of the Symposium on Detector Research and Development for the Superconducting Super Collider*, ed. T. Dombeck, V. Kelly, and G.P. Yost (World Scientific, Singapore, 1991) pp. 680-682.

[78] C.W. Park et al., "Fabrication of a Step-Index Scintillating Optical Fiber by a Coextrusion Process," *ibid.* pp. 284-286.

[79] K.F. Johnson and H.L. Whitaker, *Nucl. Instr. Meth.* **A301** (1991) 372.

[80] J. Kirkby, "Today and Tomorrow for Scintillating Fibre Detectors," CERN preprint EP/87-60.

[81] P. Mélèse et al., "Results of a Scintillating Fiber Preshower Detector for Identifying Electrons via Synchrotron Radiation," published in the Conference Record of the 1990 IEEE Nuclear Science Symposium (1990) pp. 677-681.

[82] R.E. Ansorge et al., "Performance of a Scintillating Fiber Detector for the UA2 Upgrade," CERN preprint EP/87-63 (1987).

[83] W. Worstell et al., "Cast Lead-Eutectic Solid and Liquid Scintillating Fiber Shower Calorimeters," published in the Conference Record of the 1990 IEEE Nuclear Science Symposium (1990) pp. 701-703.

[84] K. Beard et al., "Lead/Scintillating Fiber Electromagnetic Calorimeter Protoype," published in the Conference Record of the 1990 IEEE Nuclear Science Symposium (1990) pp. 731-735.

[85] P. Destruel et al., "Plastic Scintillating Fibers," *Proceedings of the Workshop on Scintillating Fiber Development for the SSC*, November 14-16, 1988, Fermilab, Batavia, Illinois, U.S.A., pp. 551-568.

[86] M. Bourdinaud and J.C. Thevenin, "Plastic Scintillating Microfibers of 50μm", *Proceedings of the Workshop on Scintillating Fiber Development for the SSC*, November 14-16, 1988, Fermilab, Batavia, Illinois, U.S.A., pp. 823-827.

[87] J. Alitti et al., "Performance of the UA2 Scintillating Fiber Detector," *Proceedings of the Workshop on Scintillating Fiber Development for the SSC*, November 14-16, 1988, Fermilab, Batavia, Illinois, U.S.A., pp. 7-34.

[88] J.C. Thevenin, "Plastic Optical Fibers Technology," *Proceedings of the Workshop on Scintillating Fiber Development for the SSC*, November 14-16, 1988, Fermilab, Batavia, Illinois, U.S.A., pp. 57-94.

[89] F. Takasaki, "Recent Development of Scintillating Fiber Detectors for SSC around KEK," *Proceedings of the Workshop on Scintillating Fiber Development for the SSC*, November 14-16, 1988, Fermilab, Batavia, Illinois, U.S.A., pp. 141-164.

[90] J.S. Frank and R.C. Strand, "Construction and Performance of a Plastic Scintillating Fiber Target for a Rare Kaon Decay Experiment," *Proceedings of the Workshop on Scintillating Fiber Development for the SSC*, November 14-16, 1988, Fermilab, Batavia, Illinois, U.S.A., pp. 361-382.

[91] K. Kuroda et al., *Nucl. Instr. Meth.* **A300** (1991) 259.

[92] D. Acosta et al., *Nucl. Instr. Meth.* **A294** (1990) 193.

[93] D. Acosta et al., *Nucl. Instr. Meth.* **A302** (1991) 36.

[94] D. Acosta et al., *Nucl. Instr. Meth.* **A305** (1991) 55.
D. Acosta et al., *Nucl. Instr. Meth.* **A308** (1991) 481.
D. Acosta et al., *Nucl. Instr. Meth.* **A309** (1991) 143.
[95] H. Blumenfeld et al., *Nucl. Instr. Meth.* **225** (1984) 518.
[96] H. Blumenfeld et al., *Nucl. Instr. Meth.* **A235** (1985) 326.
[97] H. Burmeister et al., *Nucl. Instr. Meth.* **225** (1984) 530.
[98] A. Bross et al., *Nucl. Instr. Meth.* **A286** (1990) 69.
[99] S.J. Alvsvåg et al., *Nucl. Instr. Meth.* **A290** (1990) 320.
[100] A.J. Rusi et al., *Nucl. Instr. Meth.* **A290** (1990) 109.
[101] C.M. Hawkes et al., *Nucl. Instr. Meth.* **A292** (1990) 329.
M. Kuhlen et al., "Study of Scintillating Fibers for a High Resolution Time of Flight System at the SSC," *Proceedings of the International Industrial Symposium on the Supercollider*, ed. M. McAshan (Plenum Press, New York, 1989) pp. 611-622.
R. Stroynowski, "Light Propagation and Timing with Scintillating Fibers," Caltech preprint CALT-68-1668, to be published in the proceedings of the 2nd International Conference on Advanced Technology and Particle Physics, June 11-15, 1990, Como, Italy.
M. Kuhlen et al., *Nucl. Instr. Meth.* **A301** (1991) 223.
[102] C. Angelini et al., *Nucl. Instr. Meth.* **A277** (1989) 132.
[103] J.A. Crittenden, *Nucl. Instr. Meth.* **A277** (1989) 125.
[104] K. Takikawa, "Red-Green-Blue Scintillating Fiber Calorimeter," *Proceedings of the International Workshop on Solenoidal Detectors for the SSC*, April 23-25, 1990, Tsukuba, Japan, pp. 370-374.
[105] D.W. Hertzog et al., *Nucl. Instr. Meth.* **A294** (1990) 446.
[106] L.R. Allemand et al., *Nucl. Instr. Meth.* **225** (1984) 522.
[107] F. Takasaki et al., *Nucl. Instr. Meth.* **A262** (1987) 224.
[108] R.E. Ansorge et al., *Nucl. Instr. Meth.* **A273** (1988) 826.
[109] H. Blumenfeld et al., *Nucl. Instr. Meth.* **A278** (1989) 619.
[110] H. Blumenfeld et al., *Nucl. Instr. Meth.* **A279** (1989) 281.
[111] G.W. Foster and J. Freeman, "Scintillating Tile/Fiber Calorimetry Development at FNAL," *Proceedings of the International Workshop on Solenoidal Detectors for the SSC*, April 23-25, 1990, Tsukuba, Japan, pp. 376-380.
R. McNeil et al., "Scintillating Plate Calorimeter Optical Design," *Proceedings of the Symposium on Detector Research and Development for the Superconducting Super Collider*, ed. T. Dombeck, V. Kelly, and G.P. Yost (World

Scientific, Singapore, 1991) pp. 435-437.

J. Proudfoot et al., "Simulation Studies for Design Optimization of a Scintillating Plate Calorimeter," *ibid.* pp. 410-418.

H. Spinka et al., "Scintillating Plate Calorimeter Mechanical Design," *ibid.* pp. 728-730.

[112] F.G. Hartjes and R. Wigmans, *Nucl. Instr. Meth.* **A277** (1989) 379.

[113] N.A. Amos et al., *Nucl. Instr. Meth.* **A297** (1990) 396.

[114] M. Atac et al., "A Simple Method of Fusing Plastic Fibers," Fermilab preprint FN-537 (1990).

[115] C. D'Ambrosio et al., "Reflection Losses in Polystyrene Fibres," CERN preprint PPE/91-51, submitted to Nuclear Instruments and Methods (1991).

[116] J. White et al., "A Liquid Scintillator Spaghetti Calorimeter EM Module for Forward Calorimetry at the SSC," *Proceedings of the Symposium on Detector Research and Development for the Superconducting Super Collider*, ed. T. Dombeck, V. Kelly, and G.P. Yost (World Scientific, Singapore, 1991) pp. 444-446.

[117] J. White et al., "Effect of Radiation Induced Discoloration of the Cladding on Liquid Scintillation Fibers," *ibid.* pp. 677-679.

[118] M. Chiba et al., "Measurement of Radiation Damage in Liquid Scintillators by ^{60}Co γ rays," *Proceedings of the International Workshop on Solenoidal Detectors for the SSC*, April 23-25, 1990, Tsukuba, Japan, pp. 381-392.

[119] S.G. Iverson et al., "Organic Scintillating Fiber Detectors," *Proceedings of the Workshop on Scintillating Fiber Development for the SSC*, November 14-16, 1988, Fermilab, Batavia, Illinois, U.S.A., pp. 571-581.

[120] R. Ruchti et al., "Liquids-in-Capillaries: New Fiber Detectors for High Energy Physics Applications," *Proceedings of the Workshop on Scintillating Fiber Development for the SSC*, November 14-16, 1988, Fermilab, Batavia, Illinois, U.S.A., pp. 585-593.

R. Ruchti et al., *IEEE Trans. Nucl. Sc.* **36** (1989) 146.

[121] A. Artamonov et al., *Nucl. Instr. Meth.* **A300** (1991) 53.

R. Nahnhauer and V. Zacek, "Search for $\nu_\mu \rightarrow \nu_\tau$ Oscillations with a Massive Active Target Detector based on Scintillating Fibers," CERN preprint PPE/90-138, to be published in the proceedings of the Workshop on Application of Scintillating Fibers in Particle Physics, September 3-5, 1990, Blossin, Germany.

G. Zacek, "Low Energy Neutrino Physics with Scintillating Fibers," CERN preprint PPE/91-06, *ibid.*

J. Bähr et al., *Nucl. Instr. Meth.* **A306** (1991) 169.

[122] C. Kennedy et al., *IEEE Trans. Nucl. Sc.* **37** (1990) 144.

[123] N.S. Bamburov et al., *Nucl. Instr. Meth.* **A289** (1990) 265.

[124] J.L. Pinfold et al., *Nucl. Instr. Meth.* **A286** (1990) 345.

[125] Alltech Associates Inc., Deerfield, Illinois, U.S.A.

[126] Pennwalt Corporation, Philadelphia, Pennsylvania, U.S.A.

[127] R. Bionta et al, "Liquid Scintillator Calorimetry," research and development proposal submitted to the SSC Laboratory (1990).

[128] C. Da Viá, CERN, private communication.

[129] Schott 8250 produced by Schott Glaswerke, Mainz, Germany.

[130] D. Acosta et al., "Effects of Radiation Damage on Scintillating Fibre Calorimetry," CERN preprint PPE/91-45, submitted to Nuclear Instruments and Methods (1991).

[131] V. Hagopian et al., "Radiation Damage Tests of New Scintillating Fibers and Plates," *Proceedings of the Symposium on Detector Research and Development for the Superconducting Super Collider*, ed. T. Dombeck, V. Kelly, and G.P. Yost (World Scientific, Singapore, 1991) pp. 674-676.

K.F. Johnson et al., "Radiation Damage Tests of a Scintillating Fiber Calorimeter," *ibid.* pp. 672-673.

D.W. Hertzog et al., "Can a Pb/SCIFI Calorimeter Survive the SSC?" *Proceedings of the Workshop on Radiation Hardness of Plastic Scintillator*, ed. K.F. Johnson (March 19-21, 1990, Tallahassee, Florida, U.S.A.) pp. 93-103.

[132] D.W. Hertzog et al., "High Resolution Pb/SCIFI Calorimetry: Performance and Radiation Damage Studies," *Proceedings of the First International Conference on Calorimetry in High Energy Physics* ed. D.F. Anderson et al., (World Scientific, Singapore, 1991) pp. 135-148.

[133] C.R. Hurlbut, "Development of New Scintillator Materials for the SSC," *Proceedings of the International Industrial Symposium on the Supercollider*, ed. M. McAshan (Plenum Press, New York, 1989) pp. 187-202.

[134] N.J. Turro, *Modern Molecular Photochemistry* (Benjamin/Cummings Publishing Co., Inc., Menlo Park, California, 1978).

[135] T. Kamon et al., *Nucl. Instr. Meth.* **213** (1983) 261.

[136] M. Adinolfi et al., "A High-Resolution Tracking Detector based on Capillaries filled with Liquid Scintillator," CERN preprint PPE/91-66, submitted to Nuclear Instruments and Methods.

[137] M. Kobayashi et al., *Nucl. Instr. Meth.* **305** (1991) 401.

[138] NE Technology Limited, United Kingdom.

[139] S.V. Golovkin et al., *Nucl. Instr. Meth.* **305** (1991) 385.

[140] G. Martellotti, "Progress on High Resolution Tracking with Scintillating Fibers: A New Detector based on Capillaries filled with Liquid Scintillator," CERN preprint PPE/91-136, to be published in Nuclear Instruments and Methods.

[141] C. Zorn et al., "Results of a Low Dose Rate Irradiation of Selected Plastic Scintillating Fibers," submitted to the 1991 Conference issue of the IEEE Transactions on Nuclear Science for the 1991 IEEE Nuclear Science Symposium, Sante Fe, New Mexico, Nov. 5-8, 1991.

[142] A.D. Bross and A. Pla-Dalmau, "Radiation Damage of Plastic Scintillators," contribution to the 1991 IEEE Nuclear Science Symposium, Sante Fe, New Mexico, Nov. 5-8, 1991.